

Characterization of the  
Sensory Rhodopsin II / Transducer II  
complexes from *Halobacterium  
salinarum*

Dissertation

zur Erlangung des akademischen Grades  
eines Doktors der Naturwissenschaften (Dr. rer. nat.)  
des Fachbereichs Chemie der Universität Dortmund

Angefertigt am Max-Planck-Institut für Molekulare Physiologie  
in Dortmund

Vorgelegt von

**Young Jun Kim**  
Aus Südkorea

Dortmund, 2010

Die vorliegende Arbeit wurde in der Zeit von September 2005 bis Dezember 2010 am Max-Planck-Institut für molekulare Physiologie in Dortmund, in der Abteilung physikalische Biochemie von Prof. Dr. Roger S. Goody, unter der Leitung von Prof. Dr. Martin Engelhard angefertigt.

1.Gutachter: Prof. Dr. Martin Engelhard

2.Gutachter: Priz.-Doz. Dr. Susanne Brakmann

Hiermit versichere ich an Eides statt, dass ich die vorliegende Arbeit selbständig und nur mit den angegebenen Hilfsmitteln angefertigt habe.

---

Kim, young jun

Dortmund

# CONTENTS

## ABBREVIATION AND SYMBOLS

<b>1. INTRODUCTION .....</b>	<b>1</b>
<b>1. INTRODUCTION .....</b>	<b>2</b>
1.1. Overview of chemotaxis and phototaxis signaling .....	2
1.2. Phototaxis behaviour of <i>H.salinarum</i> .....	4
1.3. Archaeal rhodopsins .....	6
1.4. Halobacterial transducers and chemoreceptors .....	8
1.5. NpSRII-NpHtrII interaction .....	10
1.6. Photocycle .....	11
1.7. The molecular Mechanisms of signal transfer .....	13
<b>2. MATERIALS AND METHODS .....</b>	<b>19</b>
<b>2.1. Chemicals.....</b>	<b>20</b>
2.1.1. Reagent Kits .....	21
2.1.2. General instruments .....	21
<b>2.2. Cell Culture Techniques .....</b>	<b>22</b>
2.2.1. Plasmids and bacterial strains .....	22
2.2.2. Preparation of competent cells .....	24
2.2.3. Transformation by electroporation .....	24
2.2.4. Media .....	24
<b>2.3. Molecular biological methods.....</b>	<b>25</b>
2.3.1. Preparation PCR .....	25
2.3.2. Polymerase chain reaction (PCR) .....	26
2.3.3. Purification of PCR products by agarose gel electrophoresis .....	27
2.3.4. DNA Restriction enzyme digestion .....	27
2.3.5. DNA Ligation .....	27
2.3.6. Transformation by electroporation .....	28
2.3.7. Preparation of plasmid DNA .....	28
2.3.8. DNA sequencing .....	28
<b>2.4 Protein expression and purification methods.....</b>	<b>29</b>
2.4.1. Protein expression .....	29
2.4.2. Protein Purification .....	29
2.4.3. Determination of the protein concentration .....	30
2.4.4. Isolation of purple membrane lipids from <i>H.salinarum</i> .....	31
2.4.5. Reconstitution in purple membrane lipids (PMLs) .....	32
<b>2.5. Analytical methods .....</b>	<b>32</b>
2.5.1. Sodium dodecyl sulfate polyacrylamide gel electrophoresis (SDS-PAGE) .....	32
2.5.2. Western blot analysis .....	33
2.5.3. Blue native gel electrophoresis (BN-PAGE) .....	33
2.5.4. LC-ESI-mass spectrometry .....	34
2.5.5. Analytical Gel filtration .....	35
2.5.6. Crystallisation by Vapour-Diffusion method .....	35
<b>2.6. Biophysical analysis.....</b>	<b>36</b>
2.6.1. Isothermal Titration Calorimetry (ITC).....	36
2.6.2. ANS fluorescence measurements .....	40

2.6.3. Intrinsic tryptophan fluorescence .....	42
2.6.4. Circular Dichroism (CD) analysis .....	43
2.6.5. Laser flash photolysis and data analysis .....	44
<b>3. RESULTS .....</b>	<b>45</b>
<b>3.1. Cloning, expression and purification of proteins .....</b>	<b>46</b>
3.1.1. <i>Halobacterium salinarum</i> sensory rhodopsin II(HsSRII) .....	46
3.1.2. Expression of halobacterial transducer II (HsHtrII) and its analogues .....	49
3.1.4. Crystallization trials for water soluble HsHtrII .....	57
<b>3.2. Biophysical and biochemical characterization .....</b>	<b>59</b>
3.2.1. Absorption spectrum of HsSRII .....	59
3.2.2. The pH dependent spectral transition and the pKa of Asp 73 .....	60
3.2.3. Photocycle of HsSRII .....	61
3.2.4. Blue native gel of the NpSRII-HsHtrII complex formation .....	67
3.2.5. Analytical Size-Exclusion Chromatography .....	68
3.2.6. Isothermal titration calorimetry (ITC) of receptor-transducer binding .....	70
3.2.7. Circular Dichroism (CD) spectroscopy of HsHtrII constructs and Tar chemoreceptor .....	75
<b>3.3. Functional characterization of HsHtrII and Tar chemoreceptor .....</b>	<b>83</b>
3.3.1. Isothermal titration calorimetry (ITC) of HsHtrII-serine interaction .....	83
3.3.2. Isothermal titration calorimetry (ITC) of Tar-aspartate interaction .....	84
3.3.3. Intrinsic tryptophan fluorescence .....	86
3.3.4. Trp fluorescence emission spectra of HsHtrII .....	87
3.3.5. Binding of serine to HsHtrII by intrinsic tryptophan fluorescence .....	89
3.3.6. ANS fluorescence emission spectra .....	91
3.3.7. Ligand induced conformational changes of HsHtrII and Tar chemoreceptor .....	96
3.3.8. Determination of the number of ANS binding sites .....	97
<b>4. DISCUSSION .....</b>	<b>102</b>
4.1. Biochemical and biophysical characterization of HsSRII .....	103
4.2. Binding of serine to HsHtrII .....	105
4.3. Ligand-induced conformational changes of HsHtrII and Tar chemoreceptor .....	107
4.4. The HsSRII-HsHtrII complex formation .....	114
<b>5. SUMMARY .....</b>	<b>118</b>
<b>6. REFERENCES .....</b>	<b>124</b>
<b>7. APPENDICES .....</b>	<b>138</b>
<b>8. ACKNOWLEDGMENTS .....</b>	<b>146</b>

## ABBREVIATIONS AND SYMBOLS

Å	Ångstrom (0.1nm)
AA	Amino acid
ANS	1-Anilinonaphthalene-8-Sulfonic Acid
APS	Ammonium Persulfate
BP	Base pair
BN-PAGE	Blue native polyacrylamide gel electrophoresis
BR	Bacteriorhodopsin
CheA	Chemotaxisprotein A
CheB	Chemotaxisprotein B
CheR	Chemotaxisprotein R
CheW	Chemotaxisprotein W
CheY	Chemotaxisprotein Y
CheZ	Chemotaxisprotein Z
CD	Circular dichroism
$\Delta$ CP	Heat capacity
Da	Dalton
DNA	Deoxyribonucleic acid
DTT	Dithiothreitol
DDM	N-Dodecyl- $\beta$ -D-maltosid
DEAE	Diethylaminoethyl
EDTA	Ethylendiaminetetraacetate
<i>E. coli</i>	<i>Escherichia coli</i>
ESI-MS	Electrospray Ionisation Mass Spectroscopy
$\Delta$ G	Free energy
<i>H. salinarum</i>	<i>Halobacterium salinarum</i>
Htr	halobacterial Transducer
HR	Halorhodopsin
$\Delta$ H	Enthalpy
IPTG	Isopropyl- $\beta$ -D-1 -thiogalactopyranosid
ITC	Isothermal Titration Calorimetry
Ka	Association constant
kDa	kilo-Dalton
KD	Dissociation constant
kJ	kilo-Joule
LB	Luria-Bertani
$\lambda$	Wavelength, Lambda
Mr	relative Molecule masse
MCP	methyl accepting chemotaxis protein
Min	Minute
Mw	Molecular Weight
Napi	sodium phosphate
<i>N. pharaonis</i>	<i>Natronobacterium pharaonis</i>
NTA	Nitrilo triacetic acid

O.D	Optical Density
PML	Purple membrane lipid
PCR	Polymerase Chain Reaction
PEG	Polyethelenglycol
PMSF	PhenylemethyIsulphonylfluoride
RNA	Ribonucleic acid
rpm	rounds per minute
RT	Room temperature
Sb	Schiff base
$\Delta S$	Entropy
SDS-PAGE	Sodiumdodecylsulphate-Polyacrylamide Gel Electrophoresis
SR	Sensory rhodopsin
Tar	aspartate chemoreceptor
Tsr	serine chemoreceptor
TM	Transmembrane
TRIS	Tris-(hydroxymethyl)-aminomethane
U	Units
UV	Ultraviolet
$\mu$ l	Microliter
$\mu$ M	Micromolar

### Amino Acids Abbreviations

Amino Acids	Three letter code	One letter Code
Alanine	Ala	A
Arginine	Arg	R
Asparagine	Asn	N
Aspartate	Asp	D
Cysteine	Cys	C
Glutamine	Glu	E
Glutamate	Gln	Q
Glycine	Gly	G
Histidine	His	H
Isoleucine	Ile	I
Leucine	Leu	L
Lysine	Lys	K
Phenylalanine	Phe	F
Methionine	Met	M
Proline	Pro	P
Serine	Ser	S
Threonine	Thr	T
Tryptophane	Trp	W
Tyrosine	Tyr	Y
Valine	Val	V

# 1. INTRODUCTION

### 1. Introduction

Motile bacteria respond to a variety of external stimuli by modulating the rotational direction of their flagella. Flagella driven motility is a necessity for coping with changing environments such as the decrease or increase of specific signaling molecules (chemotaxis), changes in the salinity (osmotaxis), temperature (thermotaxis), light intensity (phototaxis) and oxygen (aerotaxis) (1-3). Based on well-known chemotactic mechanisms in *E. coli*, signal transfer models of the events derived from chemoreceptor activation, achieve remarkable sensitivity, gain, dynamic range, and feedback control through the transmembrane signaling domain(4-10). Most of our knowledge on chemotaxis transducers is derived from the membrane-bound chemoreceptor proteins of bacteria (11,12). *E. coli* apparently evolved in an environment where sugars and amino acids served as energy sources. Therefore receptors to sense such substances are found in its inner membrane. Some ligands interact directly with the receptors in periplasmic space, such as serine with Tsr or aspartate with Tar, while ligand binding triggers a structural rearrangement of the binding protein, which allows the subsequent interaction with the receptor. Maltose, for example, is sensed by Tar through interaction with the maltose binding protein(13,14).

#### 1.1. Overview of chemotaxis and phototaxis signaling

Chemotaxis receptors such as the aspartate (Tar) and serine (Tsr) receptors in bacteria have extracellular ligand binding domains that trigger signal transduction. A special case in signal transduction is the photoreception of organism. The well known visual perception uses rodopsin as photoreceptor. Several lines of evidence support that downstream signaling cascades are essentially identical between the phototaxis and chemotaxis systems (15,16). It suggests that the signal can be transmitted through phototaxis and chemotaxis, resulting in presumably the same conformational changes in the cytoplasmic domain. Such transmembrane receptors are ubiquitously found in all cells. The physiological responses of the bacteria are controlled by a complex network system, which is composed of interlinked



## INTRODUCTION

signal transduction cascades that mediate the sensing and processing of stimuli (13,14).

As shown in Figure 1-1, motile bacteria use a two-component phosphotransfer system to regulate motor activity. As a result, the cell's motility can be controlled to migrate towards nutrients or away from repellents by sensing gradients of chemicals even under high background concentrations.

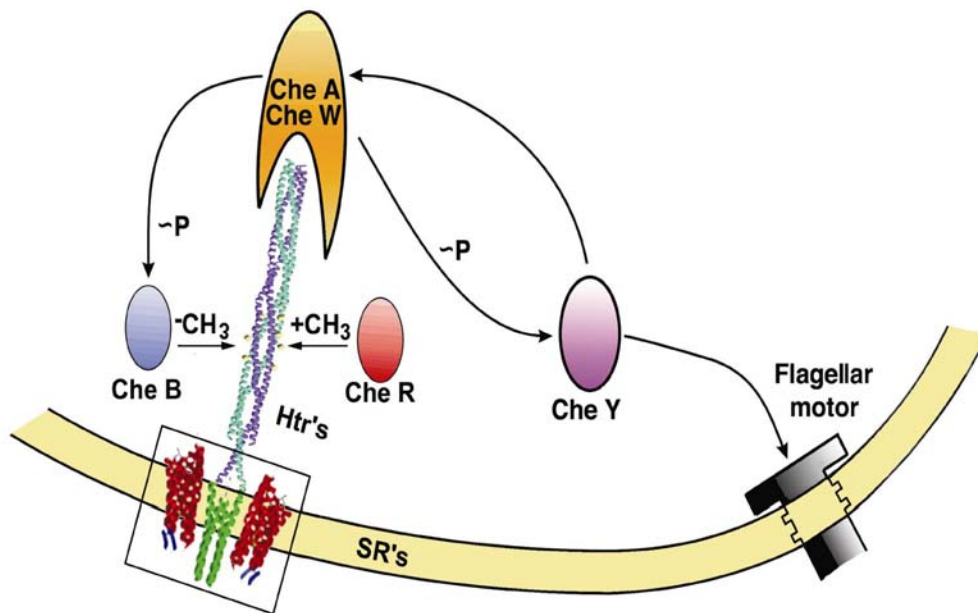


Figure 1-1. Signaling cascade of archaeal phototaxis which is analogous to the chemotactic two component system. This figure was taken from Gordeliy *et al.*, 2002 (17).

The architecture shared by the six essential Che proteins (Che A, CheW, Che Y, Che Z, Che R and Che B) has been extensively characterized in chemotaxis and phototaxis system. The light absorbed at the photoreceptor is transmitted to the transducer protein as phosphorylation signaling part. On activation of transducer protein, Che A binds to the signaling domains of the receptors *via* coupling with the protein CheW. The autophosphorylation activity of Che A depends on the signaling state of the receptors. Removal of an attractant or increase in a repellent causes increases in the level of CheA-phosphate and *vice versa*. This kinase, together with the response regulator

Che Y, forms the archetypal two-component signal transduction system, in which the phosphoryl-group is transferred from Che A to the response regulator Che Y (18,19). Phosphorylated Che Y affects the direction of rotation of the flagellar motor by binding to the switch complex of the motor (20-22). In *E. coli*, the Che Y-phosphate signal is terminated through the spontaneous hydrolysis of Che Y-phosphate as well as by Che Z, a response regulator phosphatase. The receptor methylation/demethylation creates a feedback loop that allows system adaptation of bacteria to constant stimuli (12,23). A second response regulator, a methyl-esterase Che B is responsible along with methyltransferase Che R for adaptation. Che R constitutively adds methyl groups derived from S-adenosyl-methionine to conserved glutamic residues of the receptors, while the activity of Che B is controlled by its phosphorylation. CheA-phosphate phosphorylates Che B, hydrolyzing methyl groups from the glutamates. The removal of methyl groups reset the chemoreceptor into the prestimulus signaling conformation. The Che R and Che B modifications also provide a memory mechanism that alters behavioural responses to subsequent stimuli. The nature of these modifying activities suggests that each cell has different receptor sensitivities.

### **1.2. Phototaxis behaviour of *H.salinarum***

Light is the ultimate energy resource for all forms of life and evoke the development of numerous types of microbial rhodopsins. The microbial rhodopsins are a diverse group of photosensitive pigments in all three kingdoms of life: eukaryotes, archaea and eubacteria (24,25). One of the important photoreceptors, widespread in higher organisms with more than 2000 members, is the rhodopsin-like 7-transmembrane-helix-receptors, also known as GPCRs (26). Members of this protein family interact with a guanine nucleotide-binding protein which conveys the signal from the receptor to a wide array of effectors (27,28). For example, the GPCRs family is the largest known family of cell-surface receptors, responding to a variety of stimuli such as hormones, neurotransmitters, odorant molecules and light (29-31). Another example is the microbial rhodopsin-mediated phototaxis and ion transport, which were first reported for archaeal species *H. salinarum* (32-34).

## INTRODUCTION

---

*H. salinarum* utilizes its flagella to swim back and forth by switching the rotational direction of the bundle approximately every ten seconds (35). Light and some chemical stimuli can induce or suppress this motor switching, thereby resulting in localisation of cells in a preferred location (Figure 1-2).

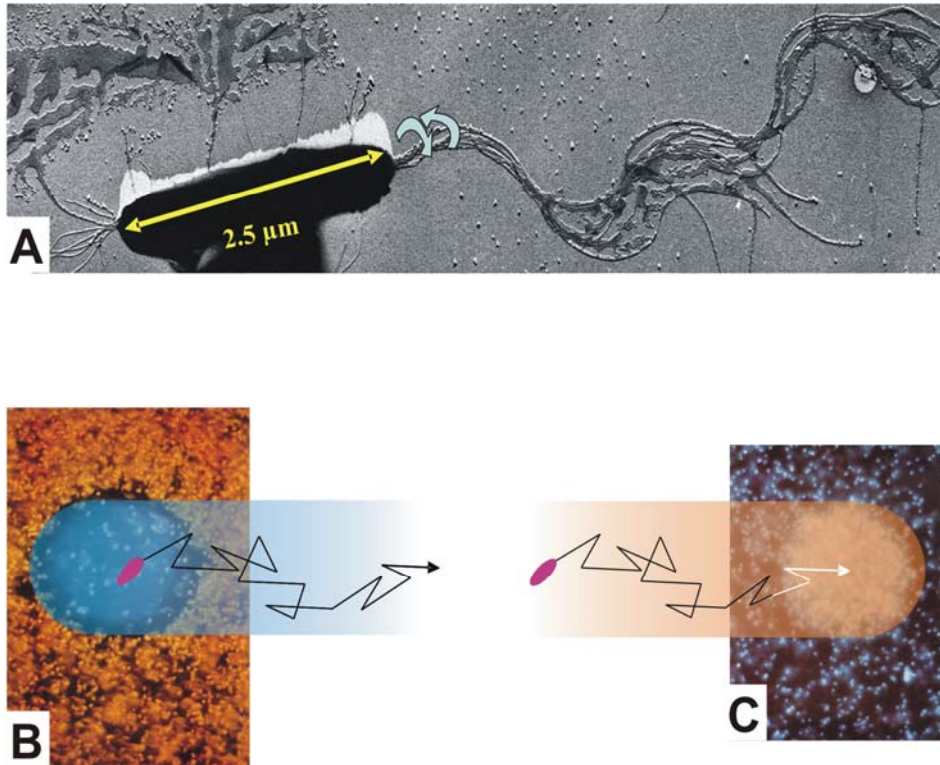


Figure 1-2. The phototactic behavior of *H. salinarum* (A) Electron micrograph of a polarly flagellated cell. Swimming movements of cells during different light irradiation (B) photophobic response to blue light (C) Photophilic response to orange light. Figure A is taken from M. Alam and Oestehelt, 1984 (36). Figure B and C were adapted from Stoeckenius *et al.*, 1974 (37).

Figure 1-2B shows that blue light and near- and far-UV light act as repellents that causes increase in the frequency of change in the rotary direction (33,38,39). On the other hand, *H. salinarum* is attracted by orange light which causes decrease in frequency of change of the rotary direction (Figure 1-2C)(40,41). The ability of movement is, at the molecular level, directly correlated to the respective photoreceptor.

### 1.3. Archaeal rhodopsins

*H. salinarum* has been studied much more extensively than other halophilic archaea because of its bioenergetic aspects. *H. salinarum* inhabits environments with high light and saturated salt concentrations such as the Great Salt Lake in the US or solar evaporation ponds. They utilize oxygen for normal respiration through the tricarboxylic acid (TCA) cycle in combination with a respiratory electron transport chain (42). However, in the absence of oxygen, they satisfy their energy needs such as synthesis of ATP by arginine fermentation,  $K^+/Na^+$  gradient and by photosynthesis of bacteriorhodopsin (BR) and halorhodopsin (HR) (43-45).

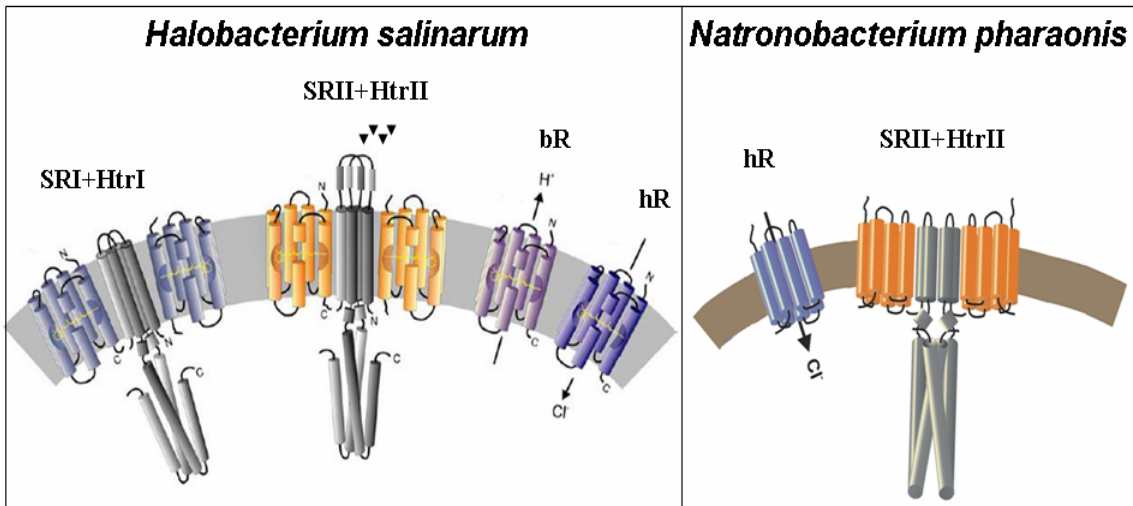


Figure 1-3. Archaeal rhodopsins. In cell membranes of archaea, there are four types of retinylidene photoreceptors. *H. salinarum* contains sensory rhodopsin I (SRI) and sensory rhodopsin II (SRII), which together with their bound transducers HtrI and HtrII, mediate phototactic and chemotactic responses. The ion pumps, bacteriorhodopsin (bR) and halorhodopsin (hR) transfer a proton or a chloride pump, respectively (left panel). *N. pharaonis* only contains halorhodopsin (hR) and sensory rhodopsin II (SRII) with its transducer II (right panel).

*H. salinarum* possesses four types of rhodopsins (46-48), while only sensory rhodopsin II and halorhodopsin are found in *Natronomonas pharaonis* (Figure 1-3) (49,50). The functions of the four archaeal rhodopsins are well characterized. These archaeal rhodopsins share a common design of seven

## INTRODUCTION

---

transmembrane helices which form a binding pocket for the covalently attached retinal-chromophore. Retinal is bound to a conserved lysine residue via a protonated Schiff base (sb) (51-53). In case of mammalian rhodopsin, this conformational change occurs from the 11-*cis* ground state to an all-*trans* excited state (54,55). Unlike eubacterial rhodopsin, the archaeobacterial rhodopsins have all-*trans* conformation in ground state that undergoes an isomerization to a 13-*cis* state after photon absorption. In addition, the chromophore does not dissociate from the protein after the absorption of a photon, but thermally relaxes in a cyclic reaction to an all-*trans* ground state.

Bacteriorhodopsin (BR) was first discovered (56,57) in *H.salinarum*. BR ( $\lambda_{\max}$  568 nm) and halorhodopsin (HR) ( $\lambda_{\max}$  576 nm) are light-driven ion pumps for protons and chloride, respectively. Accordingly, bacteriorhodopsin (BR) and halorhodopsin (HR), are expressed under low oxygen pressure and nutrient limitation. This condition is suboptimal for growth and respiration of *H. salinarum*. Therefore, on exposure to sun light, HR and BR hyperpolarize the membrane to generate a positive outside membrane potential, thereby producing inwardly electrochemical gradient that is used for generation of ATP through proton-motive force (51,58). HR further contributes to pH homeostasis by hyperpolarizing the membrane by chloride ion uptake rather than proton release, thereby providing an electrical potential for net proton uptake, which is especially important in alkaline conditions(51,58).

Sensory rhodopsin I (SRI) and Sensory rhodopsin II (SRII) are phototaxis receptors controlling the cell's swimming behaviour in response to changes in light intensity and color. The interplay of these two receptors guides the bacteria towards optimal light environments. SRI ( $\lambda_{\max}$  587nm), the first phototaxis receptor discovered, directs the movement of the bacteria towards orange light, which is also covering the absorption of the ion pumps. In the presence of harmful UV radiation, a photophobic response is induced by a two photon absorption (33). The first excitation of SRI with a photon of  $\lambda > 500$  nm triggers positive phototaxis: the attractant response. A second photon can be absorbed by a long-lived photointermediate ( $\lambda_{\max}$  373nm), thereby activating the photophobic response of the bacteria: negative phototaxis. The second phototaxis receptor, sensory rhodopsin II (or phoborhodopsin), has an action

## INTRODUCTION

spectrum with absorption maximum at 487 nm and enables the bacteria to avoid photo-oxidative stress under conditions of blue light in the presence of oxygen.

### 1.4. Halobacterial transducers and chemoreceptors

Sensory rhodopsins (SRs) exist as complexes with their cognate integral membrane Halobacterial transducers (Htrs). SRI forms a signaling complex firmly with HtrI, while SRII forms one with HtrII. In addition to two Htr's, 16 other transducer proteins that resemble their eubacterial relatives have been identified through biochemical experiments and sequence analysis of the *H. salinarum* genome (59-61).

HsHtrII	1	MSGSL VARIRGSYGT KLTLALVVVV VLSVGVGTFV YQOTTQLEF	SVRAILTQSA PARASHLAW LQARQDQL	
NpHtrII	1	MSLNVSRLLL PSRVRHSYTG KMGAVFIIVG ALTVLFGAIA YGEVTAATAA	.....	
EcTar	1	MINRI RVVTLVWVL GVFALLQLIS GSLFFSSLHN	SKSIVVSNQ LREYDELTS YNMLLQRI	
HsHtrII	76	AARRPVLAK METAI RYLE GLAADEKPE GRFAEIVYR TQTTIITASS	ATAFQVWPR EQAPATAP PFAATSLVV	
NpHtrII	50	.....	.....	
EcTar	66	ALRGAVRMM MDARMDQWA RVLLLEARK FLAQAAYK KIKSMAPLPA	MVATRRATPE RYKQVYALP ELIDITRYKH	
HsHtrII	156	VAAPFVPAA EPVVLVLP IPNTEKALI VMVMVLYR EPGQVAAS	FVVVARGSY VSRPELQVRL VGHGSRLL	
NpHtrII	50	.....	.....	
EcTar	146	TSVFA...P TQMDQAME REAQALISE KLVREIVT	.....	
HsHtrII	236	NSRTQPAVI TANGVTAAE PVDCAPVVL VRAP...HDR	AFALGDFVAS SLVGLVLITI VSLSLIGTV GSTTIVTALRQ	
NpHtrII	50	.....	TGD AAAVQEAAVS AILGLIILLG INLGLVAATL GGDTAASLST	
EcTar	182	.....	D NADDYRFAQH QLAVIALVVV LILLVAVYGI RRMLLPLAK	
HsHtrII	313	FSRRADEMAA GDLDDIDTS RNDEFGTLAE SFRSMRDSLS	ESLTDARAT ARAEDAREDA EQQRADAEA REDAEARKD	
NpHtrII	93	LAAKASRMGD GDLVLETR REDEIGDLYA AFDEMRSVR	TSLEDARNAR .....EDA EQAQKRA.....	
EcTar	223	IIAHIREIAG GNLANVLTID GRSEMGDLAQ SVSHMQRSLT	DTV.....	
HsHtrII	393	AQETARALEA AAADYEALT AVADGDLTRR VDASRDHDM	ARIGHALNDM LDDIETSVAA ATAFSDHVS DAQRVEADAG	
NpHtrII	153	.EEINTELQA EAEKFEVMD RCADGDFQR LDAETDNEAM	QSEGSFNEM MDGIEALVGR IERFADAVSE DAEAVRANAE	
EcTar	266	.....	.....	
HsHtrII	473	DAIDAGTDVS TAVDEISDGA TEQDRLHEV AGEVDDLAS	AEEVAETVAS LADTAGQAAS AVDDGRQATE DAVETMDVA	
NpHtrII	232	SVMEASEDVN RAVQNISDAA GDQETVQQI ALEMDDVSAT	TEEVAASADD IAKTARQAAE TGEAGRETAE TAITEMNEVE	
EcTar	266	.....	THVR EGSDAIYAGT REIAAGNTDL SSRTEQQASA	
HsHtrII	553	DDAEAAAAM DALDSEMADI GEIVDVIADI ADQTNMLALN	ASIEAARTGA DGDGFVAVD EVKTLAEESR DAAEDIESRL	
NpHtrII	312	SRTEQAVASM EELNEDVREI GEVSEMIADI AEQTNILALN	ASIEAARADG NSEGFVAVD EVKALAEETK AATEEIDDLI	
EcTar	340	KVVGVVVKTM HEIADSSKKI ADIISVIDGI AFQTNILALN	AAVEAARAGE QGRGFVAVG EVRNLASRSA QAAKEIKALI	
HsHtrII	633	LALQQQVSDV ADEMRSDDT VSDGRATVGD AATALDDVVS	FVADTDTAAG QIRAAADRQA HAASRVASAV DEVAGISQET	
NpHtrII	392	GTVDRTQTT VDDIRETSDQ VSEGVETVED TVDALERIVD	SVERTNDGIQ EINQSTDAQA DAAQKATTMV EDMAATSEQT	
EcTar	420	EDSVSRVDTG SVLVEAGET MNIVNAVTR VTDIMGEIAS	ASDEQSRGID QVALAVSEMD RVTQQNASLV QESAAAAAAL	
HsHtrII	713	AAQATAVADS AATQDTLSS VDDAAADLAD RAAALDDLLA	EFDAHDDTEP EDY	765
NpHtrII	472	ASDAETAET TETQAEVKE VFDLIDGLSE QADSLSETLS	RTDT.EEASA ADLDDQPTLA AGDD	534
EcTar	500	EEQASRLTQA VSAFRLAASP LTNKPQTPSR PASEQPPAQP	RLRIAEQDPN WETF	553

Transmembrane

Ligand Binding

HAMP

Signalling/Methylation

Chemoreceptor corresponding domain



## INTRODUCTION

---

Figure 1-4. Comparison of amino sequence alignment and homology of selected bacterial and archaeal transducer proteins HsHtrII, NpHtrII and *E.coli* Tar chemoreceptor. Transmembrane (yellow), ligand binding domain (blue), HAMP domains (green) and signaling/methylation domain (light grey) are marked by functional chemoreceptor corresponding domain.

Sequence alignments have revealed that the primary structural feature of *E.coli* Tar chemoreceptor is similar to other Halobacterial transducer proteins. (Figure 1-4). *E.coli* Tar chemoreceptor can be divided into five functional modules: ligand binding domain; transmembrane domain; HAMP domain; methylation domain and signaling domain (62). Compared to the primary structure of NpHtrII, *E.coli* Tar chemoreceptor and HsHtrII have a relatively large periplasmic domain. Remarkably, HsHtrII has a sequence of approximately 200 amino acids in its extracellular domain, which might act as the chemosensory domain for the flagella motor in their environment. The observation that HsSRII-HsHtrII displays a dual functionality is important with respect to a common mechanism of transmembrane signaling in photo- and chemotaxis. Hou S.B. *et al* (63) reported HsHtr II as a serine chemoreceptor. Nevertheless, the function of the ligand binding domain has yet to be determined at the molecular level. Likewise the cytoplasmic domains of Tar chemoreceptors that have high sequence homologies with the HtrIIs display typical behavior of chemotaxis. The cytoplasmic domain consists of HAMP domain, methylation domain and signaling domain. All transducers commonly share a linker domain (64,65) which plays an important role in signal uptake and propagation. Interestingly, a structural linker element between a sensor and a transmitter module is widely found in histidine kinases, adenylyl cyclases, methyl-accepting proteins and phosphatases, Therefore, these linkers were named HAMP domain (66). These domains are widely distributed through the three kingdoms of life and connect extracellular sensors with intracellular signaling domains in over 7500 proteins. This diversity in the context of function and environment implies common principles of signal relay. It is suggested that these HAMP domains possess roles of regulating the phosphorylation or methylation of homodimeric receptors by transmitting the conformational changes in periplasmic ligand binding domains to cytoplasmic signaling kinase

## INTRODUCTION

and methyl-acceptor domains (67). The recent solution structure of an archeal HAMP domain demonstrates that it adopts a homodimeric four-helical parallel coiled-coiled conformation (67,68). The following methylation domains contain four or more Glu residues that are substrates for Che R and Che B modification (36,59). The signaling domains have the highly conserved cytoplasmic tip for interaction with Che A and Che W.

### 1.5. NpSRII-NpHtrII interaction

The first structural information was obtained with NpSRII alone(69-72), which is an adequate model system for the *H.salinarum* receptor HsSRII. Subsequently structural information was obtained with the receptor-transducer complex using a shortened transducer NpHtrII [1-114] (Figure 1-5) (61).

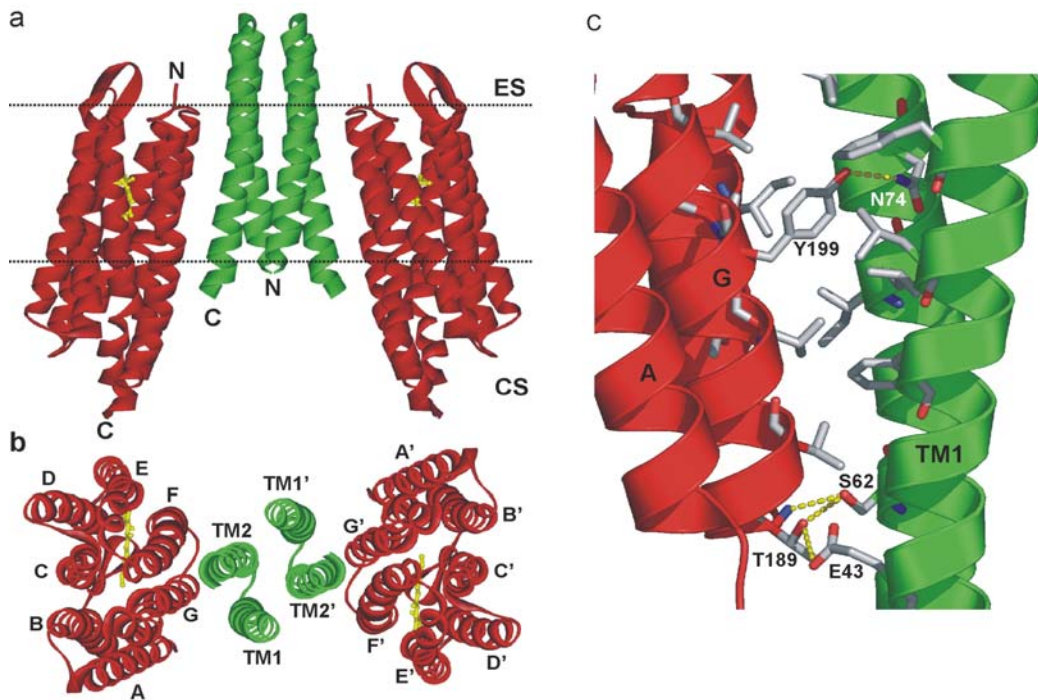


Figure 1-5. The crystal structure of the NpSRII - NpHtrII complex structure. NpSRII helices are shown in red, NpHtrII helices in green. (a) Side view and (b) upper view of the complex. CS, cytoplasmic side; ES, extracellular side. (c) Interface between receptor ( $\alpha$ -helices in red) and transducer ( $\alpha$ -helices in green) showing hydrogen bonds and van der Waals contacts.



## INTRODUCTION

---

Residues involved in hydrogen bonds (yellow dots) are labelled. This figure is taken from Johann P. Klare *et al.* (73,74).

A small fragment of NpHtrII was chosen because of technical difficulties in crystallization of the intact complex. In previous experiments, it was shown that NpHtrII [1-114] was tightly bound to NpSRII ( $K_D=200$  nM) (75). Figure 1-5a and 1-5b show that NpSRII bears retinal as the chromophore containing seven transmembrane helix and NpHtrII contain two transmembrane (TM) helices, which exist as homodimer. Each transducer molecule is bound to a receptor molecule thereby forming the signaling complex with stoichiometry of 2:2. This stoichiometry was also reported for the co-expression of SRI-HtrII complex in halobacterial membranes, indicating that this arrangement might be a general feature of archaeal photo-receptor - transducer complexes (76). The main interactions in the complex are van der Waals contacts closely between TM1-helix G, TM2-helix F, TM1-TM2' and TM1'-TM2' as shown in Figure 1-3b. Notably, only three hydrogen bonds (Tyr-199<sub>NpSRII</sub> to Asn-74<sub>NpHtrII</sub>, Thr-189<sub>NpSRII</sub> to Ser-62<sub>NpHtrII</sub> and Thr-189<sub>NpSRII</sub> to Glu-43<sub>NpHtrII</sub>) are formed. The importance of Tyr199 has already been deduced from the X-ray structure of NpSRII (71,77). It should be noted that Tyr-199 /Asn-74 hydrogen bond is not necessary for the complex formation (78) although it might be important for the receptor transducer signal transfer (79).

### 1.6. Photocycle

The mechanism of signal transfer in phototaxis was first elucidated by analysis of the photocycle (47). The photocycle is initiated by photoisomerization of retinal. On excitation by light, the retinal chromophore undergoes an all-trans  $\rightarrow$ 13-cis isomerization of a double bond of sensory rhodopsin proteins (51). After photo-excitation the protein undergoes several intermediate states that can be spectroscopically distinguished and analyzed by their different absorption maxima. The resulting sequence of intermediates has been denoted in analogue to the BR nomenclature, as K, L, M, N and O states inducing a circular chain of photochemical and structural events (37,80).

## INTRODUCTION

---

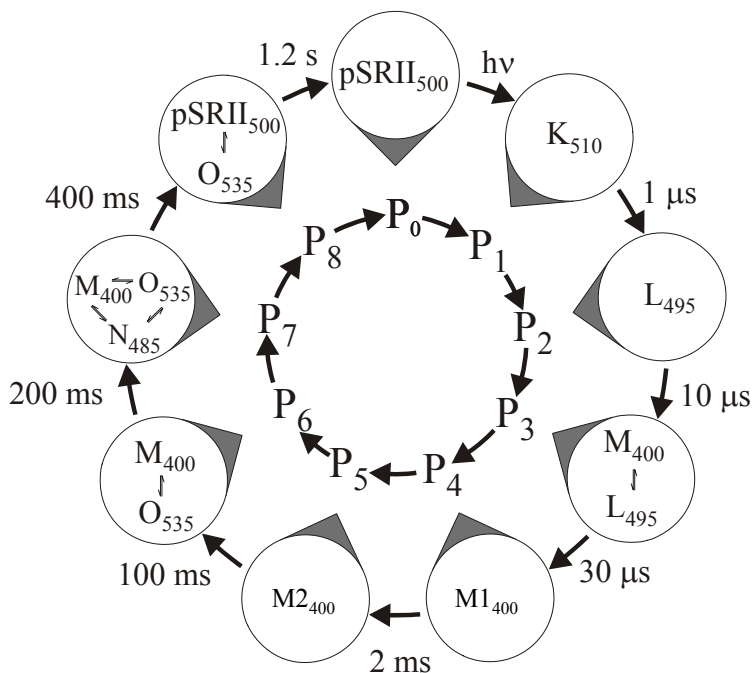


Figure 1-6. Model of the photocycle of the photophobic receptor SRII from *N. pharaonis* based on a sequence of irreversible reactions. Absorbance maxima of the spectral intermediates K, L, M, N and O states. This figure is taken from Igor chizov *et al* (47).

This photocycle was studied in detail for the NpSRII receptor (Figure 1-4). In the case of *NpSRII*, the photocycle can be described as follows: The absorption of a single photon leads to a 13-cis isomerisation of the chromophore (*NpSRII*→K). After approximately one microsecond, the protein undergoes conformational changes (K→L). This change alters the affinity of several residues toward protons leading to the donation of a proton from the Schiff base to Asp75 in the extra-cellular proton channel domain of the protein. At this point a proton is released into the medium from the extracellular site (L→M). After that, the cytoplasmic proton-channel opens and the Schiff base becomes re-protonated (M→N→O) followed by the retinal re-isomerization and the relaxation of protein to the ground state (O→*NpSRII*) (81-83). One of the intermediates, referred to as M state, is characterized by retinal isomerized from all trans to 13-cis conformation which leads to deprotonated Schiff base and conformational changes in the protein. An important result of

the photocycle experiments is that the optical silent transition state from M1 to M2 has a time constant of 2 ms.

### 1.7. The molecular Mechanisms of signal transfer

The results of the photocycle provide further information about the binding of the transducer to the receptor. The interaction of the receptor in the M state with the transducer results in the transfer of the conformational changes from the receptor to the transducer molecule (84,85). According to EPR analysis (86-88), an outward movement of helix F and the TM2 rotation is observed in the M1→M2 state with rate constant of about 2 ms. Therefore, the M-state and the following intermediates would be the signaling state. As previously reported the photocycle kinetics(87,89) have shown that NpSRII with NpHtrII does not change the photocycle kinetics. Contrary to these results in the case of *H.salinarum*, the binding of the HsHtrs with HsSRs change the turnover rate of the photocycle. Spudich and coworkers (90) have demonstrated that the binding of the HsHtrI with HsSRI increases the turnover rate of M-intermediate. In the latter photocycle experiment, J. Sasaki and Spudich (91) showed that the HsSRII-HsHtrII complex accelerates O-decay and M-decay than HsSRII in the presence of HsHtrII. They suggest that the transducer produces changes in the hydrogen network around Asp 73, thereby accelerating proton transfer reactions. The binding of HsHtrI to HsSRI has large kinetic effects on the HsSRI photocycle(92), a result which provided initial evidence for the formation of a functional complex. Recognition specificity and signal relay in the SRI–HtrI complex resides largely or entirely in the membrane embedded domain. This is because swapping of the cytoplasmic domain of the transducer (HtrI residue 60) with the corresponding portion of HsHtrII does not impair attractant and repellent phototaxis signaling by SRI. Therefore, the residues in the HtrI TM domain (residues 1–53) and the beginning part of HAMP (residues 54–60) appear to be sufficient for SRI–HtrI signal transfer (92). This complex altered the rate of S<sub>373</sub>(M) formation which was interpreted as a modulation of the electrostatic interactions of the protonated Schiff base and an optimisation of the photocycle by the transducer.

## INTRODUCTION

Over the past years, structural rearrangements upon light activation in the F and G helices and TM2 have been elucidated by time-resolved FTIR (84,93-96), EPR(86,87) and X-ray diffraction(93). Time-resolved FTIR (84,93-96) demonstrated that the signaling state occurs in the M1-M2 transition, which is mainly characterized by protein conformational changes (amide bond changes), rather than changes of the chromophore.

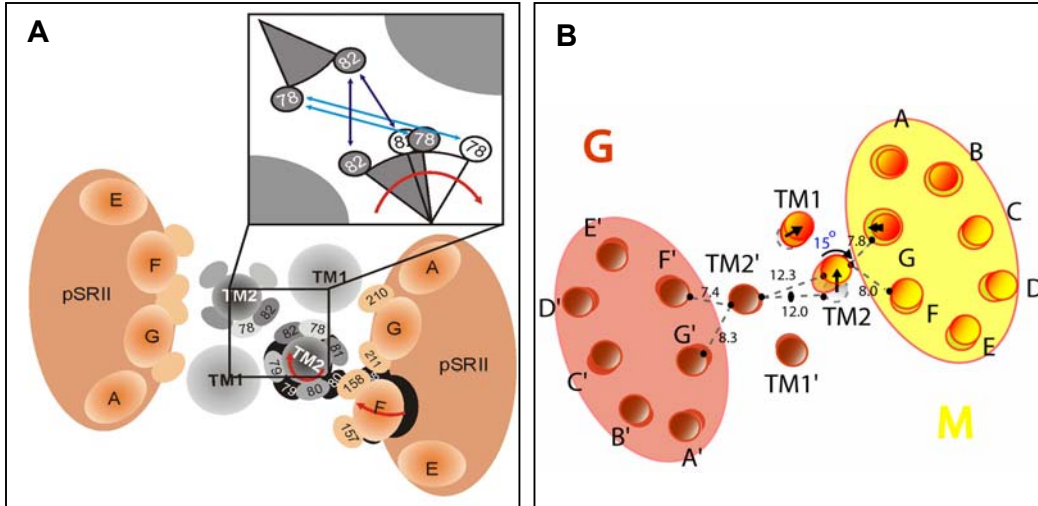


Figure 1-7. Schematic pictures of light-induced conformational changes within the transmembrane region of the 2:2 NpSRII-NpHtrII complex viewed from the cytoplasmic surface. (A) EPR-spectroscopy of M-state conformation. (B) X-ray crystallography of late M-states. Figure A is taken from Wegener.A.A *et al.*(87). Figure B is taken from Moukhametzianov. R *et al.*, (93).

Figure 1-7 illustrates a signal relay pathway based on the SRII-HtrII complex structure. A topological model for the complex was derived earlier using data from electron paramagnetic resonance (EPR) experiments. Wegener A.A *et al.*(87) and J.P. Klare *et al.* (83) demonstrated that light activated NpSRII induce outward tilting of the helix F and a 20-30° rotation of TM2 of NpHtrII during the early stages of photocycle. The reformation of F-helix original state to recovery of TM2 position is delayed by approximately 200 ms (84). It is correlated with the early steps of the photocycle and sustained until the O-intermediate decays to the initial state (87,88).

## INTRODUCTION

The activation of NpSRII-NpHtrII structure derived from EPR data was compared to that obtained by X-ray crystallography (96). A crystal structure of light activated sensory rhodopsin II- transducer II complex revealed that (i) receptor activation by light leads to a relative shift between helices F and G and (ii) the transducer responds to the activation of the receptor by a clockwise rotation of about  $15^\circ$  of TM 2. This rotation is accompanied by a slight (0.9 Å) piston-like movement. Spudich *et al*(58) proposed that F-helix tilting occurred by the disruption of the salt bridge between the protonated Schiff base of G-helix and the negatively charged carboxyl group Asp-75 in the C-helix during the signal transfer from NpSRII to NpHtrII. Both EPR and X-ray data indicates rotated TM2 to represent the activated state of the transducer.

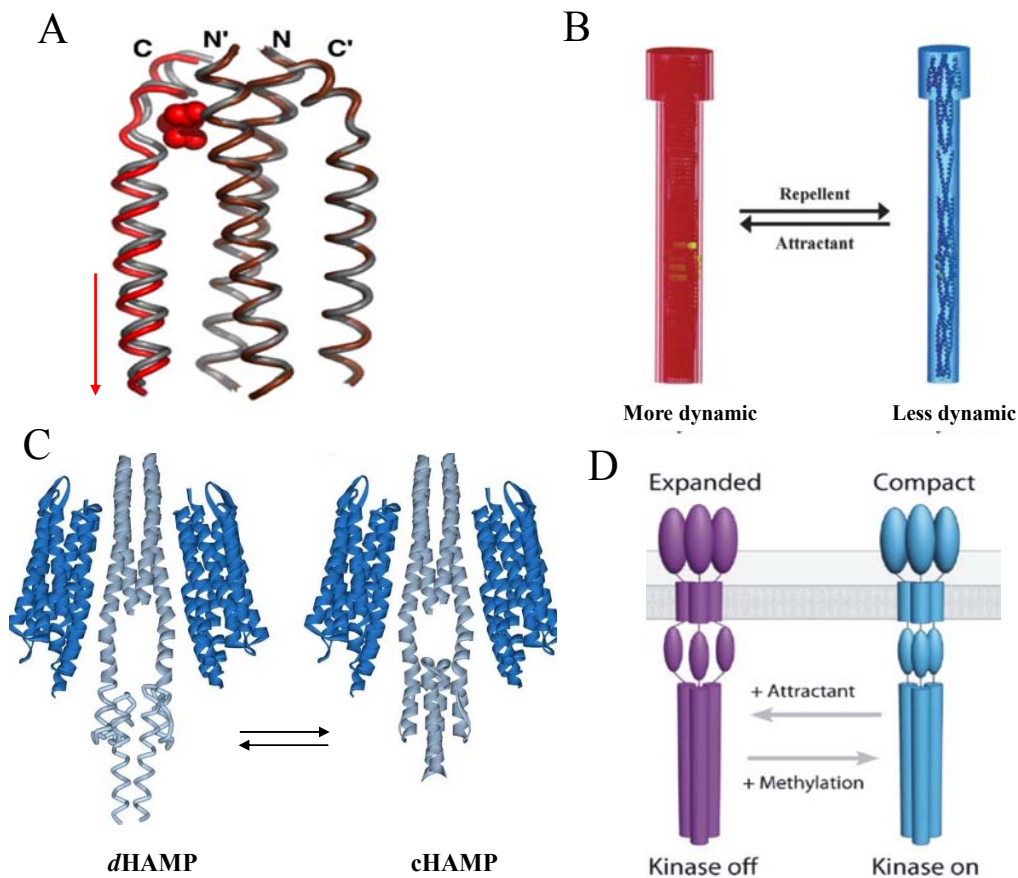


Figure 1-9. Models for transmembrane signal transfer. (A) The 'swinging-piston model' of Tar chemoreceptor. The periplasmic regions of the four helices. Gray and red helices represent

## INTRODUCTION

---

the apo and aspartate occupied structure, respectively. This figure was adopted from Chervitz, S. A. *et al*, (97,98). (B) The 'Frozen dynamic model' for Tsr signaling. Repellent and attractant binding induced less dynamic (blue) and more dynamic properties (red), respectively. This figure was adopted from Kim, S. H. *et al*,(99). (C) Two states of HAMP in equilibrium between dynamic and compact conformations This figure was adapted from Doebber, M. *et al*, (100). (D) The 'expanded and compact model' of the trimer of dimmer Tar chemoreceptor. The expanded HAMP (magenta) corresponding to the kinase off state and the compact HAMP conformation (cyan) corresponding to the kinase off state This figure was adapted from Khursigara, C. M.*et al*,(101).

Several models for transmembrane signal transfer have been proposed to explain conformational changes of activated chemoreceptors and phototransducers. As shown in Figure 1-9A, the first structural Tar chemoreceptor from *E.coli* has shown the ligand-induced displacement of the signaling helix, the so-called "swinging-piston model" (97,98). The distance difference analysis of the aspartate receptor revealed that one subunit of sensory domain is essentially unaltered by ligand binding. This static subunit has the same backbone conformation in the apo and the aspartate-occupied crystal structures of the periplasmic domain (98,102). A displacement of approximately 1.6 Å into the direction of the cytoplasm, in combination with a tilt of the helix of about 5° can be deconvoluted into a "piston" component and a "swing" component. A second model 'Frozen dynamic model' was proposed by Kim and coworkers (Figure 1-9B), where the transmembrane signaling helix ultimately enters the whole cytoplasmic domain, which leads to the rigidity of  $\alpha$ -helix in turn increasing phosphorylation activity of the histidine kinase (CheA) (99). In this model, the activation of the receptor domain decreases the dynamics of the cytoplasmic domain (repellent signaling state). The adaptation process was also explained in the frame of this model, as methylation of Glu residues would modify the dynamics of Tsr chemoreceptor (attractant signaling state). This frozen dynamic dynamic model supports the two state equilibrium of HAMP domain from NpSRII-NpHtrII complex which is proposed by Doebber *et al* (100). The HAMP domain is found to be engaged in a two state equilibrium between a highly dynamic (*d*HAMP) and a more compact (*c*HAMP) conformation depending on salt concentration, pH and temperature. The presence of the *c*HAMP conformation may results from

## INTRODUCTION

---

increasing phosphorylation activity of the histidine kinase (CheA), which might increase the amount of folded protein in equilibrium with the dHAMP conformation. Likewise, Cezar *et al* (101) observed the full length serine chemoreceptor with distinct states in which the HAMP domains are present either with compact or expanded conformations. Also, the chemoreceptor is distinct in terms of how ligand binding and methylation modulate the conformation equilibrium. Binding of the attractant serine to Tsr hexamer initiates a conformational change of transmembrane helix which then propagates to HAMP domain to favor the expanded conformation. Based on the known effects of serine binding to reduce the activity of Che A kinase, it was proposed that the expanded HAMP domain corresponds to the “kinase off” state. Conversely, an increase in chemoreceptor methylation results in the preference of the compact HAMP conformation, which corresponds to the “kinase on” state. This implies that ligand-induced helix movements provide a plausible mechanism for the dynamic range of the HsHtrII-HsSRII complex during phototaxis.

Although there have been detailed descriptions of the mechanism for signal transduction of transmembrane receptors, yet the most fundamental questions on the enteric response in chemoreceptors are still unanswered, such as ;

- (i) How the signals from various receptors sensing different ligands in a chemically diverse environment are integrated to compute an adequate output signal is not known well.
- (ii) How signal is transferred to Histidine kinase remains still unclear.
- (iii) Upon transducer activation, signal amplification and integration have not yet observed.

### 1.8. Objectives of this work

The elucidation of the distribution, dynamics, and function of membrane proteins is essential for the understanding of the phototaxis and chemotaxis transduction system of *H.salinarum*. The aim of the present study is to characterize the molecular function how membrane proximal signaling events are triggered by extracellular and/or membrane associated ligand binding. The model system employed in this study consists of the photoreceptor sensory rhodopsin II (HsSRII) and halobacterial transducer II (HsHtrII).

In order to study the biochemical and biophysical properties of HsHtrII and HsSRII protein, laser flash photolysis, ITC, analytical size chromatography and blue native gel were performed. In order to analyze the photocycle of HsSRII and in complex with HsHtrII, laser flash photolysis was performed. Isothermal titration calorimetry (ITC) was used to determine the dissociation constant ( $K_D$ ) of HsHtrII–HsSRII and HsHtrII-Ser interactions based on the enthalpy and the stoichiometry of the binding interaction. Furthermore, oligomerization and complexation of HsHtrII with HsSRII was studied by analytical size chromatography and blue native gel.

Another aim of the study was to elucidate the molecular mechanism of HsHtrII as a serine chemosensor by studying their dynamics and conformational changes. The investigation of conformational changes has focused not only the HsHtrII functions for serine binding, but also on identifying folding intermediate such as molten globule like protein. Molten globule state has been suggested to be involved in many important physiological processes, including signal transduction and interactions with molecules. 1-Anilinonaphthalene-8-Sulfonic Acid (ANS) and intrinsic tryptophan fluorescence study allows understanding the role of chemoreceptor by pointing to its interaction with serine, and it can also identify molten globule like protein. Because the molten globule conformation is characterized by maintenance of or increase in secondary structure, the structural integrity of HsHtrII constructs was also studied in the various ranges of temperature and different salt conditions by CD measurements.



## **2. MATERIALS AND METHODS**

## 2.1. Chemicals

The chemicals used and the corresponding companies are presented.

Chemical	Supplier
Acetic acid	Merck (Darmstadt, DE)
Acetonitrile	JT Baker (Deventer, NL)
1-Anilinonaphthalene-8-Sulfonic Acid	Cayman (Tallinn NL)
Acrylamid/Bisacrylamide (37.5:1, 30 % w/v)	Applichem (Darmstadt, DE)
Arginine	Roth (Karlsruhe, DE)
Aspartate	Roth (Karlsruhe, DE)
Ammonium persulfate (APS)	Merck (Darmstadt, DE)
Ampicillin (Amp)	Serva (Heidelberg, DE)
Ammonium chloride	Baker (Griesheim, DE)
Bromphenol blue	Serva (Heidelberg, DE)
Bovine serum albumine (BSA)	Sigma
Bis-Tris	Roth (Karlsruhe, DE)
Chloroform	JT Baker (Deventer, NL)
Chloramphenicol (Cam)	Merck (Darmstadt, DE)
Coomassie Brilliant Blue G250+R250	Serva (Heidelberg, DE)
N-Dodecyl- $\beta$ -D-maltoside (DDM)	Calbiochem
Dimethylsulfoxide(DMSO)	Fluka
D <sub>2</sub> O	Roth (Karlsruhe, DE)
Dithiothreitol (DTT)	Gerbu (Gaiberg, DE)
Ethylenediaminetetraacetic acid (EDTA)	Gerbu (Gaiberg, DE)
Ethanethiol	Fluka
Ethanol	JT Baker (Deventer, NL)
Ethidium bromide	Sigma
GdmHCl	Calbiochem(Darmstadt, DE)
Hydrochloric acid	JT Baker (Deventer, NL)
Imidazol	Gerbu (Gaiberg, DE)
Isopropyl- $\beta$ -D-thiogalactopyranoside (IPTG)	Applichem (Gaiberg, DE)
Kanamycin	Boehringer (Mannheim,DE)
Methanol	Applichem (Darmstadt, DE)
$\beta$ -Mercaptoethanol	Serva (Heidelberg, DE)

## MATERIALS AND METHODS

---

Phenylmethylsulfonylfluoride (PMSF)	Sigma
Potassium dihydrogenphosphate	JT Baker (Deventer, NL)
2-Propanol	JT Baker (Deventer, NL)
Serine	Roth (Karlsruhe, DE)
Sodium chloride	Fluka
Sodium dihydrogenphosphate,	JT Baker (Deventer, NL)
Sodium dodecylsulphate (SDS)	Gerbu (Gaiberg, DE)
Sodium hydroxide	JT Baker (Deventer, NL)
<i>N,N,N',N'</i> -tetramethylethylenediamin (TEMED)	Roth (Karlsruhe, DE)
Trihydroxymethylaminomethane (TRIS)	Roth (Karlsruhe, DE)
Triton X-100	Serva (Heidelberg, DE)
Urea	JT Baker (Deventer, NL)
Yeast extract, peptone 140	Gibco (Eggenstein, DE)

### 2.1.1. Reagent Kits

QIAprep Spin Miniprep Kit	Qiagen
QIAquick Gel Extraction Kit	Qiagen
Perfect 1kb-DNA standard	Invitrogen (Karlsruhe)
Wide Range, SDS7 protein marker	Sigma (Deisenhofen)

### 2.1.2. General instruments

Instruments	Supplier
Avanti J-20 XP centrifuge with JLA 8.1 000 rotor	Beckman Coulter, Palo Alto, CA, USA)
Biorad PE 9700 thermocycler	Applied Biosystems (Weiterstadt, DE)
Cell incubator	New Brunswick (Nürtingen, Germany))
Centrifuge Avanti J20-XP	Beckman Coulter (Palo Alto, USA)
Centrifuge Optima L-70K Ultracentrifuge	Beckman Coulter (Palo Alto, USA)
GenePulser for electroporation	Bio-Rad (Munich, Germany)

## MATERIALS AND METHODS

Deionized water apparatus	Millipore (Eschborn, DE)
Gel-electrophoresis system	Bio-Rad (München, DE)
High pressure liquid chromatography (HPLC)	Waters (Eschborn, DE)
HPLC-ESI-MS	Agilent, Finnigan
Isothermal titration calorimeter	MicroCal (Northampton, USA)
Microfluidizer	Microfluidics (Newton, MA, USA)
PH-meter 761	Calimatic Knick (Berlin, DE)
SDS-PAGE Mini-Protean II system	Bio-Rad (München, DE)
Shaker	Infors (Bottmingen, CH)
Spex Fluoromax-3 Spectrofluorometer	Jobin Yvon Horiba Group (NJ, USA)
Ultrasonic cell disruptor (SONIFIER)	Branson (Danbury, CT, USA)
UV/Visible Spectrometer DU 640	Beckman Coulter (Palo Alto, USA)
Jasco J-815 spectropolarimeter	JASCO Inc(Easton, MD,USA)

## 2.2. Cell Culture Techniques

### 2.2.1. Plasmids and bacterial strains

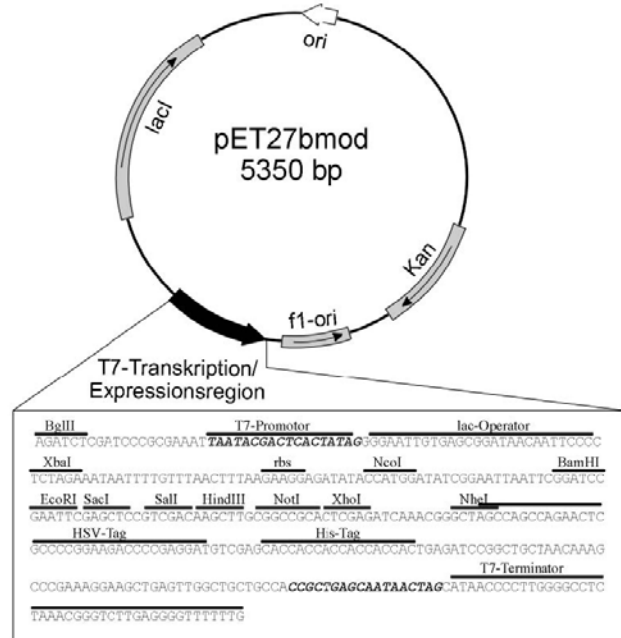
#### Plasmids

Plasmid Name	Insert	Resistance
pET27b(+)-HsSRll	<i>Hssopll</i>	Kan
pET27bmod-HsSRll	<i>Hssopll</i>	Kan
pET27bmod-HsHtrll[1-765]	<i>Hshtrll</i> [1-765]	Kan
pET27bmod _HsHtrll(1-765ΔLBD)	<i>Hshtrll</i> (1-765ΔLBD)	Kan
pET27bmod _HsHtrll[1-398]	<i>Hshtrll</i> [1-398]	Kan
pET27bmod _HsHtrll(1-398ΔLBD)	<i>Hshtrll</i> (1-765ΔLBD)	Kan
pET27bmod _HsHtrll-LBD	<i>Hshtrll</i> (42-285)	Kan
pET27bmod _HsHtrll-HAMP	<i>Hshtrll</i> (303-465)	Kan
pET27b(+)-Tar	<i>Tar</i> (1-553)	Kan
pET27b(+)-Tar-LBD	<i>Tar</i> (1-265)	Amp

Empty pET27b (+) vector was obtained from Novagen (Abingdon). pET27(+) is a plasmid containing the C-terminal six histidine residues and pET27(+) bmod containing the C-terminal seven histidine residues modified

## MATERIALS AND METHODS

by Klostermeier *et al* for use in Nickel chromatography for protein purification(103). The pET27bmod-HsHtrII [1-765] was gifts from Dr. Nadine mennes. The pRS constructs were kindly provided by Dr. Ralf Seidel.



Empty pET 27bmod plasmid

The overexpression of proteins in *E.coli* is under control of a T7 promoter that precedes the lac-operator sequence which is controlled by IPTG. Addition of IPTG activates the T7 polymerase transcription and induces the expression of desired protein.

### Bacterial strains

### Genotypes

XL1 Blue (Stratagene)	<i>recA1</i> , <i>endA1</i> , <i>gyrA96</i> , <i>thi-1</i> , <i>hsdR17</i> , <i>supE44</i> , <i>relA1</i> , <i>lac</i> [ <i>F'</i> , <i>proAB</i> , <i>lacI<sup>q</sup>ZΔM15</i> , <i>Tn10</i> ( <i>Tet<sup>r</sup></i> )]
BL21 (Novagen)	<i>F<sup>-</sup></i> , <i>ompT</i> , <i>lon</i> , <i>hsdS</i> ( <i>r<sub>B</sub><sup>-</sup></i> , <i>m<sub>B</sub><sup>-</sup></i> ), <i>dcm</i> , <i>gal</i> ,
BL21(DE3) $\lambda$ (DE3) (Novagen)	<i>F<sup>-</sup></i> , <i>ompT</i> , <i>lon</i> , <i>hsdS</i> ( <i>r<sub>B</sub><sup>-</sup></i> , <i>m<sub>B</sub><sup>-</sup></i> ), <i>dcm</i> , <i>gal</i> (DE3)
BL21(DE3) Rosetta	<i>F<sup>-</sup></i> , <i>ompT</i> , <i>lon</i> , <i>hsdS</i> ( <i>r<sub>B</sub><sup>-</sup></i> , <i>m<sub>B</sub><sup>-</sup></i> ), <i>dcm</i> , <i>gal</i> , $\lambda$ (DE3),

(Novagen)

pRARE2 (Cam<sup>R</sup>)

### **2.2.2. Preparation of competent cells**

One liter of LB medium was inoculated with 1 mL of an overnight-grown culture of XL-1 blue competent cells. Cells possessing antibiotic resistance genes were grown in the presence of the corresponding antibiotics. The culture was incubated at 37° C on a shaker, until the OD<sub>600</sub> reached 0.5 (ca. 3 - 4 h). The culture was cooled on ice for 20 min, transferred to sterile centrifugation vessels and centrifuged for 10 min at 4°C at 2000 g. The supernatant was discarded. The bacterial cell pellet was gently resuspended in 5 mL of ice-cold sterile GYT (0.125 % (w/v) yeast extract, 0.25 % (w/v) tryptone, 10 % (v/v) glycerol) and recentrifuged as described above. Cell pellet were resuspended in 1 mL GYT, dispensed in 50 µl aliquots, shock frozen in liquid nitrogen and stored at -80° C.

### **2.2.3. Transformation by electroporation**

Fifty microliter of the competent cells were incubated with approximately 100 ng of DNA in a dry and previously chilled electro competent cuvette and then transformed using a transformation apparatus controlled at a voltage of 2.5 kV. The cells were then transferred to 1 ml of LB medium and were grown at 37°C for 1 hour. The cells were then centrifuged carefully discarding 900 µl supernatant. The bacteria were suspended with 100 µL of LB medium and plated on an agar selection medium containing the appropriate antibiotic.

### **2.2.4. Media**

#### **2-TY Medium**

16g/L Pepton-140, 10g/L yeast extract, 5g/NaCl, pH 7.2

#### **LB Medium**

10g/L Batotryptone, 5g/L yeast extract, 10g/NaCl, pH 7.4

## MATERIALS AND METHODS

---

### Minimal Medium

Na <sub>2</sub> HPO <sub>4</sub>	7.5 g	10 x SL4:	
K <sub>2</sub> HPO <sub>4</sub>	3 g	EDTA	0.5g
NaCl	0.5 g	FeSO <sub>4</sub> • 7H <sub>2</sub> O	0.2 g
MgSO <sub>4</sub> • 7H <sub>2</sub> O	0.25 g	SL6:	
CaCl <sub>2</sub> •2H <sub>2</sub> O	0.014 g	MnCl <sub>2</sub>	0.03 g
Glucose	10 g	ZnSO <sub>4</sub>	0.1 g
NH <sub>4</sub> Cl (or N15H <sub>4</sub> Cl)	1 g	H <sub>3</sub> BO <sub>3</sub>	0.3 g
Trace elements (see below)	10 ml	CuCl <sub>2</sub>	0.010 g
		Na <sub>2</sub> MoO <sub>4</sub>	0.025 g
Trace elements:		CoCl <sub>2</sub> •6H <sub>2</sub> O	0.2 g
10 x SL4 9 ml		NiCl <sub>2</sub>	0.020 g
SL6 10 ml		Na <sub>2</sub> MoO <sub>4</sub>	0.030 g
Add distilled water to 1L			

The media were sterilized at 120°C for 20 minutes. For the over-expression of proteins in *E. coli* the respective medium was supplemented with 50 µg/ml kanamycine

## 2.3. Molecular biological methods

### 2.3.1. Preparation PCR

The appropriate 5'- primers and 3'-primers were designed. The PCR reaction mixture was prepared in steps shown in Table 2.1. The mixture was incubated in Biorad PE 9700 thermocycler (Applied Biosystems) using PCR program as described in table 2.2. The following oligodeoxynucleotides were purchased from MWG Biolabs (Ebersberg, Germany).  $T_m$  (melting temperature) of primer can be calculated by following equation.

$$T_m = 4^\circ\text{C} \cdot \sum(n_G + n_C) + 2^\circ\text{C} \cdot \sum(n_A + n_T)$$

$$T_{m\text{Red}} = T_m - \left( 1^\circ\text{C} \cdot \frac{n_{\text{mismatch}}}{n_{\text{total}}} \right)$$

## MATERIALS AND METHODS

---

Table 2.1. Primer sequences

Name	Sequences( 5'→ 3')
T7 promotor -for	5'- TTA ATA CGA CTC ACT ATA GGG GAA-3'
T7 terminator-rev	5'- CTA GTT ATT GCT CAG CGG TGG C-3'
HsSRII-for	5'- AGATATAACCATGGCACTCACGAC-3'
HsSRII-rev	5'- CCGGACGGCGACGAATTCGC-3'
HsHtrII[1-765] - for	5'- GAGATATAACCATGGGGTCCGGATT-3'
HsHtrII[1-765] - rev	5'- TGCGAATTCTCGTAGTCTCCGGTTTCG-3'
HsHtrII[1-398] - for	5'- ATATAACCATGGGGTCCGGAT-3'
HsHtrII[1-398] - rev	5'- GATGAATTCTCGGGAGCCGTTTCTTGG-3'
HsHAMP(303-465) - for	5'- ATATAACCATGGGCTCGACCACG-3'
HsHAMP(303-465) - rev	5'- TCGAAGCCGACGCCGAATTCGCACCACCA-3'
HsLBD(42-285) - for	5'- GAGATATAACCATGGAACCTCGAAAC-3'
HsLBD(42-285) - rev	5'- ACGACCGCAAGCTTGAATTCGCA-3'
HsHtrII(Δ38-280) Linker1-for	5'- GCAGGTAACCGCCGCCGCGGACCGG-3'
HsHtrII(Δ38-280)Linker1- rev	5'- CCGGTCGCGGGCGGCGGCGTTAC-3'
HsHtrII(Δ38-280) Linker2-for	5'-CCGCCGCCGCGACCGGTGATGCCGCAGCCGTACAG-3'
HsHtrII(Δ38-280)Linker2- rev	5'-TGTACGGCTGCGGCATCACCGGTGGCGGCGGCG-3'
Tar (1-265) -for	5'- AGATATAACCATGGCACTCACGAC-3'
Tar (1-265) -rev	5'- AGATATAACCATGGCACTCACGAC-3'
Tar LBD(34-182) -for	5'- GGCAGTCTGTCCATGGCTTCCCTT-3'
Tar LBD(34-182) -rev	5'- GCAAATCGGGAATTCTCTGCGTTG-3'
Tar (1-553) - for	5-GGGAAACATTGAATTCAGCTTGCGGC-3
Tar (1-553) -rev	5'- AGATATAACCATGGCACTCACGAC-3'

### 2.3.2. Polymerase chain reaction (PCR)

Amplification of DNA fragments was carried out using High Fidelity Expand Polymerase from Roche (Mannheim) according to standard procedures. In brief, a 50 µL reaction mixture contained 1 – 10 ng of template DNA, 10 pM of forward and reverse primers, 100 µM of dNTP mixture, 2 – 4 units of High Fidelity Expand Polymerase mix from Roche (Mannheim) as well as the corresponding reaction buffer. The PCR-reaction was performed with a MJ



Research PTC-200. Firstly, a denaturation step was performed for 1 min at 96 °C, followed by annealing for 30 sec at 55 – 65 °C depending on primer length and GC content. The extension step occurred at 72 °C for 2 – 3 min, depending on the length of the template DNA fragment. In general, ca. 20 cycles were performed for amplification. Prior to further use, the salts in the reaction buffer were removed from the PCR reaction mixture using the Cycle-Pure Kit from PeQLab (Erlangen, GE).

### **2.3.3. Purification of PCR products by agarose gel electrophoresis**

DNA was separated by gel electrophoresis using gels with 0.7 % to 1 % agarose in TBE buffer (90 mM TrisHCl, 90 mM boric acid, 1 mM EDTA, 0.6 mg/l ethidium bromide, pH 8.9). Before separation, the samples were mixed with 3x sample loading buffer (TBE buffer, 10 % ficoll, 0.025 % bromphenol blue, 0.025 % xylencyanol). The desired DNA fragment was cut out of the agarose gel and extracted using the QIAquick gel extraction kit from Qiagen (Hilden, Germany).

### **2.3.4. DNA Restriction enzyme digestion**

Both vector and purified PCR product were digested by the appropriate restriction enzymes. Digestions of DNA fragments were performed as recommended by the manufacturer at 37°C for 2 h using restriction enzymes and buffers from New England Biolabs (Beverly) or Fermentas (St. Leon-Rot) and stopped by addition of DNA loading buffer. The digested fragments were separated using agarose gel electrophoresis, which was followed by isolation using the Gel Extraction Kit.

### **2.3.5. DNA Ligation**

For ligation, 1-10 pmol of linear plasmid DNA was mixed with a 10 fold molar excess of insert fragment. Ligation was performed in ligation buffer in a volume of 20 µl, using 5 units of T4 DNA ligase with T4 DNA ligase buffer (50

mM TrisHCl, 10 mM MgCl<sub>2</sub>, 1 mM ATP, 1 mM DTT, 5 % PEG 8 000, pH 7.6) in 20 µl for 3 h at 37°C (Roche Diagnostics, Mannheim, Germany). Subsequent the reaction mix was diluted with 3 volumes of sterile H<sub>2</sub>O.

### **2.3.6. Transformation by electroporation**

For transformation of plasmid DNA into *E.coli* cells, electroporation was performed (52). Seventy five microliter of electro-competent cells was mixed with 20 µl of diluted DNA ligation mix on ice in a cuvette for 2 minutes. The transformation was made by electroporation with a BioRad Gene Pulser apparatus (2 mm electrode gap, 800 Ω ohmic resistors, 1.5 kV voltages and 25 µF capacities). After an electrostatic discharge the mixtures were suspended in 0.5 ml antibiotic free LB medium and incubated for 1 h at 37 °C and then plated out on selective medium. Selection was carried out on agar plate containing 50 mg/l kanamycin.

### **2.3.7. Preparation of plasmid DNA**

Preparation of plasmid DNA was performed using a modified plasmid midi-prep-kit (Qiagen, Hilden, Germany). After cell lysis and centrifugation, the cleared supernatant was incubated with 10 µg/ml RNase A for one hour at 37 °C and subsequently purified using the provided anion exchange column. The purified plasmid DNA was additionally precipitated with ice-cold ethanol and washed with 70 % ethanol in water. Finally elute the plasmid DNA with 30-50 µL sterile water by centrifugation (10,000 rpm, 1 min).

### **2.3.8. DNA sequencing**

DNA sequencing was carried out according to180 using the BigDyeDesoxy terminator cycle sequencing kit (Applied Biosystems, Weiterstadt). A sequencing reaction mixture typically included 500 ng DNA, 4 µl terminator mix, 3.2 pmol sequencing primer in a volume of 10 µl. The sequencing PCR and DNA precipitation was carried out according to the protocols of manufacturer. Analysis of the sequencing products was performed on an ABI PRISM 3700 DNA Analyzer (Applied Biosystems, Langen).

## 2.4 Protein expression and purification methods

All buffers were prepared with reagent grade chemicals and distilled water that was subsequently treated with a Milli Q (Millipore, Bedford, MA) water purification system.

### 2.4.1. Protein expression

The proteins were expressed in *E. coli* BL21(DE3) *Rosetta* essentially as described (104,105). An overnight culture from a single colony from a LB agar plate was grown and diluted with fresh medium suspended with 50 mg/l ampicillin and 30 mg/l chloramphenicol. The cells were grown at 37°C with vigorous shaking until an  $OD_{600} = 0.6$ . Protein expression was induced using 1mM isopropyl- $\beta$ -D-thiogalactoside (IPTG) for 3 hours at 37°C. The cells were harvested by centrifugation for 15 minutes at 6000 rpm. Cells were harvested after 3 h, washed in approximately 100-150 ml cell washing buffer (150 mM NaCl, 25 mM NaPi, 2 mM EDTA, pH 8.0) and stored at  $-80^{\circ}\text{C}$ .

### 2.4.2. Protein Purification

Cells were harvested by centrifugation and lysed in a Microfluidizer (Microfluidics Corporation, Newton, MA). Membranes were sedimented at  $100,000 \times g$  for 1.5 h at  $4^{\circ}\text{C}$  and solubilized in buffer A (2% (w/v) *n*-dodecyl- $\beta$ -D-maltoside (DDM) (Calbiochem), 4 M NaCl, 50 mM MES, pH6) for 16 h at  $4^{\circ}\text{C}$ . After centrifugation of the solubilized membrane proteins ( $100,000 \times g$ , 1.5 h,  $4^{\circ}\text{C}$ ) the supernatant was purified using Ni-NTA chromatography. The Ni-NTA superflow (Qiagen, Hilden, Germany) was pre-equilibrated with buffer B (4M NaCl, 50 mM MES, pH 6.0, 0.05% DDM) for 1 h at  $4^{\circ}\text{C}$  while slowly shaking the vessel. The loaded resin was filled onto a chromatography column and washed extensively with buffer C (buffer B + 60mM imidazole). Purified his-tagged protein was then eluted from the column with buffer D (buffer B + 250 mM imidazole). For preparation of soluble constructs, The Ni-

NTA superflow (Qiagen, Hilden, Germany) were equilibrated in buffer (4M NaCl, 50 mM MES, pH 6) for HsHtrII and in buffer (150mM NaCl, 20mM Tris/HCl pH 7) for Tar protein. And the column was washed with equilibrium buffer containing 60mM imidazole. Purified his-tagged protein was then eluted with equilibrium buffer with 250 mM imidazole. Thereafter, imidazole was removed by using an Econo-Pac 10DG desalting column (Bio-Rad). HsSRII concentration was determined by the optical density at 487 nm ( $\epsilon = 48,000 \text{ M}^{-1} \text{ cm}^{-1}$ ). The yield of HsHtrII and Tar concentrations were calculated from the optical density at 280 nm ( $\epsilon = 24,000$ ) and 280 nm ( $\epsilon = 39,880$ ), respectively.

### 2.4.3. Determination of the protein concentration

Absorption spectra necessary for determination of the protein concentration were obtained using a spectrophotometer (Beckman, Palo Alto, USA). The concentration of the HsHtrII proteins were determined using the method of Ehresmann (106) by measuring the absorption at 228.5nm and 234.5 nm in a 1ml quartz cuvette. The protein concentration was calculated using the following equation:

$$C = \frac{(A_{228.5} - A_{234.5})}{3.14}$$

$A_{228.5}$  : Absorption at 228.5nm

$A_{234.5}$  : Absorption at 234.5nm

$C$  : Protein concentration in mg/ml

For the HsSRII, ANS and highly pure HsHtrII variants, the concentration was determined using the Lambert-Beer equation and the calculated extinction coefficients

$$A = \epsilon \cdot c \cdot d$$

$$C = \frac{A}{\epsilon \cdot d}$$

$A$  : Absorption

$\epsilon$  : Extinction coefficient of the protein ( $M^{-1} \text{ cm}^{-1}$ )

$d$  : Path length of the cuvette (cm)

$c$  : Molar Mass of Proteins (M)

### 2.4.4. Isolation of purple membrane lipids from *H. salinarum*

Samples of purple membrane lipids were kindly supplied by A. Göppner. The applied method was introduced by Kates *et al* (107). The purple membranes were extracted from *Halobacterium salinarum*. The purple membrane (BR content 300 to 350 mg) was suspended in 200 ml 4 M NaCl. After addition of 500 ml methanol and 250 ml chloroform, the mixture was stirred in nitrogen liquid tank. The obtained suspension was centrifuged for 15 min at 3800 rcf in metal tubes. The yellow supernatant was again pooled under nitrogen flow. The extraction of pellets was washed with 500 ml methanol and 250 ml chloroform. Then, the pooled supernatants were filtered using a paper filter (Whatman No.1) in methanol/chloroform 1:1 for 2 hours. Afterwards 500 ml sterile H<sub>2</sub>O and 500 ml Chloroform was added to the filtrate and extraction was performed using shaking. Phase separation was carried out under argon flow. The chloroform phase was separated and subsequently evaporated at 30 °C using a rotary evaporator (Büchi, Essen, Germany). The obtained residue was suspended in 12 ml chloroform and centrifuged at 24 000 rcf, 4 °C for 30 minutes. The chloroform containing supernatant was evaporated again and the pellet was suspended in 45 ml acetone at 0 °C using ultrasonic pulses. After the addition of 1 ml 10 % MgCl<sub>2</sub> in methanol, the suspension was centrifuged at 1 000 rcf (4 °C). The supernatant was discarded and the obtained pellet was extracted three times with 10 ml acetone until off-white extracts were obtained. The remained pellet was dried in vacuum, weighted and dissolved in methanol/chloroform 1:1 to obtain a 40 g/l solution. This solution was mixed with 20 volumes of 50 mM NaPi, pH 8.0

under argon flow. The obtained suspension was homogenized using ultrasonic pulses and subsequently lyophilized. The obtained lipids were suspended in phosphate buffer (2 g/L) which was stored at  $-80\text{ }^{\circ}\text{C}$ .

### **2.4.5. Reconstitution in purple membrane lipids (PMLs)**

For the reconstitution in PM lipids, membrane protein solutions containing 0.05 % DDM were used. The solubilised protein or protein complex was mixed 1:1 (w/w) with lipids and incubated for 10 min at  $4\text{ }^{\circ}\text{C}$ . Subsequently detergent absorber Bio beads (Bio-Rad, Munich, Germany) were added (1 g/100 mg DDM) and this mixture was shaken and incubated overnight at  $4\text{ }^{\circ}\text{C}$ . After incubation, the beads were separated by glass silk. A reconstituted protein is centrifuged at 12000rpm. This pellet was washed twice and finally suspended appropriate buffer.

## **2.5. Analytical methods**

### **2.5.1. Sodium dodecyl sulfate polyacrylamide gel electrophoresis (SDS-PAGE)**

For the analysis of proteins, one-dimensional gel electrophoresis was carried out using denaturing 15% SDS-polyacrylamide gel electrophoresis (SDS-PAGE) according to the standard protocol. Separation of proteins of different molecular weight was performed according to Laemmli using denaturing 15% SDS-polyacrylamide (108,109). The running gel was composed of 15% acrylamide, 0.4% bisacrylamide, 0.1% (w/v) SDS and 375 mM Tris, pH 8.8. The polymerisation of the gel material was initiated by adding  $14\text{ }\mu\text{M}/\mu\text{l}$  N,N,N,N-Tetramethyl-Ethylenediamine (TEMED) and 0.5 mg/ml ammonium persulphate (APS). The gel was casted by pouring it into the casting chamber and covering it with isopropanol/water 1:1. After polymerisation, the isopropanol/water mixture was replaced by the stacking gel composed of 5% acrylamide, 0.13% bisacrylamide, 0.1% (w/v) SDS, 125 mM Tris, pH 6.8,  $14\text{ }\mu\text{M}/\mu\text{l}$  TEMED and 0.5% mg/ml APS. Prior to application on the gel, proteins with SDS sample buffer were denatured by incubation for 2 minutes at  $95\text{ }^{\circ}\text{C}$ . The protein molecular weight marker (LMW-Standard,

Amersham Biosciences) was composed of protein phosphorlylase B (97 kDa), albumin (67 kDa), ovalbumin (43 kDa), carboanhydrase (30 kDa), trypsin inhibitor (20.1 kDa) and lysozyme (14.4 kDa). The electrophoresis took place at 60 mA in SDS running buffer. The gels were stained with a Commasie Blue solution and then destained with destaining buffer containing 5% Ethanol and 10% Acetic Acid for visible protein bands.

### 2.5.2. Western blot analysis

Proteins separated by SDS-PAGE were electrotransferred to a nitrocellulose membrane (Bio-Rad) for 20 minutes at 4 mA /cm<sup>2</sup>. Before transferring proteins to nitrocellulose membrane, the gel was incubated in the cathode buffer and the membrane in the anode buffer. The membrane was blocked for 1 hour at room temperature in 5% blocking solution (Roche) diluted in TBS buffer and incubated for 1hour with polyclonal antibodies against poly histidine in 0.5% blocking solution-TBS. After reaction, membrane was washed 3x 10minutes with TBS-Tween, incubated with goat-rabbit IgG-horseradish peroxidase (Promega) for 1hour, washed again, and then the bands were visualized by chemiluminescence (BM Chemiluminescence Blotting Substrate,Roche) or fluorescence (ECF western blotting reagent, Amersham)

Cathode buffer	30mM Tris, 300mM ε–aminocapronic acid pH 8.8
Anode buffer	300mM Tris, 100mM Tricine pH 8.6
TBS	50mM NaCl pH 7.5
TBS-Tween	TBS containing 0.1% Tween-20

### 2.5.3. Blue native gel electrophoresis (BN-PAGE)

Blue native PAGE (BN-PAGE) can be used for determination native protein masses and oligomeric states and to identify physiological protein–protein interactions. Blue-native polyacrylamide gel-electrophoresis (BN-PAGE) was performed as outlined by Schägger and Jagow (110) using a discontinuous system with 4% acrylamide in the stacking gel followed by a 10%-20% gradient for separation. Prior to the electrophoresis the solubilized NpSRII and

## MATERIALS AND METHODS

---

the truncated HsHtrII are incubated together for 1 h at room temperature. Using the system Hoefer<sup>®</sup> SE-400 (Pharmacia) the electrophoresis conditions were 150 V, 25mA and 20W for accumulation of samples in the stacking gel. Voltage was then set to 500V with the current limited to 15 mA for separation at 4°C. Selected bands from the BN-PAGE were grinded to small pieces, and incubated for 15 minutes at 40°C in SDS-buffer. The supernatant was analyzed by SDS-polyacrylamid-gelelectrophoresis (SDS-PAGE). For gel preparation the following buffers were used:

Acrylamide solution :	48 % acrylamide, 1.5 % bisacrylamide
Gel buffer :	150 mM bis-trisHCl, 1.5 M ε-aminocaproic acid, pH 7.0
3x Sample buffer :	4.5 ml glycerol, 0.31 g bis-trisHCl, ad 10 ml H <sub>2</sub> O, pH 7.0
Cathode buffer :	50 mM tricine, 15 mM bis-tris, 0.02 % Coomassie Serva blue G, pH 7.0, filtered
Anode buffer :	50 mM bis-trisHCl, pH 7.0
Stacking gel (4 %) :	0.8 ml acrylamide solution, 3.33 ml gel buffer, 120 µl 10 % APS, 12 µl TEMED add 10 ml H <sub>2</sub> O
Gradient solution (10 %) :	3 ml acrylamide solution, 5 ml gel buffer, glycerol, 20 µl 10 % APS, 7 µl TEMED, add 15 ml H <sub>2</sub> O
Gradient solution (20 %) :	6 ml acrylamide solution, 5 ml gel buffer, 3 g glycerol, 70 µl 10 % APS, 7 µl TEMED, add 15 ml H <sub>2</sub> O

### 2.5.4. LC-ESI-mass spectrometry

Mass spectrometry is an analytical technique used for measuring the Molecular Weight (Mw) of samples. Mass spectrometers use the difference in mass-to-charge ratio ( $m/z$ ) of ionized atoms or molecules to separate them from each other. Mass spectrometry is therefore useful for quantitation of atoms or molecules and also for determining chemical and structural information about molecules. Molecules have distinctive fragmentation patterns that provide structural information to identify structural components. Mass spectrometers can be divided into three fundamental parts, namely the ionisation source, the analyser, and the detector. Liquid Chromatography-



Electrospray Ionization-Mass Spectrometry (LC-ESI-MS) analysis was performed on an Agilent 1100 series chromatography system (Hewlett Packard) equipped with an LCQ ESI mass spectrometer (Finnigan, San Jose, USA) using Jupiter C4 columns (5  $\mu\text{m}$ , 15 x 0.46 cm, 300  $\text{\AA}$  pore-size) from Phenomenex (Aschaffenburg, Germany) for proteins and 125/21 NUCLEODUR 5  $\mu\text{m}$  C18 columns for peptides. For LC separation a gradient of buffer B (0.1 % formic acid in acetonitrile) in buffer A (0.1 % formic acid in water) with a constant flow-rate of 1 mL/min was applied, with a gradient program. Mass spectra data evaluation and deconvolution was performed using the X-calibur software package.

### **2.5.5. Analytical Gel filtration**

Analytical gel filtration (GF) chromatography were performed on a Waters 600 chromatography instrument equipped with a Waters 2487 absorbance detector and a Waters 2475 fluorescence detector (Waters, Milford, MA, USA). The column was pre equilibrated with respective buffer the flow rate was 0.5ml/min and the absorbance of the eluent was monitored at 280nm. The HsSR<sub>II</sub>, HsHtr<sub>II</sub> and mixtures were loaded on on a Superdex 200-HR 10/30 column (Pharmacia) with a flow rate of 0.5 mL/min and an injection volume of 0.5 mL. The buffer was 50 mM MES pH 6.0, 4 M NaCl, 1 mM EDTA, and 0.05 % n-dodecyl  $\alpha$ -d-maltoside, and the protein concentration of the samples was 1-2 mg/mL. Fractions of samples were collected and analyzed by SDS/PAGE. The column had previously been calibrated with proteins of known molecular mass.

### **2.5.6. Crystallisation by Vapour-Diffusion method**

In the most common methods of growing protein crystals, purified protein is dissolved in an aqueous buffer containing a precipitant such as ammonium sulfate or polyethylene glycol at a concentration just below that is necessary to precipitate the protein. By far the vapour diffusion method is the most common and popular technique for crystallising proteins. In this technique a

drop containing protein, stabilizing buffers, precipitants and crystallization aids is allowed to equilibrate in a closed system with a much larger reservoir. The reservoir usually contains the same chemicals minus the protein but at an overall higher concentration so that water preferentially evaporates from the drop. If conditions are right this will produce a gradual increase in protein and precipitant concentrations so that a few crystals may form. Water-soluble HsHtrII [1-765] and Tar(1-553) were thawed and subjected to screening using Classic I and Classic II. The protein concentration was screened at 0.5 and 1.0 mg/ml for HsHtrII[1-765] and 1 and 2 mg/ml for Tar(1-553) by dilution of the protein stock with gel filtration buffer. The vapour diffusion method with drops consisting of 1.2  $\mu$ l protein and 1.2  $\mu$ l precipitant solutions was used throughout. All crystallization trials were carried out at 20 °C. The conditions were checked for the appearance of crystals periodically.

## 2.6. Biophysical analysis

### 2.6.1. Isothermal Titration Calorimetry (ITC)

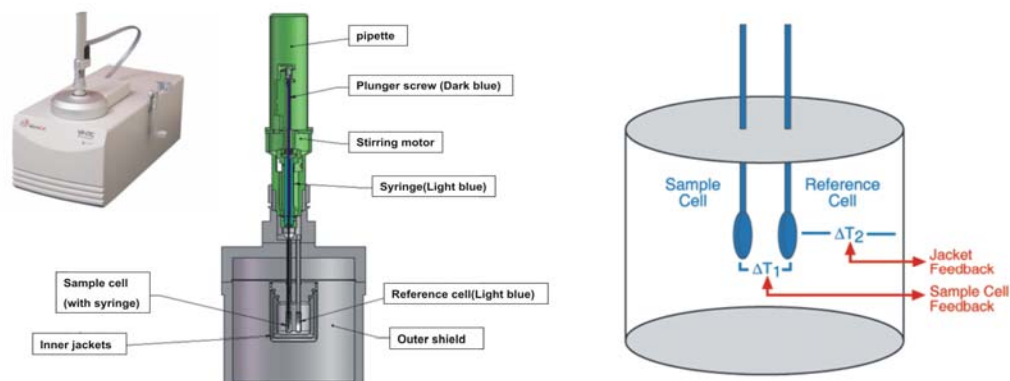
In an ITC experiment, the macromolecule solution is placed in the sample cell. In a typical ITC experiment, a solution of a one biomolecule (“ligand” such as a drug, protein, DNA molecule, etc) is titrated into a solution of its binding partner. Measurement of heat changes allows accurate determination of binding constants ( $K_a$ ), reaction stoichiometry ( $n$ ), enthalpy ( $\Delta H$ ) and entropy ( $\Delta S$ ), thereby providing a complete thermodynamic profile of the molecular interaction in a single experiment. The binding of two molecules is regulated by the thermodynamics of the binding event, in particular, the overall change in free energy accompanying binding. The change in free energy is defined as:

$$\Delta G = -RT \ln K_a = \Delta H - T \Delta S$$

Where,  $G$  is Gibbs free energy,  $R$  the gas constant, and  $T$  the absolute temperature. Change in heat and energy can contribute to  $\Delta H$ , as well as the change in exposed surface area of a molecule. Conformational entropy,

## METERIALS AND METHODS

rotational/translational entropy, and the hydrophobic effect can all contribute to  $\Delta S$ . Structural and dynamical properties of the system can help elucidate these parameters. The heat released upon their interaction ( $\Delta H$ ) is monitored over time. As successive amounts of the ligand are titrated into the ITC cell, the quantity of heat absorbed or released is in direct proportion to the amount of binding.



MicroCal Isothermal Titration Calorimeter. Diagram of ITC cells and syringe. The syringe rotates in place during the ITC experiment. Sample and reference cells are presented as two ovals that are immersed into water bath. The end of the syringe has been adapted to provide continuous mixing in the ITC cell. The plunger is computer-controlled and injects precise volumes of ligand.

The schematic drawing of the ITC cells and syringe is shown that twin coin-shaped cells are mounted in a cylindrical adiabatic environment, and connect to the outside through narrow access tubes. The reference cell contains buffer or water minus the macromolecule. Prior to the injection of the titrant, a constant heat is applied to the reference cell. This signal directs the feedback circuit to activate the heater located on the sample cell to differentially measure and compensate for heat produced (exothermic) or absorbed (endothermic). The temperature difference between the sample and reference cells ( $\Delta T_1$ ) is kept at a constant value (i.e. baseline) by the addition or removal of heat to the sample cell, as appropriate, using the feed back system. The integral of the power required to maintain equal temperatures between the two cells. For endothermic reactions the reverse will occur, meaning the feedback circuit will increase power to the sample cell to

## MATERIALS AND METHODS

---

maintain the temperature. As the macromolecule in the cell becomes saturated with ligand, the heat signal diminishes until only background heat of dilution is observed. The AVP-ITC MicroCalorimeter (MicroCal, USA) was used throughout the experiments. For sample preparation, proteins were dialyzed at 4°C over night against the buffer. All buffers were degassed prior to use. HsSR11 and ligands were injected into the reaction chamber (1.5 mL buffer A, 20 µM transducer protein) in 12 µl increments (in 3 min intervals) at a concentration of between 300 µM to 500 µM. A 290µl injection syringe with 300 rpm stirring was used to give a series of 12µl injections at 3min intervals. Control experiments for heats of mixing and dilution were performed under identical conditions and used for data correction in subsequent analysis. Titrations were carried out the temperature in 25 to 35°C. In control experiments buffer was titrated into protein. Data acquisition and subsequent nonlinear regression analysis were done in terms of a simple binding model, using the ORIGIN 7 software package.

At the beginning of an experiment, the cell of calorimeter is filled with macromolecule solution (working volume  $V_0$ ) and the injection of ligand solution drives an equivalent volume ( $V_{inj}$ ) of solution in the injector. The concentration of macromolecule decreases at injection number  $i$  as:

$$M_{tot,i} = nM_{tot,0} \left(1 - \frac{V_{inj}}{V_0}\right)^i \quad (\text{eq. 1})$$

where  $M_{tot,i}$  is the total concentration of protein in the cell after injection step  $i$ ,  $M_{tot,0}$  is the total concentration of protein in the cell before injection, which is a known quantity.  $V_0$  is the volume of the cell,  $V_{inj}$  is the injection volume, and  $n$  is the number of binding sites. The total concentration of the titrant ligand increases with each injection step as:

$$L_{tot,i} = L_{tot,0} \left(\frac{V_{inj}}{V_0}\right)^i \quad (\text{eq. 2})$$

where  $L_{tot,i}$  is the total concentration of ligand in the cell after injection step  $i$  and  $L_{tot,0}$  is the total concentration of ligand in the injection syringe.

The total concentration of macromolecule and ligand is equal to the sum of the bound and the free (unbound) forms at injection number  $i$ , and is given as:

## METERIALS AND METHODS

---

$$M_{tot,i} = M_i + ML_i = M_i(1 + K_a L_i) \quad (\text{eq. 3})$$

$$L_{tot,i} = L_i + ML_i = L_i(1 + K_a M_i) \quad (\text{eq. 4})$$

where  $M_i$ ,  $L_i$  and  $ML_i$  are the concentrations of free macromolecule, free ligand and ML complex at injection number  $i$ ,  $K_a$  is the binding constant.

Eq. 3 can be rearranged to give the concentration of free M as:

$$M_i = \frac{M_{tot,i}}{1 + K_a L_i} \quad (\text{eq. 5})$$

Eq. 5 can be substituted into eq. 4 and rearranged to give the following quadratic expression:

$$K_a L_i^2 + [1 + K_a (M_{tot,i} - L_{tot,i})] L_i - L_{tot,i} = 0 \quad (\text{eq. 6})$$

The meaningful solution of this quadratic equation gives the concentration of free ligand after any injection step:

$$L_i = \frac{-[1 + K_a (M_{tot,i} - L_{tot,i})] + \sqrt{[1 + K_a (M_{tot,i} - L_{tot,i})]^2 + 4K_a L_{tot,i}}}{2K_a} \quad (\text{eq. 7})$$

The heat that is absorbed or produced for each injection in an ITC experiment is the difference in heat content before and after the injection. The heat for injection number  $i$  is defined as:

$$Q_i = \langle \Delta H \rangle_i M_{tot,i} V_0 - \langle \Delta H \rangle_{i-1} M_{tot,i-1} (V_0 - V_{inj}) \quad (\text{eq. 8})$$

where  $\langle \Delta H \rangle$  is the cumulative enthalpy change per mole of macromolecule.

In case of one to one binding, the cumulative enthalpy change is given as:

$$\langle \Delta H \rangle_i = \Delta H \frac{ML_i}{M_{tot,i}} = \Delta H \frac{ML_i}{M + ML_i} = \Delta H \frac{K_a L_i}{1 + K_a L_i} \quad (\text{eq. 9})$$

where  $\Delta H$  is the enthalpy change for binding one mole of ligand to one mole of macromolecule,  $M_{tot,i}$  and  $ML_i$  are the concentrations of total and bound macromolecule at injection number  $i$ . Replacing  $\langle \Delta H \rangle$  in eq. 9 with eq. 8 results in:

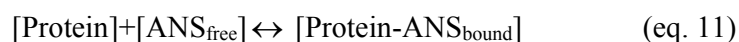
$$Q_i = \frac{\Delta H K_a L_i M_{tot,i} V_0}{1 + K_a L_i} - \frac{\Delta H K_a L_{i-1} M_{tot,i-1} (V_0 - V_{inj})}{1 + K_a L_{i-1}} \quad (\text{eq. 10})$$

where the  $M_{tot,i}$  and  $L_{tot,i}$  can be calculated from eq. 1 and 2, respectively, while  $L_i$  can be substituted using eq. 7. Therefore, eq. 10 is a quadratic

equation of  $K_a$ . Fitting the ITC data to this equation allows for direct determination of  $\Delta H$ ,  $K_a$  and  $n$ .

### 2.6.2. ANS fluorescence measurements

The fluorescence measurements were performed on a Spex Fluoromax-3 spectrofluorometer (Jobin Yvon, Edison, NJ, USA) equipped with a temperature controller. All samples were in 4 NaCl 25 mM MES at pH 6 with various ligand concentrations in 1ml quartz 1 cm path length cell in 15C°. For 8-Anilino-1-naphthalenesulfonic acid (ANS) binding fluorescence experiments, the excitation wavelength was set at 380nm and the emission spectra was recorded in the range of 400nm-600nm. Approximately 10 mM ANS (Sigma, St. Louis, MO) stock solution was prepared by dissolving ANS in 10 % glycerol. ANS concentration was determined by using molar absorption coefficient,  $\epsilon_{350} = 5000 \text{ M}^{-1} \text{ cm}^{-1}$  (111). To obtain the amount of ANS bound per protein, ANS fluorescence titrations were carried out. The binding of ANS to protein was monitored at 470 nm. The observed fluorescence intensity was corrected by subtracting the fluorescence of the sample containing 0 $\mu$ M ANS. In a reversible second-order reaction shown in equation 11:



The dissociation constant is defined as:

$$K_d = \frac{[\text{Protein}][\text{ANS}]}{[\text{Protein - ANS}]} \quad (\text{eq. 12})$$

$N$  is defined as the average number of bound ANS molecules per macromolecule described in equation 13:

$$N = \frac{[\text{Bound ANS}]}{[\text{Bound ANS}] + [\text{Free ANS}]} = \frac{[\text{Free ANS}]}{K_d + [\text{Free ANS}]} \quad (\text{eq. 13})$$

## METERIALS AND METHODS

---

The fluorescence intensities were plotted against the total concentration of ANS and the apparent  $K_D$  was obtained by fitting the data to equation 14, where  $F$  is the corrected fluorescence intensity at 470 nm,  $F_{max}$  is the fluorescence intensity upon saturation of the ANS binding sites,  $[ANS]$  is the total concentration of ANS, and  $K_D$  is the apparent dissociation constant results in:

$$F = \frac{F_{Max}[ANS]_{free}}{[ANS]_{free} + K_D} \quad (\text{eq. 14})$$

To examine the binding stoichiometry, a Scatchard analysis was performed (112,113). To estimate the fluorescence of 5 $\mu$ M ANS when completely bound to protein, the plot of fluorescence intensity versus total protein concentration was then fit to Equation 15.  $[\text{protein}]$  is the total protein concentration which is given as:

$$F = \frac{F_{Max}[\text{Protein}]}{[\text{Protein}] + K_D} \quad (\text{eq. 15})$$

The ANS titration data were then extrapolated to the Scatchard plot in terms of the concentrations of bound and free ANS. The concentrations of bound and free ANS were determined by equations 16 and 17, respectively, where  $F$  is the corrected fluorescence intensity at 470 nm for each point of the ANS titration and  $F_{Max}$  is the fluorescence intensity when 1 $\mu$ M ANS is completely bound by protein given as:

$$[ANS]_{bound} = \frac{F(1\mu\text{M ANS})}{F_{Max}} \quad (\text{eq. 16})$$

$$[ANS]_{free} = [ANS]_{total} - [ANS]_{bound} \quad (\text{eq. 17})$$

$$\frac{N}{ANS} = \frac{1}{K_d} - \frac{N}{K_d} \quad (\text{eq. 18})$$

The Scatchard plot is then constructed by replotting the ANS titration data as  $N/[ANS]_{\text{free}}$  versus  $N$ . A graph of  $N/[ANS]$  against  $N$  gives a straight line whose slope is  $-1/K_d$ . The number of binding sites per HsHtrII protein is equal to the value of the x-intercept of the line obtained by a fit of the data to the Scatchard equation given by equation 18.

### 2.6.3. Intrinsic tryptophan fluorescence

For intrinsic emission fluorescence measurement, the samples were excited at 295nm and taken from 305nm to 405nm. For the effect of unfolding on chemical induced denaturation, fluorescence-monitored Gd-HCl denaturation was performed. In order to measure affinity of HsHtrII with serine, titrations were performed to estimate the  $K_D$  (dissociation constant) of HsHtrII to serine. The excitation wavelength was at 295nm and the emission spectra were at 340nm. For each point in titration, the fluorescence HsHtrII which contains tryptophan residues was added to a quartz cuvette containing 1 mL buffer with continuous stirring. Serine was then titrate to the cuvette, until the fluorescence signal change reached saturation. The ligand-induced fluorescence quenching as a function of proteins were monitored by trptophan fluorescence titration. Increasing amounts of ligand. The corrected fluorescence values were then fitted to an equation of a single class of ligand binding by the nonlinear least-squares method for determining dissociation constants. All spectra of the buffer was subtracted after plotting the data. The change in fluorescence was corrected for light scattering as well as dilution and plotted as a function of the reactant concentration. The data was fitted to the following equation 19:

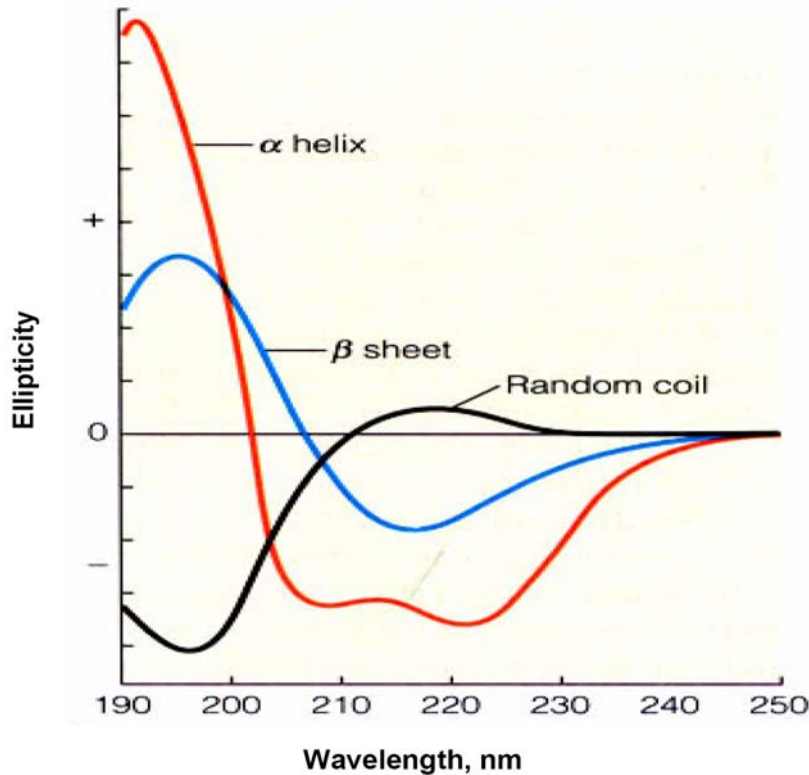
$$F = F_{\min} + \left( K_d + A_0 + E_0 - \sqrt{(K_d + A_0 + E_0)^2 - 4A_0E_0} \right) \frac{F_{\max} - F_{\min}}{2A_0} \quad (\text{eq. 19})$$



where  $F$  is the observed fluorescence intensity after each step of titrant  $E$  addition,  $E_0$  is the total (cumulative) concentration of titrant  $E$ ,  $A_0$  is the concentration of fluorescent reactant  $A$ ,  $F_{\min}$  is the initial fluorescence intensity at  $E_0 = 0$ ,  $F_{\max}$  is the final fluorescence intensity at  $E_0 = \infty$ , and  $K_d$  is the dissociation constant, which is to be determined. Data analysis was performed with the program GraFit 5.0 (Erithacus software, Surrey, UK)

#### 2.6.4. Circular Dichroism (CD) analysis

Circular dichroism (CD) is an important technique in the structural characterization of protein and especially for secondary structure determination (114). The experimentally measured parameter in CD is the difference in absorbance for left- and right- handed circularly polarized light that when encountered by a protein's specific secondary structure gives rise to characteristic bands of secondary structural elements, such as  $\alpha$ -helix,  $\beta$ -sheet, and random coil structures.



Computed circular dichroism spectra for the evaluation of protein conformation. Each

wavelength denoted an  $\alpha$ -helix (blue),  $\beta$ -sheet (purple) and random coil (light blue).

The CD spectrum of secondary structure motif can well be distinguished. An element of  $\alpha$ -helices exhibit distinct minima at 208 and 222 nm and a large maximum between 190 and 200nm. The  $\beta$ -sheets exhibit small maxima in the range of 190 – 200 nm. A disordered structure, a so called random coil, appeared in the CD spectrum with a large maximum in the range between 210 nm and 240nm and a minimum at 190nm. The far-UV CD spectra of protein samples were recorded between 190 and 250 nm (300 $\mu$ L sample volume) on a Jasco J-815 spectropolarimeter equipped with a temperature-controlled incubator and buffer background was always subtracted. The optical path length was 0.5 mm with a 1.0 nm bandwidth a scan speed of 50 nm/min under nitrogen flow. An accumulation of 10 spectra was obtained for blank and protein scans. The secondary structure percentages were calculated using CD computer-modeling program (CCA, Continll, CDSSTR). Thermal denaturation of proteins was monitored the ellipticity at 220nm. For full length HsHtrII and HsHtrII-398, the samples were first incubated at 20 °C for 10min and increased temperature to 80 °C at 0.5 °C per minute. The results were expressed as mean residue ellipticity in units of degree/cm<sup>2</sup>/dmol. Data was fit to a two-state model to determine the T<sub>m</sub> (melting temperature) values. Plots of T<sub>m</sub> changes were fit in Origin 7 using non-linear curve fitting function.

### **2.6.5. Laser flash photolysis and data analysis**

The photocycle experiments and the analysis of the data were done as described by Chizhov and coworkers (83,115). HsSRII, HsHtrII and HsHtrII analogues are reconstituted into PM-lipids and were immobilized in gels (16.5% acrylamide). Prior to these experiments, the gel slice was equilibrated with the appropriate buffer (4 M NaCl, 50 mM MES, pH ranging from 6 to 1) for at least 30 minutes. The transient absorption changes were recorded at 360 nm, 490 nm and 540/550 nm wavelength, respectively.

## 3. RESULTS

## RESULTS

### 3.1. Cloning, expression and purification of proteins

#### 3.1.1. *Halobacterium salinarum* sensory rhodopsin II(HsSRII)

In order to characterize HsSRII, the protein was over-expressed as an N-terminal His-tagged fusion protein and purified from solubilized membrane fractions by Ni-NTA affinity chromatography. The left panel in Figure 3-1 shows the expression vector for production of HsSRII constructs. *E. coli* XL1-Blue was used as host for DNA manipulation. The *HssopII* gene was amplified by PCR from genomic DNA extraction of *H. salinarum*. The 5'-primer introduced an *NcoI* site including the start codon. The 3'- primer added a coding region for seven times histidines followed by two stop codons. An *EcoRI* site was subcloned into a pET 27bmod expression vector (116). The plasmid was then transformed into *E.coli* Rosetta pLysS competent strain. Positive clones were verified by DNA sequencing.

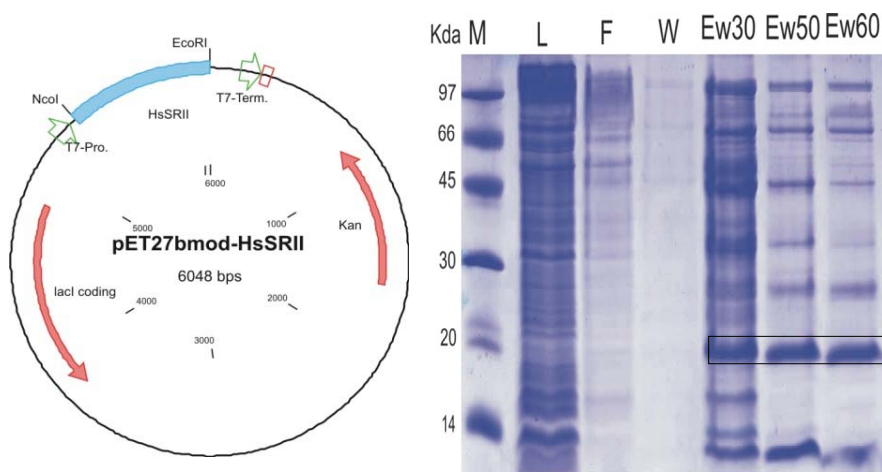


Figure 3-1. Left panel; The expression vectors pET 27bmod, Right panel; SDS-PAGE of purified HsSRII proteins (box) (M = marker, kDa; L= crude lysate; F = flow through of Ni-NTA column; W = washing with equilibrium buffer; Ew30 = Eluate after washing with 30mM Imidazole; Ew50 = Eluate after washing with 50mM Imidazole; Ew60 = Eluate after washing with 60mM Imidazole.

Initial tests were carried out to determine the optimal conditions for over-expression and purification. Expression of the fusion gene is under the control of the T7 promoter(117) and regulated by IPTG due to the presence of a *lac I*

## RESULTS

gene. The protein was over-expressed and purified using Ni-NTA affinity column. However, after the first step of purification, the designed HsSR11 construct (Figure 3-1, box) was not pure and protein contaminants were present in the eluate (lane Ew30, Ew50 and Ew60) (Figure.3-1). From the analysis of SDS gel, it was seen that purification could not be achieved by increasing imidazole concentration up to 60mM in the washing step. Only 50% pure HsSR11 protein was obtained.

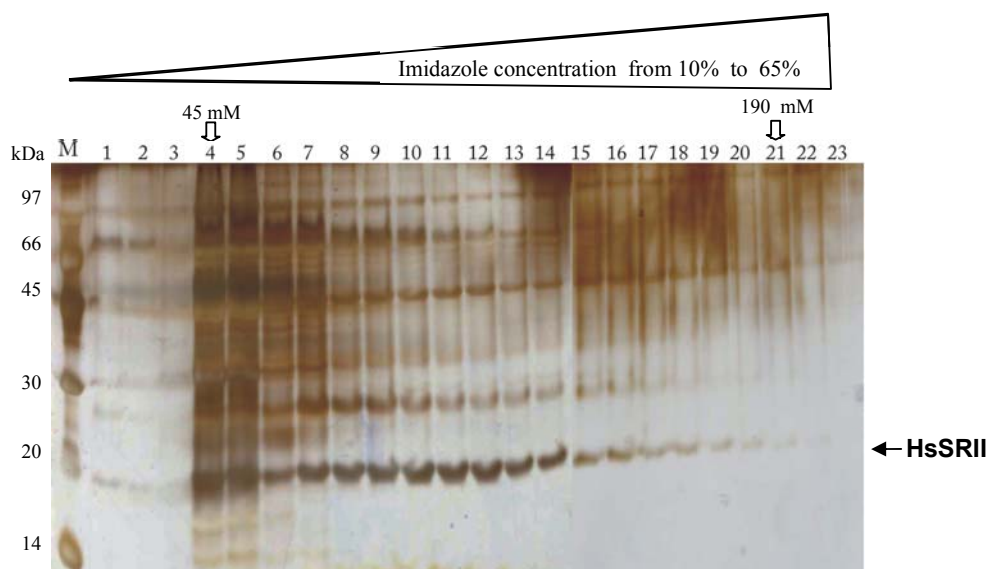


Figure 3-2. The silver-staining of purified HsSR11; Eluent fractions of HsSR11 from Ni-NTA column and eluted with a step gradient of 10 mM imidazole. Fraction size: 1 ml, gradient: 0 to 300 mM imidazole in 4M NaCl, 50 mM MES, 0.05% DDM, pH 6.0 at 4°C, in 300 min at a flow rate of 0.5 ml/min. Fraction numbers are indicated above the respective lanes. The proteins were separated by SDS-PAGE and silver-stained.

To minimize the impurity during the purification, several different approaches were adopted. A concentrated fraction of purified protein was loaded again onto a Ni-NTA column (Hi-Trap Chelating, Qiagen), equilibrated in appropriate buffer with 0 mM imidazole (buffer A) on an Äkta Prime FPLC system (Pharmacia). The column was washed with 6-8 column volumes of buffer A containing 2% with 300 mM imidazole (buffer B). After this, the bound protein was eluted with a gradient of imidazole concentration of 2 to 100% (buffer B). The protein fractions were analyzed by SDS-PAGE and silver

## RESULTS

---

staining (Figure 3-2). The desired HsSRII protein fractions appeared in the elution containing imidazole gradient ranging from 45 mM to 190 mM. This method, however, did not achieve a desirable level of purification, and unwanted protein bands with molecular weights between 25 and 97 kDa showed up. The reason could be that HsSRII might interact with hydrophobic proteins under this high salt condition. It is also possible that the histidine rich proteins or the highly negative charges of proteins are strongly bound to the Ni-NTA resin whose affinity is similar to that of HsSRII protein.

HsSRII protein also could not be purified by size exclusion chromatography. It seems likely that other protein-detergent micelles are of the same size as the micellar HsSRII (data not shown).

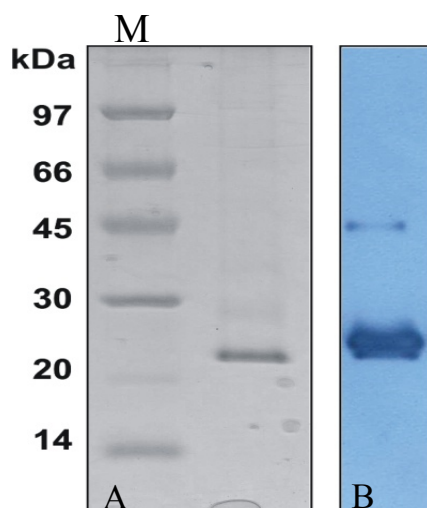


Figure 3-3. Gel electrophoresis of purified His-tagged HsSRII Coomassie stained protein (A) and (B) the corresponding immuno blot was developed with monoclonal anti-poly histidine peroxidase conjugate.

To further optimize the purification of the HsSRII protein, pET27bmod which contained the *hssopII* gene was transformed into another *E.coli* C41 competent strain. This strain is effective in overexpressing toxic and membrane proteins from all classes of organisms, eubacteria, archaea, yeast, plant, and mammals. After purification, HsSRII was at least 95% pure as judged by SDS-PAGE and UV/Vis absorption spectroscopy. Proteins were detected by western blots developed with antibody against the His-tag (Figure.3-3). The HsSRII protein preparation exhibits two dominant bands

## RESULTS

corresponding to the mass of the monomeric (24 kDa) and dimeric (48 kDa), respectively. Cell membrane lysate with 20mM imidazole was applied onto Ni-NTA column and further washed again with buffer with 50mM imidazole. A better over-expression of HsSRII was obtained when a lower concentration of IPTG was used (0.5 mM) and induction time was extended to 4 hours when cells were concomitantly cultured in minimal medium (See materials and methods). UV-vis spectroscopy of HsSRII proved that the protein sustained absorption maxima ( $\lambda=487$  nm) between pH 4 and pH 6. Therefore, the pH of washing buffer was adjusted to 5. Approximately 5-7 mg of purified protein could be obtained from 1L cell culture.

### 3.1.2. Expression of halobacterial transducer II (HsHtrII) and its analogues

In order to investigate the biochemical properties of HsHtrII such as substrate binding or the complexation of HsSRII with HsHtrII, the following transducer constructs were designed.

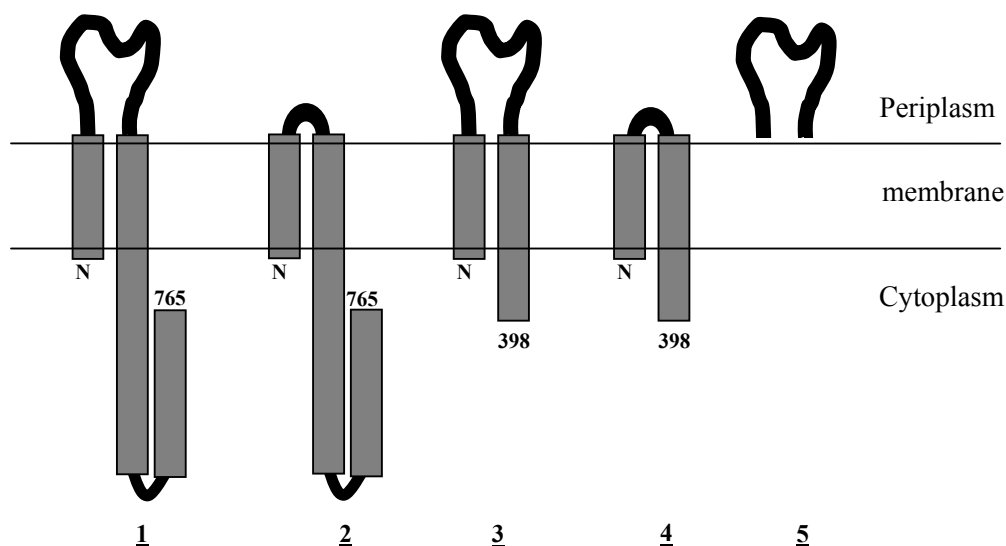


Figure 3-4. Scheme of HsHtrII constructs used in this work. 1: full length transducer (HsHtrII[1-765]); 2: full length transducer without serine binding domain (HsHtrII[1-765 $\Delta$ 38-280]); 3 shortened transducer (HsHtrII[1-398]); 4: shortened transducer without ligand binding domain (HsHtrII[1-398 $\Delta$ 38-280]); 5: ligand binding domain (HsHtrII[38-280]).

## RESULTS

---

Figure 3-4 provides a schematic representation of the HsHtrII constructs and fusion HsHtrII constructs with extracellular linker between TM1(Transmembrane 1) and TM2(Transmembrane 2) from NpHtrII. HsHtrII and its analogues encompassed a full length HsHtrII (HsHtrII[1-765]) (**1**), shortened transducer with ligand binding domain (HsHtrII[residue1-398]) (**2**), full length transducer without ligand binding domain (HsHtrII[residue1-765 $\Delta$ 38-280]) (**3**), shortened transducer without ligand binding domain (HsHtrII[residue1-398 $\Delta$ 38-280]) (**4**), and ligand binding domain (HsHtrII [38-280]) (**5**). In **2** and **4**, the extracellular serine binding domain (HsHtrII [residues 38-280]) was replaced by a short turn sequence from NpHtrII [residues 44-59] which lost the ligand binding activity. The corresponding receptors, equivalent to NpHtrII-157 (118,119), a N-terminal sequence of 398 amino acid residues was selected. The HsHtrII [residues1-398] construct was truncated at the amino acid 398 so that it contains the transmembrane domains (TM1, TM2) and the 48 residues extension of TM2 into the cytoplasm. In HsHtrII constructs, the 5'-primer was introduced to an *NcoI* site including the start codon. A coding region for seven histidines was added to 3'- primer followed by two stop codons and an *EcoRI* site. All PCR constructs were cloned into the pET27bmod expression vector. The gene sequence was confirmed by DNA sequencing.



## RESULTS

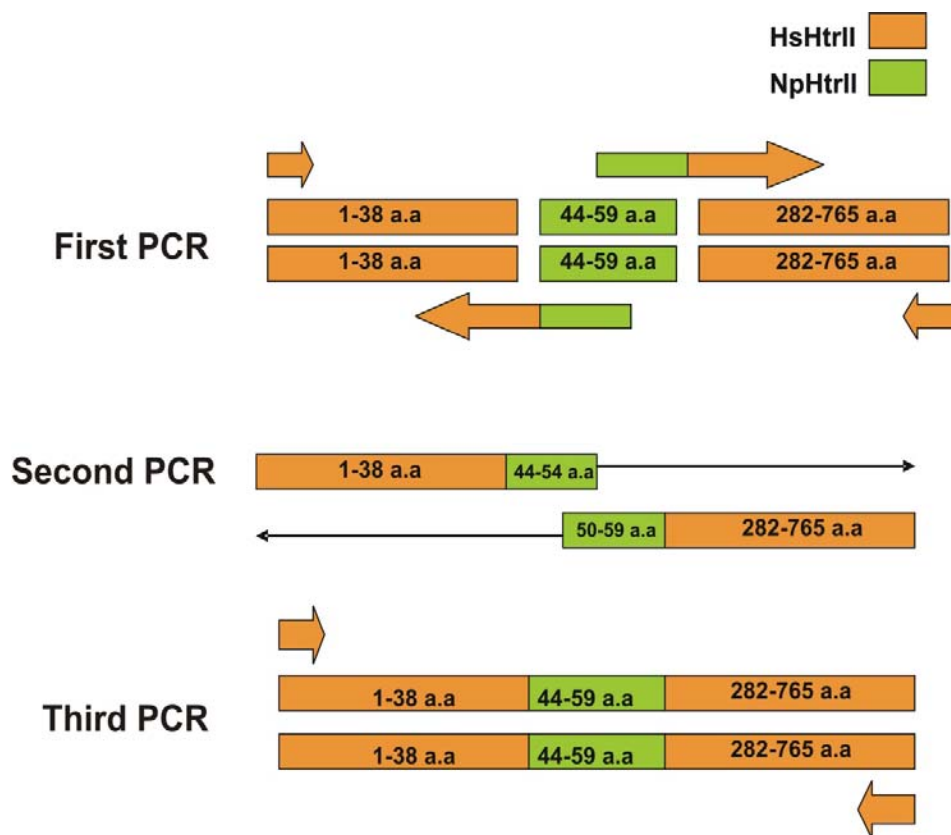


Figure 3-5. Schematic representation of the construction of a gene replacement cassette.

The PCR-based fusion technique was used to obtain HsHtrII mutants lacking the extracellular domain (Figure 3-5). This method can be accomplished by amplifying the selective marker with chimeric primers(120). In the constructs lacking the serine binding domain, *HshtrII* [38-280] of HsHtrII was replaced by DNA sequence corresponding to residues 44-59 from NpHtrII turn. The *HshtrII* genes and the *HshtrII* analogues were amplified by PCR from genomic DNA extraction of *H. salinarum*. The individual components were separately amplified by a conventional PCR. For confirmation of *NphtII* [49-59] gene replacement, the *HshtrII* [1-38] fragment with 5' forward primer and HshtrII [282-765] fragment with 3' reverse primer were amplified with a 3' reverse primer and 5' forward primer containing 10-11 overlapping homologous sequences of NphtII [44-54] and NphtII [50-59], respectively. The two chimeric genes, (*HshtrII*[1-38]-*NphtII*[44-54]) and (*NphtII*[50-59]-

## RESULTS

*HshtrII*[282-765]), were amplified without any specific primers, as the overhanging chimeric extensions act as primers. Finally, the fusion PCR product (*HshtrII* [1-38]-*NphtrII*[44-59]-*HshtrII*[282-765]) was amplified with a 5' forward primer and 3' end of *HshtrII*. The chimeric HsHtrII mutant was cloned into the pET27bmod expression vector. The gene sequence was confirmed by DNA sequencing.

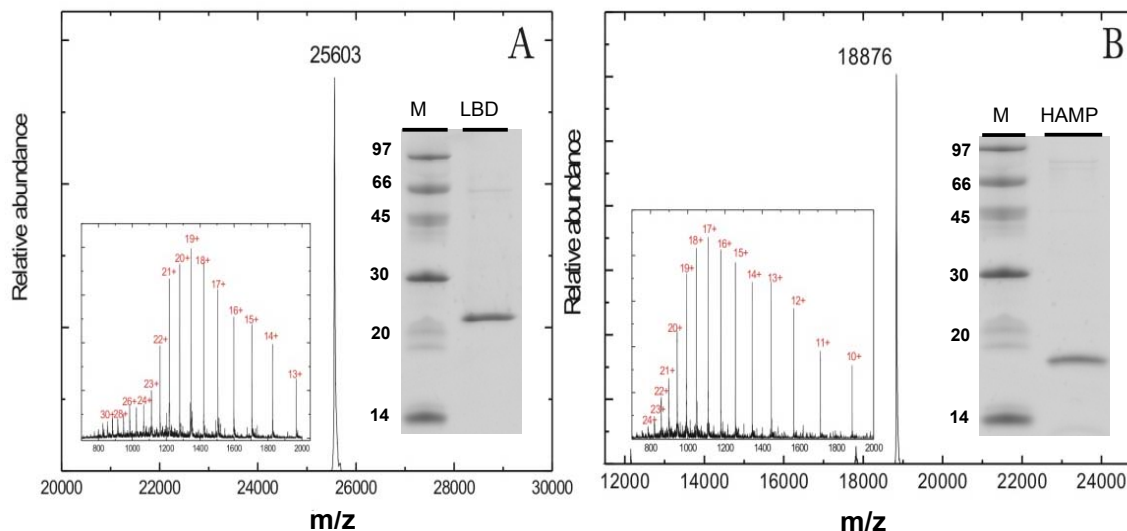


Figure 3-6. The ESI mass spectrum of purified protein. (A) Ligand binding domain (LBD) [42-285] of HsHtrII (B) Two HAMP domain [303-465]. The inset of panel shows SDS-PAGE of purified proteins and the original mass spectrum before deconvolution. The identified mass peaks were marked with bold numbers corresponding to those reaction products shown in above the scheme.

To characterize the purified HAMP domain (linker domain), and the ligand binding domain (LBD) of HsHtrII, they were first expressed in *E. coli* Rosetta pLysS competent strain as a strategy to optimize the purification. As shown in the inset of Figure 3-6, both proteins were purified by a single step of Ni-NTA affinity chromatography which yielded a purity of more than 95% with minor contaminations. Mass spectrometry was used to measure the Molecular Weight (MW) of samples. Figure 3-6 shows the LC-ESI-MS analysis of HAMP and LBD. The purified HAMP domain and extracellular domain of HsHtrII were subjected to mass spectroscopy analysis. Thirty microliters of the protein sample with a concentration of 10-20  $\mu$ M were directly injected into the spray capillary tube for the measurement. The m/z spectrum of HAMP and LBD

## RESULTS

convert to a molecular mass profile. The analysed m/z spectrum shows a Gaussian-type distribution of multiple charged ions. In the electrospray ionization mass spectrum of ligand binding domain of HsHtrII, the molecule with molecular mass of 25.603 kDa of single peak was identified. The mass profile of HAMP domain is found to have the molecular mass of 18.876 kDa. The observed molecular mass is in good agreement with the theoretical molecular mass of 25.840 (LBD) and 19.005 (HAMP), respectively.

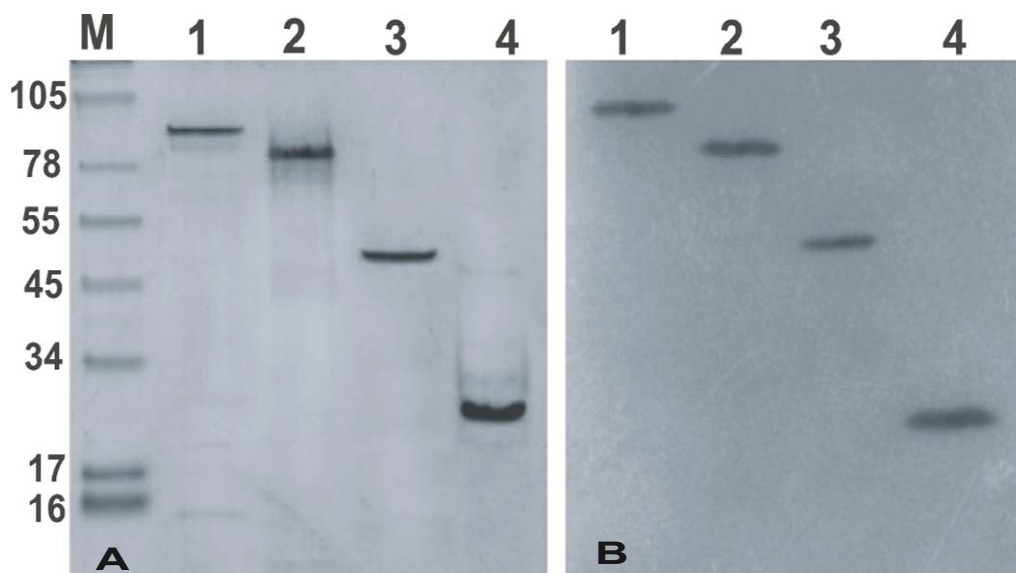


Figure 3-7. SDS-PAGE of purified proteins (A) coomassie stain of HsHtrII and its analogues: lane 1 HsHtrII[1-765] (**1**); lane 2 HsHtrII(1-765Δ38-280); (**2**); lane 3 HsHtrII[1-398] (**3**); lane 4 HsHtrII(1-398Δ38-280) (**4**). (B) Immuno blot (peroxidase conjugated monoclonal anti-poly histidine). The proteins were dissolved in 4M NaCl, 50mM MES, 0.05% DDM, pH 6.

To investigate the interaction between the ligand binding domain and its respective ligand, HsHtrII and its analogues, were heterologously expressed in *E. coli* (DE3) as an N-terminal seven His-tag fusion protein in *E. coli* Rosetta (DE3) and purified using His-tag affinity chromatography. Recombinant proteins were purified by a single step of Ni-NTA affinity chromatography which yielded a purity of more than 95% with minor contaminations as seen by SDS-PAGE (Figure 3-7). The corresponding immune-blot (right panel) was developed with monoclonal anti-poly histidine peroxidase conjugate. Most transducer proteins migrated at a position somewhat higher than the

## RESULTS

---

calculated molecular weight, as is common for transmembrane protein. The higher apparent molecular weight can be explained by the rod like conformation of the molecule, thereby leading to a bigger Stokes radius. Similar results were also observed for other membrane proteins (121-123). The proteins were purified to homogeneity with yields in the mg/L range. The purified transducer and transducer analogues are summarized in table 1.

Table. 1 Expressed HsHtrII and its analogues

<b>Protein Name</b>	<b>Molecular weight (kDa)</b>	<b>Yield (mg/mL)</b>
HsHtrII[1-765]	80	0.5
HsHtrII[1-765 $\Delta$ LBD]	57	1.0
HsHtrII[1-398]	43	5.0
HsHtrII[1-398 $\Delta$ LBD]	19	1.0
HsHtrII-LBD[42-285]	26	7.0
HsHtrII-HAMP[303-465]	19	10

## RESULTS

### 3.1.3. Expression of Aspartate chemoreceptor (Tar)

In order to compare the properties of HsHtrII with those of full length Tar [1-553] chemoreceptor and Tar receptor with one HAMP domain (1-265), they were expressed and purified. The genes were cloned into the pET 27bmod expression vector and expressed in *E.coli* BL-21(DE3) as N-terminal seven His tagged proteins.

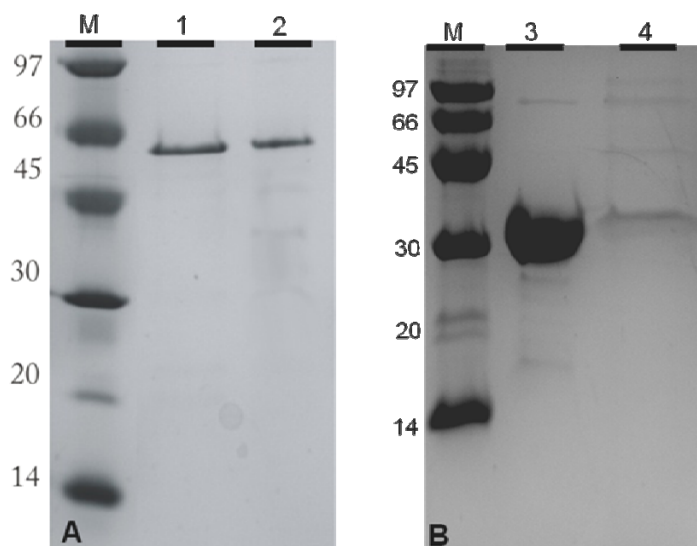


Figure 3-8. (A) Tar [1-553] (B) Tar [1-265] with and without detergent. Coomassie Brilliant blue stained SDS-PAGE of lane 1: Tar [1-553] and lane 3: Tar [1-265] purified from membrane. Lane 2: Tar [1-553] and lane 4: Tar [1-265] purified from cytosol.

In order to test solubility of Tar proteins, membrane and cytosolic Tar proteins were purified using His-tag affinity chromatography. For the preparation of cytosolic Tar, the protein was purified from the cytosolic fraction of cell extracts which do not contain detergent or lipid. After purification, proteins were almost pure as judged from the SDS-PAGE (Figure. 3-8). The SDS-PAGE analysis showed that Tar [residue 1-265] constructs were mainly found in the membrane fraction and that only a very low percentage of the total protein is soluble. However, a similar yield was obtained for Tar [residues 1-553] from both conditions which are depicted in Table 2. These proteins had

## RESULTS

---

an apparent size of approximately 60 (Tar [1-553]) and 30 kDa (Tar [1-265]), as determined by calculation of molecular weight.

Table. 2 Expressed HsHtrII and its analogues

<b>Protein Name</b>	<b>Molecular weight (kDa)</b>	<b>Yield (mg/mL)</b>
Membrane Tar [1-553]	60	2
Cytosolic Tar [1-553]	60	2
Membrane Tar [1-265]	30	5
Cytosolic Tar [1-265]	30	0.4

In contrast to the membrane Tar protein, the cytosolic Tar protein is not stable in the absence of detergent. The cytosolic Tar protein at higher concentration (>1mg/ml) showed the tendency to aggregate. Therefore, only the concentrations within 1mg/ml were biochemically characterized for the cytosolic Tar protein.

## RESULTS

### 3.1.4. Crystallization trials for water soluble HsHtrII

The structure of HsHtrII might provide an insight into the ligand binding of the chemoreceptor family. Water soluble HsHtrII [1-765] as well as HsHtrII [1-398] were used to crystallize. To optimize crystallization conditions, various screens were set up, varying the pH, the molecular weight of the PEG, the concentration of PEG and concentration of ammonium sulfate.

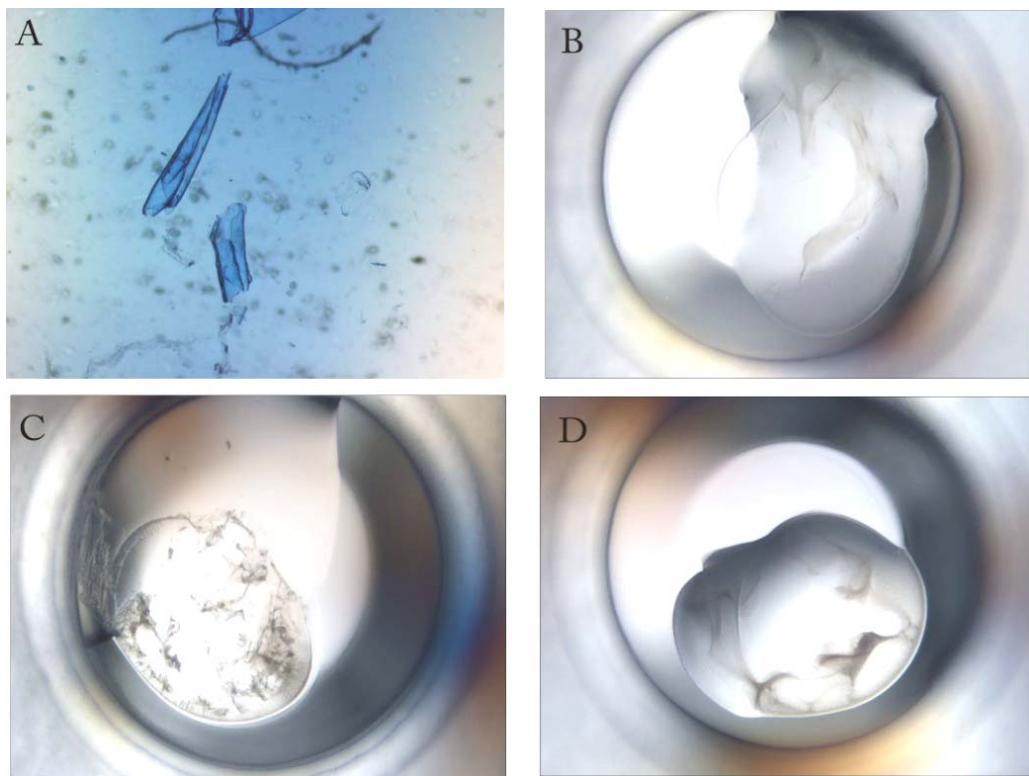


Figure. 3-9 Crystallization screen of cytosolic HsHtrII protein[1-398]. (A) After concentration of protein (~2mg/mL) (B) Classics, (C) JCSG and (D) PACT. Each screening method depends on the content of the reservoir solution. The results were obtained using the vapour diffusion method at 30 °C with protein at concentration of 1 to 2 mg/mL in 30 mM Tris-HCl pH 7.5, 150 mM NaCl, 1 mM EDTA

None of the crystallization trials produced positive results in terms of protein crystals. Water soluble HsHtrII [1-765] quickly precipitated in the buffer under all conditions tested at different pH values. Since full length HsHtrII[1-765] did not yield protein crystals, an alternative strategy was chosen to investigate the

## RESULTS

---

shortened HsHtrII [1-398] and possibly obtain structural data of analogy of the transducer. Interestingly, when HsHtrII [1-398] protein is highly concentrated, it produced sheet-like agglomeration which is fragile (Figure. 3-9A). In order to reduce the protein agglomeration and to increase the growth of single crystals, HsHtrII protein was screened against different additives. The screen of Classics (Figure 3-9B), JCSG (Figure 3-9C) and PACT (Figure 3-9D) condition resulted in similar pattern of protein aggregation. Although various crystallization conditions were tested, crystal of cytosolic HsHtrII protein was not obtained. Absence of detergent may not be a sufficient condition for cytosolic HsHtrII protein.



## 3.2. Biophysical and biochemical characterization

### 3.2.1. Absorption spectrum of HsSRII

To examine the biochemical and biophysical properties of HsSRII protein, the purity was first determined by UV/Vis spectroscopy. As can be seen in Figure 3-10, the ratio between the optical density at 487 nm and 280 nm is calculated to be 1:1.6, corroborating the SDS-PAGE analysis of highly homogeneous protein.

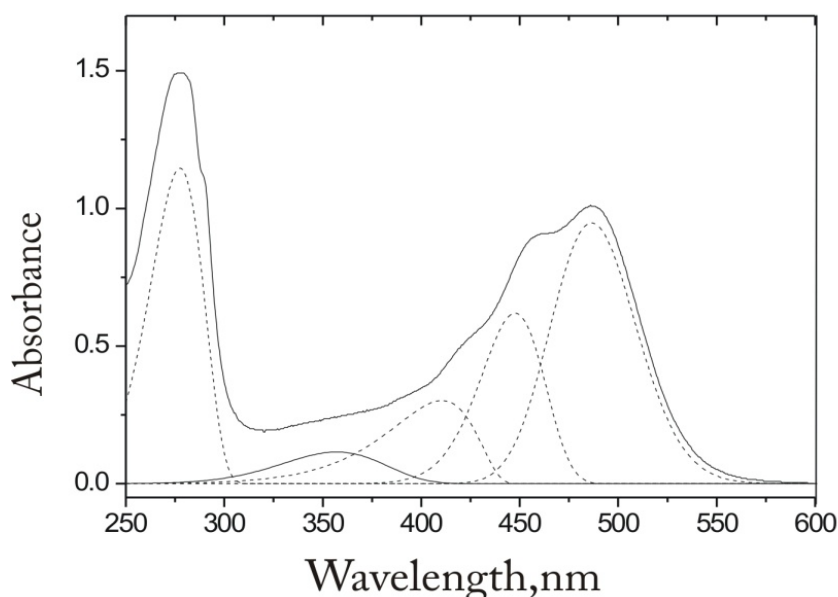


Figure 3-10. UV/Vis absorption spectrum of purified HsSRII. The result of a multi-Gaussian fit (dashed line) show the corresponding spectra of components. The protein was dissolved in 4M NaCl, 50 mM MES, 0.05% DDM, pH 6.

The spectrum displays the typical fine structure observed for SRII proteins (119,124-126). Their absorption maximum in the visible range is at 487 nm accompanied by two distinct vibronic bands at 460 nm and 420 nm. The five dotted bands were derived from the calculated spectrum using skewed multi-Gaussian convolution ((127), (83)). The maxima absorption is found at 487nm and shoulders at 448nm, 411nm, and 364nm, which are close to the values taken directly from the spectrum. Compared to NpSRII maxima absorption

## RESULTS

(497nm, 457nm, 420nm, 370nm), HsSR<sub>II</sub> displays a blue-shift of about 10 nm for maxima absorption.

### 3.2.2. The pH dependent spectral transition and the pK<sub>a</sub> of Asp 73

The carboxyl group of aspartate of the protonated Schiff base is present for all microbial rhodopsins, except halorhodopsin. Protonation of aspartate residue leads to red shift of absorption maxima. The absorption maximum shifts from the 487 nm at pH 6.0 to 530 nm at pH 1.0. Concomitantly, the well-pronounced vibrational fine structure is lost (Figure 3-11, left panel, pink line).

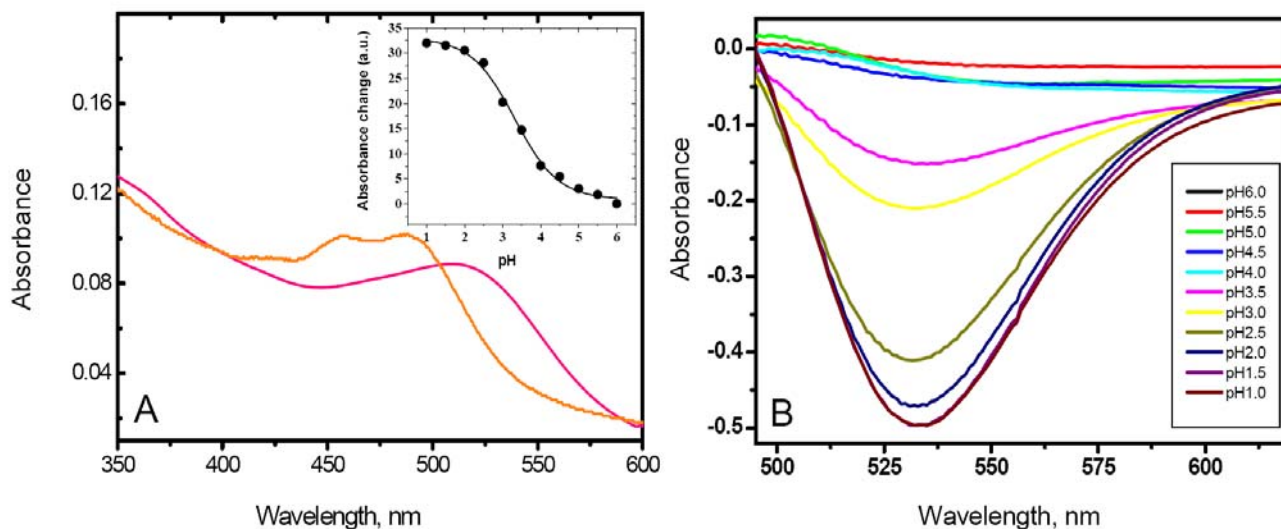


Figure 3-11. Absorption spectrum and pH dependence of HsSR<sub>II</sub>. (A) Absorption spectrum of PML reconstituted HsSR<sub>II</sub> at pH 6.0 (orange line) and pH 1.0 (pink line). (B) Absorption spectra of HsSR<sub>II</sub> embedded in polyacrylamide in the range of pH 6.0 to pH 1.0. Differential spectra were calculated by subtraction of the absorptions recorded at pH 6.0 from each spectrum at lower pH. The integrals of the differential bands were plotted against the pH, and the data were fitted by a sigmoidal function ( $pK_a=3.2$ ).

In order to obtain the pK<sub>a</sub>, HsSR<sub>II</sub> was reconstituted into purple membrane lipids of *H. salinarum*. The spectral shape and the position of the chromophore absorption band of HsSR<sub>II</sub> exhibit significant pH dependence (Figure 3-11). This absorption can be used to determine the pK<sub>a</sub> of Asp 73. The spectrum of

## RESULTS

---

HsSRII was recorded at 11 different pH values in the range from pH 6.0 to 1.0. Differences between spectra were obtained by subtraction of the spectrum taken at pH 6.0 from those measured at lower pH values. The integrals of the negative difference bands were plotted against the pH (Figure. 3-11A, inset). From this curve, a  $pK_a$  for Asp73 of 3.2 was calculated. The  $pK_a$  of aspartate of the four achaeal rhodopsins is depicted in Table 3.

Table. 3 The  $pK_a$  of aspartate

Protein	amino acid	$pK_a$
NpSRII	Asp-75	5.6
BR	Asp-85	2.2
HsSRI	Asp-76	7.2
HsSRII	Asp-73	3.1

FTIR experiments proved that Asp73, the counterion of the Schiff base, is the Schiff base proton acceptor (94). A similar bathochromic shift and loss of fine structure has been described for NpSRII (83) and attributed to the neutralization of the Schiff base counterion. Interestingly, the  $pK_a$  of HsSRII is two order of magnitude lower than that of the corresponding Asp75 in NpSRII ( $pK_a = 5.6$  (83)). A light-dark adaptation noted by Minorova *et al* (124) or small amounts of 13-cis retinal in the dark-adapted protein were not observed in this study. In BR, Asp85, which is crucial in proton pumping has a  $pK_a$  of 2.2 (128). Interestingly, the  $pK_a$  of Asp76 in HsSRI increases from 7.2 to 8.7 upon binding of cognate HsHtrl protein (129).

### 3.2.3. Photocycle of HsSRII

Upon light excitation, all microbial rhodopsins undergo all-trans to 13-cis isomerization, which leads to cyclic reaction sequences. The resulting sequences of intermediates have been denoted analogous to the BR-nomenclature K, L, M, N, O and ground state (115). The photocycle involves not only reversal of the isomerization of retinal but also ion transfer steps and conformational changes of the protein. It has been suggested that the light - activated trans-cis isomerization of retinal allows the transfer of the Schiff

## RESULTS

base proton to the Asp counterion (Asp75)(82,130). In the case of BR and HR, completion of a photocycle takes less than 100 milliseconds, which is effective for ion pumping. On the other hand SRI and SRII possess longer photocycles around 1 sec, which are inefficient pumps. In case of BR pumps, the efficiency of the ion pump requires a high turnover rate, whereas, in sensory SRs, the signaling state has to be sustained long enough to transmit the signal to cognate transducer proteins. The photochemical cycle of HsSRII has not yet been well characterised due to its sensitivity towards external conditions (125). Few data show a photocycle with a sequence of intermediates corresponding to blue shifted L, M intermediates and red shifted O intermediate (33,33,91,131,131,132).

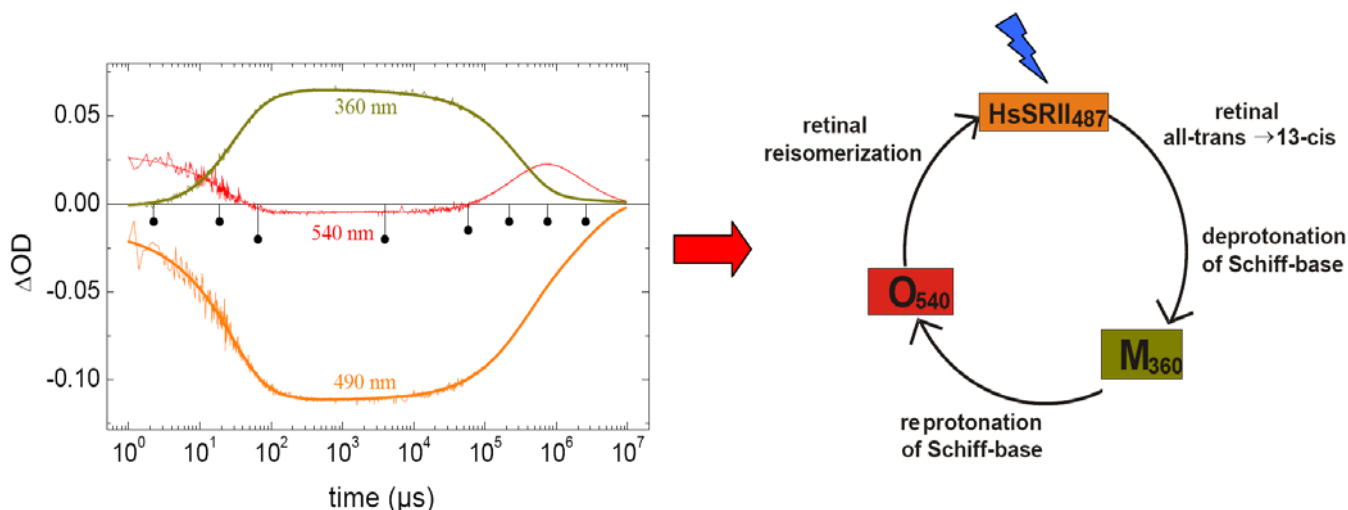


Figure 3-12. Traces of transient absorption changes after pulsed photoexcitation of HsSRII. The protein was dissolved in 4M NaCl, 50mM MES, 0.05% DDM, pH 6. Traces of the transient absorption changes after photoexcitation of HsSRII at 25°C (left panel). The time courses are shown for three selected wavelengths (360, 490 and 540 nm). Simplified scheme of the HsSRII photocycle (right panel).

In order to analyze the photocycle of HsSRII, Laser Flash Photolysis was performed with transient absorption measurements within a short range from microsecond to millisecond. Traces of selected wavelengths are shown in figure 3-12 which are quite similar to those published earlier (124). The solubilized HsSRII was measured at wavelengths 490 nm, 360 nm and 540 nm (Figure 3-12), respectively. The single wavelength excitation (360, 490 and 540 nm) generates each individual intermediate. These wavelengths

## RESULTS

were selected to follow the formation and decay of the characteristic ground-, M and O- photocycle intermediates. The time courses of transient absorption changes allow the calculation of the eight exponents by using multiexponential global analysis (eight closed circles). The schematic drawing (right panel) shows a photocycle with a sequence of intermediates. The upper trace (dark yellow line), monitored at 360nm, and represents the formation and decay of the M-intermediate. The red line, recorded at 540 nm of the red-shifted intermediates O is responsible for reprotonation of Schiff-base and switching to its ground state. The orange line of the ground state is monitored at 490nm.

Table.4 Parameters of the Gaussian fit of the spectra of the HsSRII

	$A_{\max}$	$\rho$	$\Delta\nu, \text{cm}^{-1}$	$\lambda_{\max}, \text{nm}$
$S_1$	$1.00 \pm 0.01$	$1.0 \pm 0.1$	$2116 \pm 113$	$487 \pm 0.9$
$S_2$	$0.67 \pm 0.06$	$1.3 \pm 0.2$	$1944 \pm 255$	$448 \pm 2.1$
$S_3$	$0.31 \pm 0.1$	$1.9 \pm 0.3$	$3264 \pm 1272$	$411 \pm 9.3$
$S_4$	$0.13 \pm 0.1$	$1.3 \pm 0.4$	$4988 \pm 1005$	$364 \pm 12$
$S_5$	$1.87 \pm 0.01$	$1.54 \pm 0.02$	$4342 \pm 36$	$278 \pm 0.06$
$\chi^2$	0.0001			
K	$0.6 \pm 0.2$	$1.1 \pm 0.1$	$3100 \pm 360$	$498 \pm 6$
L, N	$0.4 \pm 0.2$	$1.9 \pm 0.1$	$5930 \pm 440$	$454 \pm 9$
M	$0.72 \pm 0.01$	$1.22 \pm 0.03$	$4990 \pm 50$	$358 \pm 0.4$
O	$0.3 \pm 0.2$	$1.9 \pm 0.6$	$5770 \pm 1630$	$521 \pm 18$
$\chi^2$	0.002			

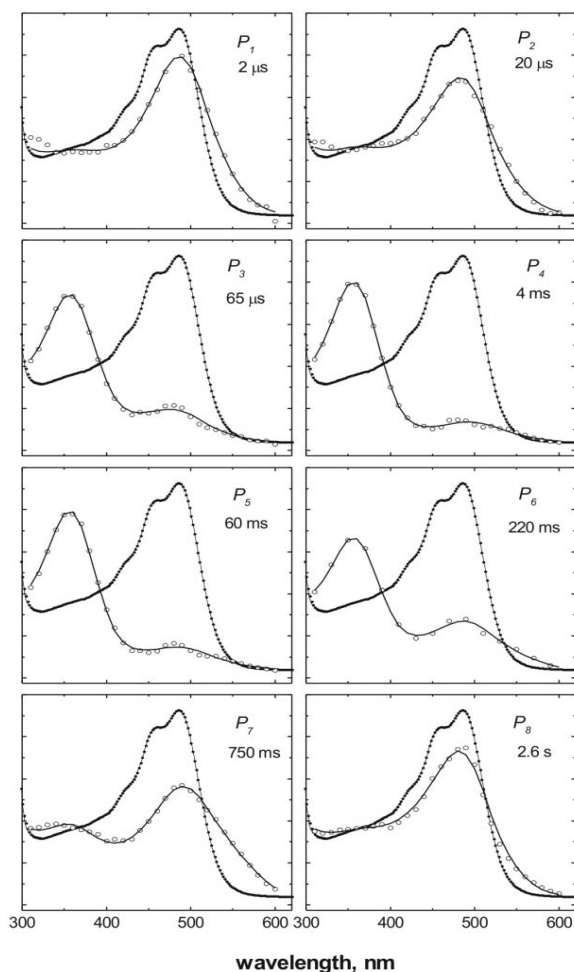


Figure 3-13. Absolute spectra of eight kinetic states  $P_1$ - $P_8$  of the HsSRII photocycle measured at 25 °C. For the sake of comparison, the initial spectrum of HsSRII is also shown in each panel. The figure shows the experimental data (dots) and Gaussian fit (solid lines) of

## RESULTS

---

the absorption spectra of the initial state and those of the kinetics states  $P_1$ - $P_8$ , which were fitted globally using four archetypal chromophore states (i.e. K, L(N), M, and O). The spectra of kinetic states were derived from the difference spectra by variation of the fraction cycling value. Optimal fit of the data were obtained for  $15 \pm 1$  % of cycling molecules after excitation of sample by  $8 \text{ mJ/cm}^2$ , 5 ns, 480 nm laser pulses.

As illustrated in Figure 3-12, the time-resolved photocycle kinetics measured at different wavelengths. By using multiexponential global analysis, the apparent half times ( $\tau_1$  to  $\tau_8$ ) were assigned to the intrinsic transitions assuming an irreversible eight kinetic states ( $P_1$  to  $P_8$ ) of the model. This model allow the calculating the differential spectra from the amplitude of the derived exponential terms. By taking into account fraction of cycling molecules and adding them to spectra of the initial states, the absolute spectra of kinetic states were obtained(133). Figure 3-13 shows the ground spectrum with absolute spectra in each panel. Fitting parameters are given in Table 4. From the fit, the number of spectral states and their amplitudes are obtained for each kinetic state. By comparing their appearance and relative spectral position with the intermediates of the BR photocycle, one can describe them as K-, L(N)-, M- and O-like spectral intermediates (HsSRII<sub>500</sub>, HsSRII<sub>460</sub>, HsSRII<sub>360</sub>, HsSRII<sub>520</sub>, respectively). The relative concentrations of the spectral states can be calculated from the corresponding amplitudes. From the absorption maxima, the first emerging kinetic state ( $P_1$ ) revealed at 498 nm which corresponds to K- like intermediate of HsSRII (2  $\mu\text{s}$  at 25°C). The next  $P_2$  kinetic state (20  $\mu\text{s}$ ) shows a single maximum ( $\lambda_{\text{max}}=460 \text{ nm}$ ), which corresponds to the L-intermediate. The  $P_3$  (65  $\mu\text{s}$ ) kinetic state fits two intermediate spectra ( $\lambda_{\text{max}}=460$  and 360 nm), which correspond fast quasi-equilibria between two archetypal chromophore states (L- and M-likes intermediate). It is obvious that almost pure M-like intermediates ( $\lambda_{\text{max}}=360 \text{ nm}$ ) exist ( $P_4$  and  $P_5$ ), which are connected by a spectrally silent transition (4ms). The  $P_6$  and  $P_7$  states represent fast equilibrium between the other neighbouring spectral intermediates. It should be noted that the normalized sum of the species of all kinetic states are always close to unity, thus indicating that the assumption of quasi-equilibria is valid. A scheme of photocycles is shown in Figure 3-14. The kinetic state  $P_8$  has the longest

## RESULTS

lifetime (2.6 s at 25°C) of all intermediates. Compared to NpSRII spectral intermediates (  $L_{495}$  and  $M_{400}$ ), photocycle intermediates of HsSRII displays a blue-shift of about 40 nm (  $L_{460}$  and  $M_{360}$ ). In comparison with the kinetic states of the NpSRII, the kinetic of HsSRII is nearly two times slower than that of NpSRII. It is important to note that the functionally important  $M_1$ - $M_2$  transition (4 ms) is two folds lower than that of NpSRII (2 ms).

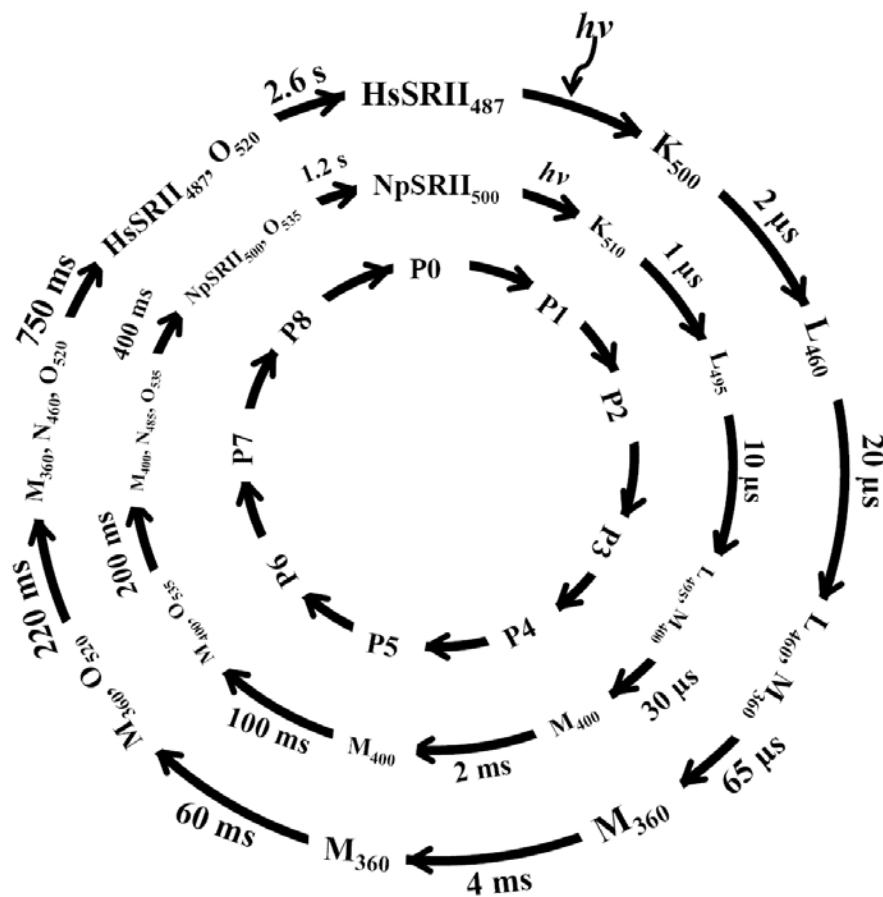
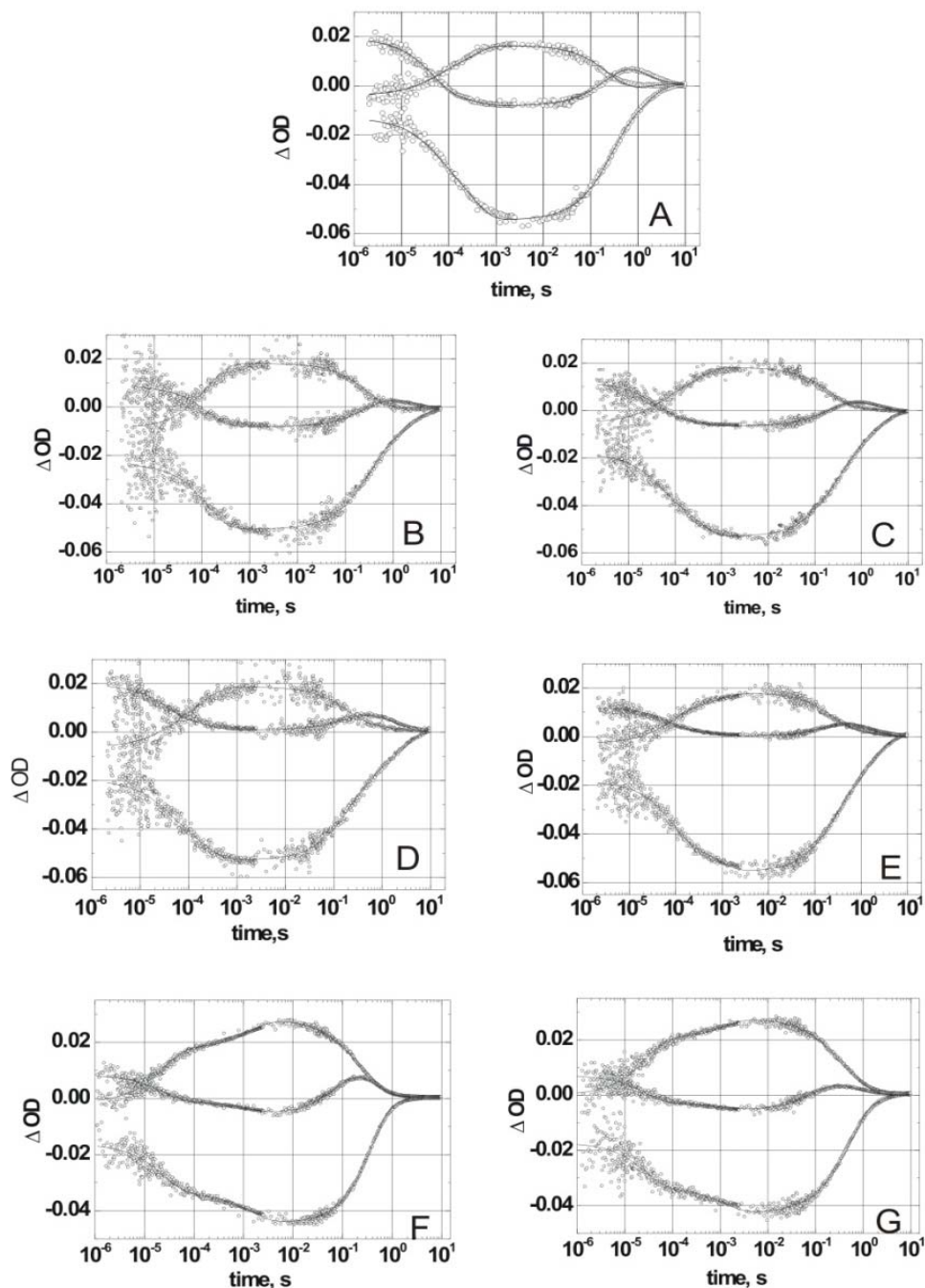


Figure 3-14. Photocycles for HsSRII and NpSRII

In order to analyze photocycle kinetics of HsSRII in complex with HsHtrII, the solubilized HsSRII-HsHtrII complex was reconstituted into purple membrane lipid from *H. salinarum*. The flash induced absorption changes of HsSRII and its complex with HsHtrII analogues are shown in Figure 3-15. The traces at 490 nm represent depletion and recovery of the ground state and those at 350 nm and 550 nm display formation and decay of M- and O-

## RESULTS

intermediate, respectively. The four rate constants were obtained by using the global fit analysis (Table 5). According to the result of the kinetic evaluation described above, it was not sufficient to fit the experimental data with eight exponential components. Only four rate constants could be fitted for reconstituted proteins in the global fit analysis, probably due to noisy transient absorption changes with a poor quality of signal-to-noise ratio.





## RESULTS

Figure 3-15. Photocycle measurements of receptors and its five complexes. Measurements were performed at 25 °C (4M NaCl, 50 mM MES, pH 6) at three different wavelengths (360 nm, 490 nm, 540nm). (A) HsSRII, (B) HsSRII-HsHtrII[1-398] (C) HsSRII- HsHtrII[1-765] (D) HsSRII-HsHtrII[1-398 $\Delta$ 38-280], (E) HsSRII- HsHtrII[1-765 $\Delta$ 38-280] (F) NpSRII, (G) NpSRII-HsHtrII[1-398]. Absorbance changes are depicted for 360 nm, 490 nm and 540 nm for HsSRII and its complexes. The absorbance changes for NpSRII and its NpSRII-HsHtrII[1-398] complex were measured at 360 nm, 490 nm and 540nm. These wavelengths are characteristic for the formation and decay of the M-like, ground-, and O-like state, respectively.

Table 5. Rate constants of HsSRII and HsSRII/HtrII complexes

	$\tau_1$	$\tau_2$	$\tau_3$	$\tau_4$
HsSRII pH 6	40 $\mu$ s	290 $\mu$ s	235ms	1.4s
HsSRII pH 3	80 $\mu$ s	490 $\mu$ s	80ms	0.6s
HsSRII/HsHtrII(1-765)	47 $\mu$ s	130 $\mu$ s	283ms	2.45s
HsSRII/HsHtrII(1-765) $\Delta$ LBD	36 $\mu$ s	200 $\mu$ s	210ms	2.14s
HsSRII/HsHtrII(1-398)	40 $\mu$ s	300 $\mu$ s	226ms	1.94s
HsSRII/HsHtrII(1-398) $\Delta$ LBD	80 $\mu$ s	840 $\mu$ s	232ms	1.70s
NpSRII	20 $\mu$ s	1.42ms	100ms	0.34s
NpSRII /HsHtrII(1-398)	30 $\mu$ s	1.22ms	112ms	0.62s

Turnover and rate constants are hardly affected by binding of HsHtrII or its analogues to HsSRII although O-intermediate amplitude is reduced on transducer binding (minor differences obtained for HsHtrII[1-398 $\Delta$ 38-280] are probably due to low concentration of sample). This observation indicates, as discussed by Sasaki and Spudich (91), an influence of the transducer on the equilibrium between late photocycle intermediates. Interestingly, binding of HsHtrII to NpSRII also reduces the amplitude of the O-intermediate (panel F & G) indicating that a functional complex is formed (Figure 3-15). The light-induced transient absorption changes of NpSRII and NpSRII-HsHtrII-398 complex measured at representative wavelengths (350nm, 490nm and 540nm /550nm) shows that the photocycle properties of HsSRII in the presence of HsHtrII are quite similar to that of NpSRII.

### 3.2.4. Blue native gel of the NpSRII-HsHtrII complex formation

The photocycle experiments indicated that the NpSRII -HsHtrII [1-398] complex forms a structurally similar HsSRII -HsHtrII [1-398] interface. To

## RESULTS

verify this assumption, the blue native gel electrophoresis was carried out with HsHtrII [1-398] which is the expected interaction partner of NpSRII. In a typical experiment, HsHtrII[1-398] was mixed with increasing amounts of NpSRII.

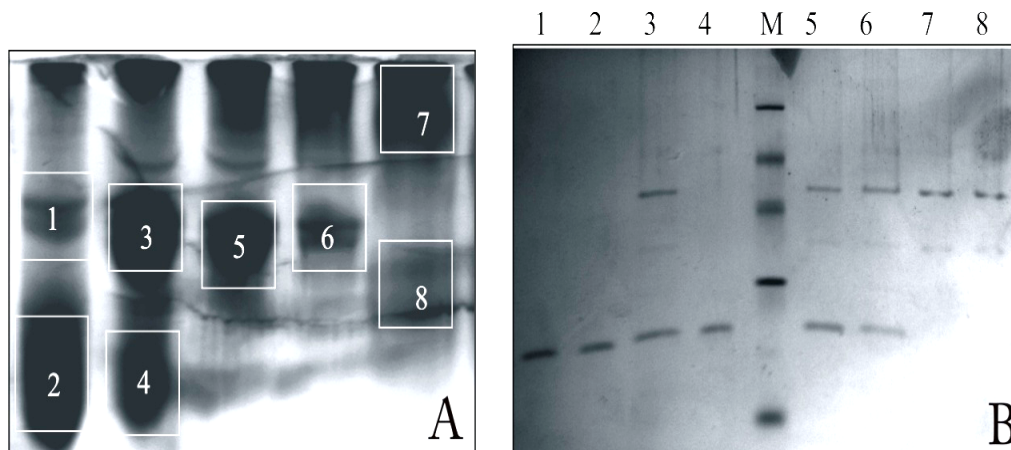


Figure 3-16. BN-PAGE of NpSRII and HsHtrII[1-398] at different concentrations (A) The solubilized proteins NpSRII (lane 1) and HsHtrII [1-398] (lane 5) were mixed at molar ratios of 5:1 (lane 2), 1:1 (lane 3) and 1:5 (lane 4). (B) Analysis of the marked bands with SDS-PAGE. After incubation of the samples for one hour at room temperature aliquots were loaded on the gel. The numbered boxes correspond to those in the BN-PAGE.

To identify the individual proteins and complex, the selected bands (numbered boxes) were excised from the gel, equilibrated with SDS buffer, and subjected to 12% SDS-PAGE. Although the amount of HsHtrII[1-398] mixed with NpSRII was five times smaller than NpSRII (Figure 3-16A, lane 2), NpSRII forms complex with HsHtrII [1-398] and the unbound NpSRII (box 2) is substantially reduced (box 4) in the presence of HsHtrII [1-398]. At a mixing ratio of 1:1 only a major band of NpSRII-HsHtrII[1-398] complex was observed in box 5. An effect of ionic strength on the dimerisation and heterocomplex formation was not observed. Taken together, these results indicate that HsHtrII interacts with NpSRII with a 1:1 binding stoichiometry.

### 3.2.5. Analytical Size-Exclusion Chromatography

The stoichiometry of HsSRII-HsHtrII complexes, as well as the affinity of the interactions, is not yet known. Furthermore, no data is available to draw

## RESULTS

conclusions about possible oligomerization of each protein. Due to the necessity of high salt concentration for HsSRII stability (4M NaCl), blue native gel electrophoresis (max. 50 mM NaCl buffer) could not be performed at physiological salt concentration.

To test whether HsSRII is able to bind with shortened HsHtrII[1-398] and to characterize possible oligomeric states of the transducer molecule and its complex with HsSRII at high salt concentration (4M NaCl), analytical gel filtration and SDS-PAGE analysis were chosen.

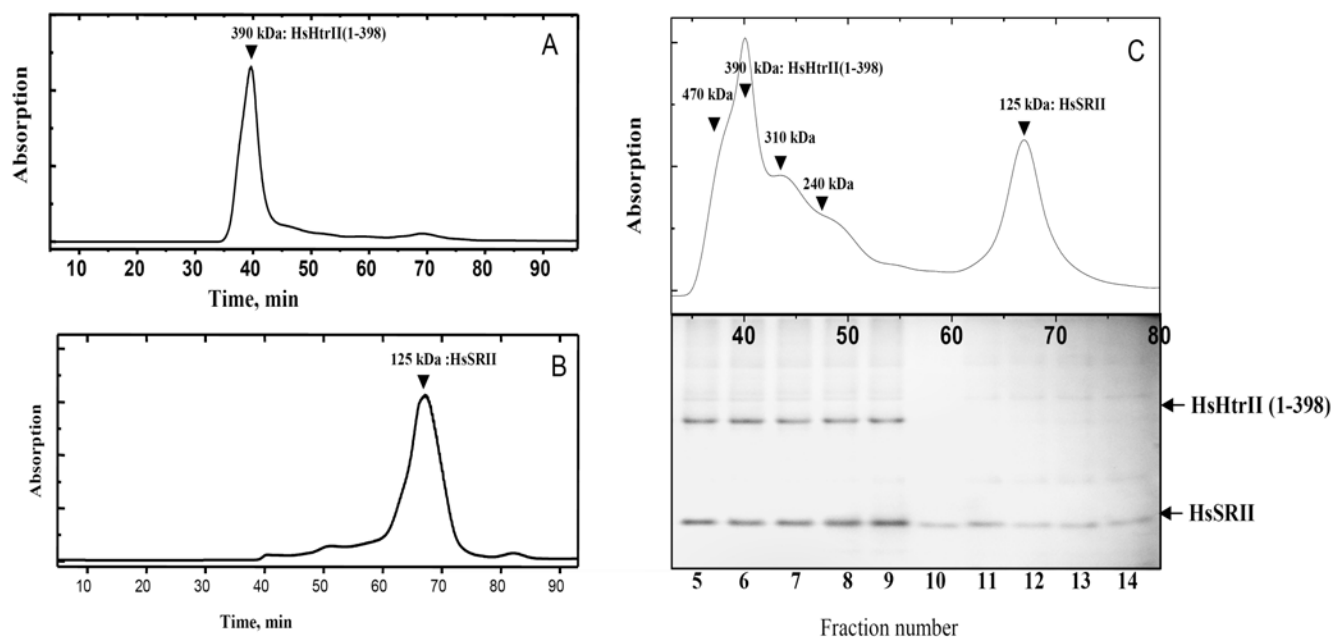


Figure 3-17. Size exclusion chromatogram (Superdex 200 10/300 GL) of solubilized (A)HsHtrII [1-398], (B)HsSRII and (C) HsSRII-HsHtrII mixture and SDS PAGE (low panel); All fractions show a single band on an SDS-PAGE which represents monomeric HsHtrII and HsSRII. The absorbance was monitored at 280 nm.

The HsHtrII[1-398] eluted at retention times from 35 min to 45min (Figure 3-17A). These molecular weights were calculated from the combination of proteins and an average DDM micelle size of around 70-74 kDa (134). Taking the molecular weight of HsHtrII[1-398] (43 kDa) and the micelle size into account, it appears to be a hexamer with a molecular size of about 320 kDa or an even higher-order oligomer. HsSRII eluted at retention times from 60 min to 75 min (Figure 3-17B). The elution profile of HsSRII showed a single peak

## RESULTS

---

with an apparent size of ~125 kDa, which is in good agreement with a dimeric state of HsSRII. For analysis of complexes, equimolar mixture of HsSRII with and HsHtrII was pre-incubated for one hour at 4°C. After incubation, the mixture was separated on a 10/300 superdex column in 4M NaCl 50 mM MES and 0.05% DDM at pH 6 (Figure 3-17C, upper panel). The chromatogram changed when HsSRII is added to HsHtrII[1-398] in a 1:1 stoichiometry. The fractions from the HsHtrII/HsSRII mixture were collected and analyzed with SDS-PAGE (Figure 3-17C, low panel). HsSRII band is detected in all fractions from 5 to 14. The complex formation was observed as a shift in retention times of peak that are eluted from 35 min to 50 min with several shoulders (470, 310, 240 kDa). SDS-PAGE of each of the fractions revealed that most of HsSRII were forming complexes with HsHtrII [1-398].

### **3.2.6. Isothermal titration calorimetry (ITC) of receptor-transducer binding**

The association of microbial rhodopsin proteins to form a functional complex has only been elucidated in a few examples. Especially, quantitative thermodynamic information of membrane protein assembly is mostly lacking due to the special nature of this protein family. It has been shown that NpHtrII binds to its receptor NpSRII with a dissociation constant in 100 nanomolar range (135,136). It was observed that the reactions of NpSRII with the transducer fragments are exothermic with  $\Delta H = -17.9 \text{ kJ mol}^{-1}$  for shortened construct NpHtrII[1-157] and  $\Delta H = -17.6 \text{ kJ mol}^{-1}$  for NpHtrII[1-114]. Compared to NpSRII, HsSRII is very labile and tends to aggregate at temperature over 25°C in a low salt concentration. Thus, in order to prevent aggregation, ITC measurement was performed at high salt concentration (4M NaCl) as shown in Figure 3-18. All constructs have dissociation constants of around 1  $\mu\text{M}$ . As can be seen from Table 6, the dissociation constants ( $K_D$ ) of these complexes were estimated to be  $1.14 \pm 0.8 \mu\text{M}$  for HsHtrII[1-765],  $1.42 \pm 0.3 \mu\text{M}$  for HsHtrII[1-765 $\Delta$ LBD],  $0.86 \pm 0.7 \mu\text{M}$  for HsHtrII[1-398] and  $1.09 \pm 0.4 \mu\text{M}$  for HsHtrII[1-398 $\Delta$ LBD]. Experiments with the HsSRII as well showed an exothermic reaction with  $\Delta H = -16.8 \text{ kJ mol}^{-1}$  for HsHtrII-765,  $-25.5 \text{ kJ mol}^{-1}$

## RESULTS

for HsHtrII[1-398],  $-15.7 \text{ kJ mol}^{-1}$  for HsHtrII[1-765 $\Delta$ LBD] and  $-21.4 \text{ kJ mol}^{-1}$  for HsHtrII[1-398 $\Delta$ LBD].

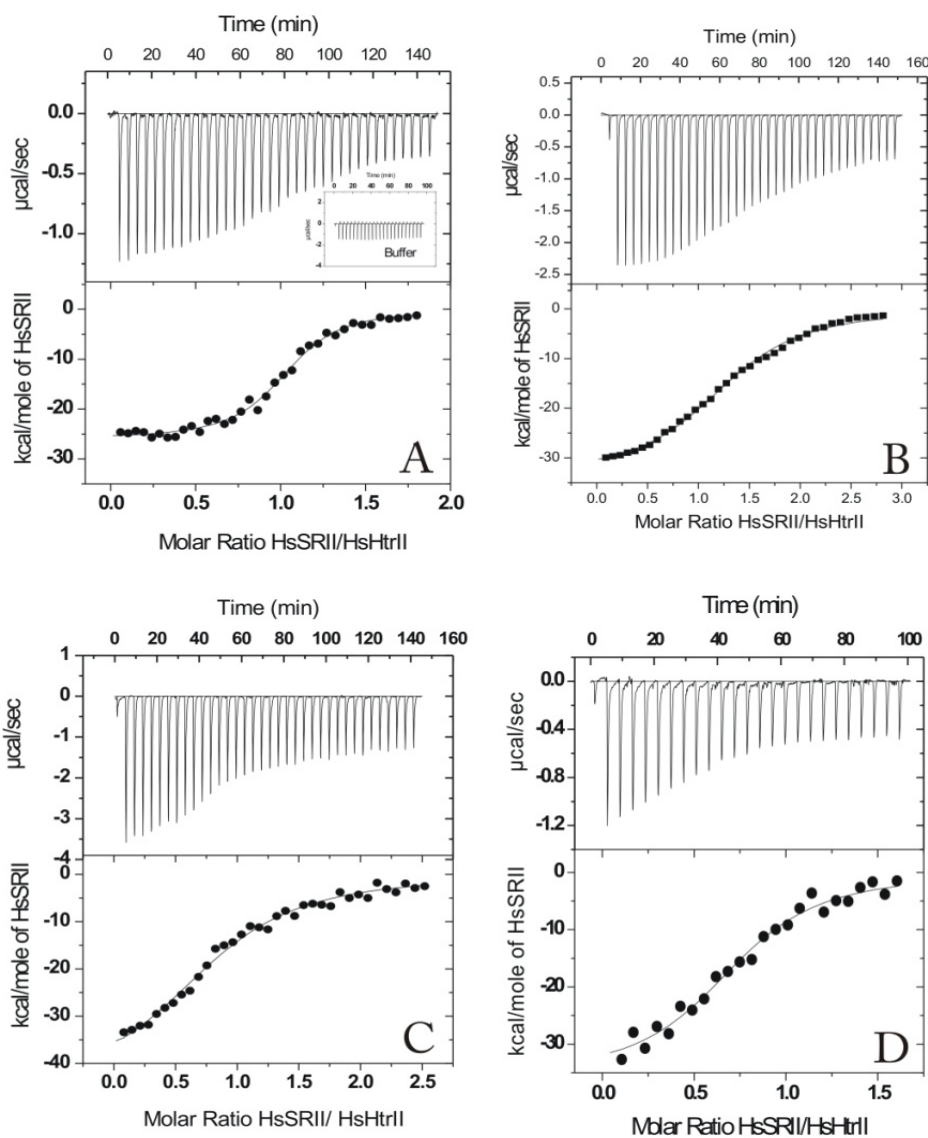


Table 6. Thermodynamic parameters

	pH	T(K)	$\Delta H^\circ(\text{kJ mol}^{-1})$	K ( $\text{M}^{-1} \cdot 10^5$ )	$\Delta G(\text{kJ mol}^{-1})$	$T\Delta S(\text{kJ mol}^{-1} \cdot \text{K}^{-1})$	$K_D(\mu\text{M})$
HsHtrII (1-765) (HsSRII)	6	293	-26.8	8.7	-12.6	-14.2	1.14
HsHtrII(1-765) $\Delta$ 38-280 (HsSRII)	6	293	-45.7	7.3	-18.7	-27.2	1.42
HsHtrII(1-398) (HsSRII)	6	298	-31.5	11.6	-20.3	-11.2	0.86
HsHtrII(1-398) $\Delta$ 38-280 (HsSRII)	6	298	-36.4	9.1	-11.6	-24.8	1.09
HsHtrII(1-398) (NpSRII)	7	308	-20.2	4.7	-21.9	1.7	2.12
HsHtrII(1-147) (HsSRI)	6	303	-11.5	9.5	-21.4	9.9	1.05

Figure 3-18. Isothermal titration calorimetry: receptor-transducer. (A) HsSRII- HsHtrII[1-765], inset: buffer control (B) HsSRII-HsHtrII[1-398], (C) HsSRII- HsHtrII[1-765 $\Delta$ 38-280], (D)

## RESULTS

HsSRII-HsHtrII[1-398 $\Delta$ 38-280]. The upper panels represent the raw data after baseline correction. In the lower panels, the integral of the upper spikes (enthalpy change) are plotted against the molar ratio of receptor to transducer analogues. The binding parameters are listed in Table 3.

The x-ray crystallographic structure of the NpSRII-NpHtrII complex shows that five amino acids were important for binding and comprise Thr-189 and Tyr-199 in NpSRII which form hydrogen bonds with NpHtrII residues Asn-74, Ser-62, and Glu-43 (17,137-139). Homologous amino acids are also found in *H. salinarum* system. Thr-187 and Tyr-197 in HsSRII correspond to Thr-189 and Tyr-199 in NpSRII, respectively. Ser-282, Ser-294 and Gln-38 in HsHtrII correspond to Ser-62, Asn-74 and Glu-43 in NpHtrII, respectively (140).

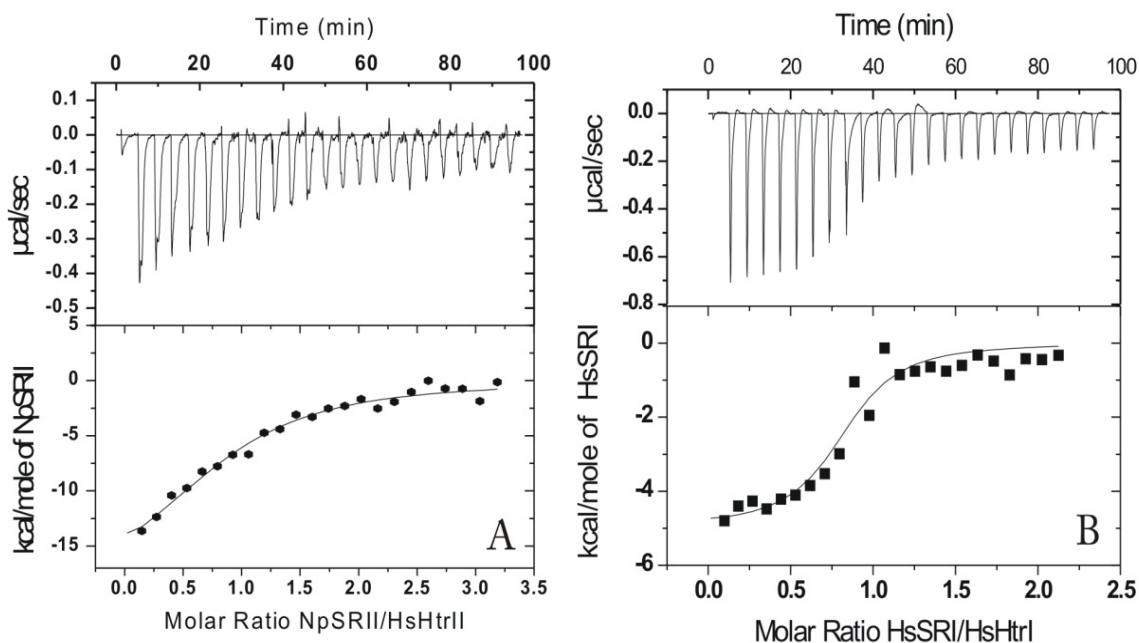


Figure 3-19. Isothermal calorimetric titration of (A) NpSRII (170 $\mu$ M) into a HsHtrII[1-398] solution (20 $\mu$ M) and titration of (B) HsSRI (250  $\mu$ M) into a solution of HsHtrI [1-147](20  $\mu$ M), in 50Mm MES, 4M NaCl, 0.05% DDM at pH 6. The upper panels represent the raw data after baseline correction. In the lower panels the integral of the upper spikes (enthalpy change) are plotted against the molar ratio of receptor to transducer analogues. The binding parameters are listed in Table 3

## RESULTS

---

These similarities suggest that HsHtrII might not only bind to its cognate receptor HsSRII but also to NpSRII. In order to test this assumption, calorimetric titrations were performed. It is also interesting to compare this data with HsSRI-HsHtrI from *H.salinarum*. The binding parameters of thermodynamic data are listed in Table 3. As shown in figure 3-19A, ITC measurement showed that NpSRII binds to HsHtrII, although the affinity was two-fold lower with estimated  $K_d$  value of 2.12  $\mu$ M. (Table 3). Apparently, HsSRII can be substituted by NpSRII without losing substantial binding affinity, suggesting that the binding of HtrIIs to SRIIs is not very species-specific at variance from that observed for the SRII /SRI system (141). The experimental data also indicates that neither the extracellular domain of HsHtrII nor its cytoplasmic domain is involved in binding to HsSRII. These results corroborate data obtained for NpHtrII showing that a minimal binding domain comprising the two transmembrane helices (NpHtrII[1-114]) is sufficient for binding(135).

For all constructs, a binding stoichiometry close to 1:1 was obtained. Salt dependency of the complex formation was found to be negligible, indicating that mainly hydrophobic interactions contribute to the binding of HsHtrII to HsSRII, in agreement with the natural habitat of *H. salinarum*. The specificity of the latter protein-protein interaction is certainly due to the fact that both receptor systems occur in *H. salinarum*. Spudich and coworkers (142) demonstrated that a minimal fragment (1-147) of the HtrI transducer leaves the wild type pH-insensitive photocycle unaffected.

## RESULTS

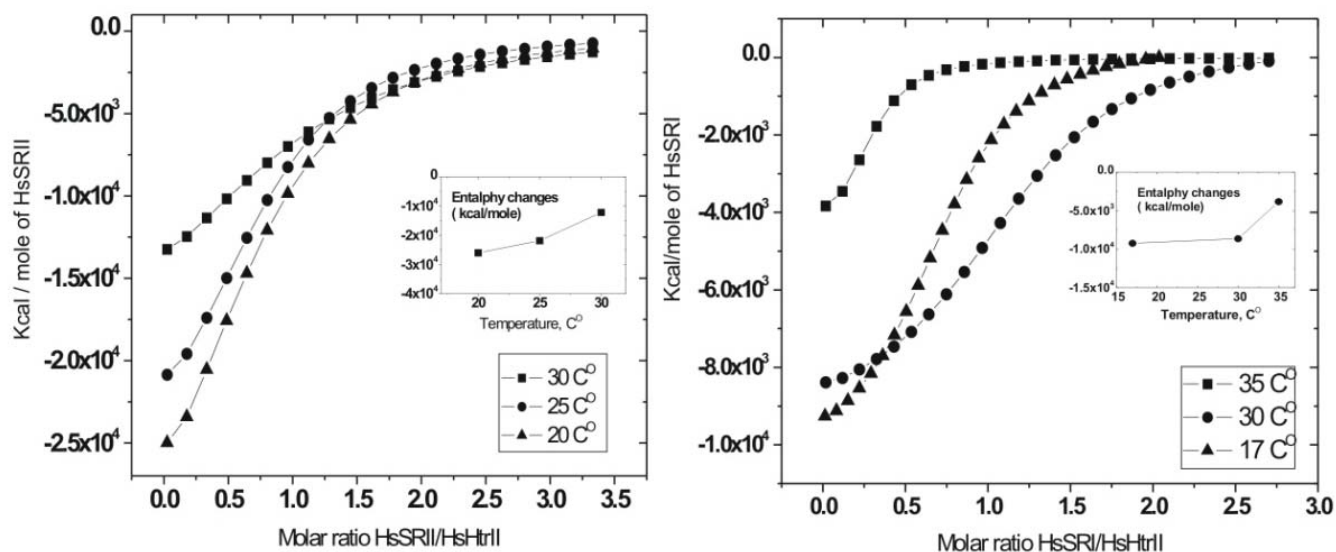


Figure 3-20. Temperature dependence of HsSRII-HsHtrII-398 interaction. (A) ITC measurements of HsSRII with HsHtrII[1-398] (B) HsSRI with HsHtrI[1-147] performed at different temperatures ranging from 20 to 35 °C. Inset: Binding enthalpy changes ( $\Delta H$ ) are shown in each panel.

To obtain more insight into this process and to determine temperature dependency and enthalpy changes, the heat capacity measurements for complex formations of HsHtrII-HsHtrII[1-398] and HsSRI-HsHtrI[1-147] were carried out by ITC in 4M NaCl, pH 6, 50 mM MES, 0.05% DDM at different temperature. As shown in Figure 3-20A, ITC titration of HsSRII with HsHtrII[1-398] at three different temperatures 20, 25 and 30 °C yielded equilibrium binding constants  $K_D = 1.2 \mu\text{M}$ ,  $1.7 \mu\text{M}$  and  $3 \mu\text{M}$ , respectively. The raw data of temperature changes were collected from fitted curves of HsSRII binding to HsHtrII[1-398] and HsSRI binding to HsHtrI[1-147] (Figure 3-20). These values are then plotted and  $\Delta C_p$  values were estimated in Figure 3-20 (inset). In the case of HsSRII-HsHtrII[1-398], the value of heat capacity obtained from the temperature range between 20 and 25 °C ( $0.82 \text{ kcal/mol K}$ ) is different from the range between 25 and 30 °C ( $1.9 \text{ kcal/mol K}$ ) as shown in Figure 3-20A. Similar results were obtained for the binding affinity of SRI and HsHtrI (1-147). The dissociation constant for the binding was determined to be  $1.05 \mu\text{M}$  at 17 °C. For HsSRI-HsHtrI[1-147] complex formation,  $\Delta C_p$  is much lower than that of the HsSRII-HsHtrII[1-398] complex formation. The values for



## RESULTS

---

temperature ranges between 17 and 30°C and between 30 and 35°C are calculated as 0.047 and 0.96 kcal/mol K, respectively.

$\Delta C_p$  is obtained as the slope of a plot of  $\Delta H$  versus the temperature. In general, heat capacity change has been directly related to the solvent-exposed hydrophobic surface area. Both complexes showed temperature dependence with lower negative enthalpy ( $\Delta H$ ) which suggests an unfavourable interaction. The heat capacity change was found to be positive, indicating that a hydrophobic surface of protein is exposed to solvent. Low  $\Delta C_p$  (0.047 kcal/mol K) suggests that a very low number of hydrophobic groups become exposed to water. At temperatures below 30°C, the HsSRI-HsHtrI[1-147] complex is stable with substantial affinity range ( $K_D=1-3 \mu\text{M}$ ), whereas the affinities drastically decrease above 35°C ( $K_D > 20 \mu\text{M}$ ). Brounillette et al (143) have shown that the thermal denaturation of bacteriorhodopsin (BR) yields an enthalpy change about 100 kcal/mol at 100°C. The temperature-dependent enthalpy changes above 80°C yield a  $\Delta C_p$  of 0.046 kcal/mol K, whereas the only loop region yields a  $\Delta C_p$  of 1.2 kcal/mol K. One can conclude that the loop regions (extramembrane part) become exposed to water more than the transmembrane part of bacteriorhodopsin (BR). These results carry implications for conformational changes of complex formation. The relatively small value of  $\Delta C_p$  (0.047 kcal/mol K) for HsSRI-HsHtrI[1-147] complex formation indicates retention of thermal stability of a transmembrane  $\alpha$ -helix. However, the high value of  $\Delta C_p$  (1.9 kcal/mol K) reflects that a very large number of hydrophobic groups become exposed to water, indicating that a relatively high temperature may mainly affect the flexible extramembrane of HsHtrII-HsHtrII[1-398] complex.

### 3.2.7. Circular Dichroism (CD) spectroscopy of HsHtrII constructs and Tar chemoreceptor

CD analysis of HsHtrII constructs; In order to study the structural integrity of HsHtrII protein, the salt dependence of HsHtrII constructs was investigated at two different salt conditions by CD measurements. UV-CD spectra of four analyzed HsHtrII constructs at 20°C are shown in Figure 3-21. The circular dichroism spectra of various HsHtrII constructs exhibit double negative minima at 208 and 222nm, which are typical for  $\alpha$ -helical structure.

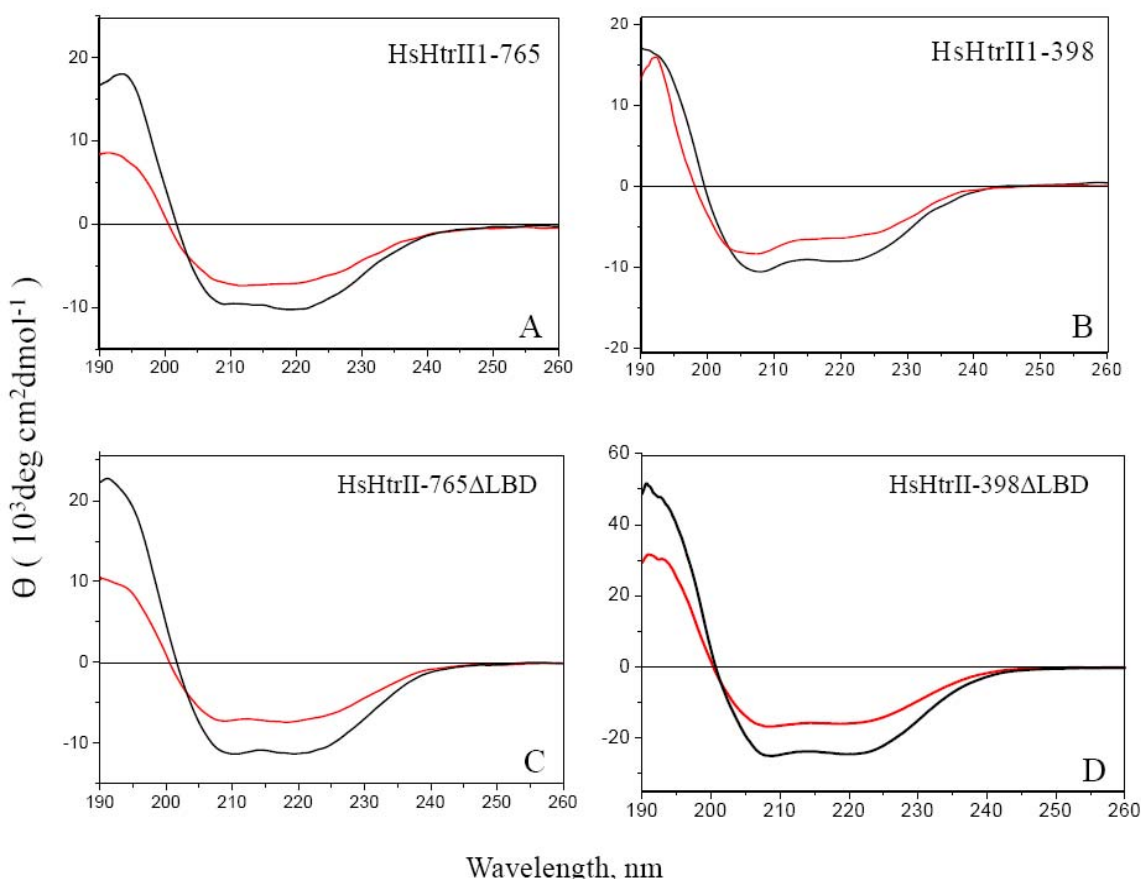


Figure 3-21. CD spectra of HsHtrII and its analogues. Salt-induced conformational changes of (A) HsHtrII[1-765], (B) HsHtrII[1-398], (C) HsHtrII[1-765 $\Delta$ 38-280] and (D) HsHtrII[1-398 $\Delta$ 38-280] in 4M KF, 20 mM KPi, 0.05% DDM, pH 6.0 (black curve) and proteins in 50 mM KF, 20 mM KPi, 0.05%, pH 6.0 (red curve). The CD signal is given in arbitrary units. Protein was diluted in the respective buffer to a concentration suited for CD spectroscopy. Data collection was performed at 20°C.

## RESULTS

Dramatic reduction in the negative molar ellipticity was observed when high salt concentration (4M, black curves) was exchanged by low salt concentration (50mM, red curves). The intensities of HsHtrII constructs significantly decrease in the  $\alpha$ -helical negative molar ellipticity at 208 and 222nm. The secondary structures of various constructs were calculated using computer-modeling program (CCA, ContinII, CDSSTR) which are depicted in Table 7. The best fit of the CD spectrum of HsHtrII[1-765] in 4M KF buffer (black curve) (Figure 3-21A) indicated that 77% were  $\alpha$ -helices, 2% were  $\beta$ -sheets and the rest were random coil. The content of the  $\alpha$ -helical in 50 mM salt buffer was estimated to be 56.4%. Similar results were obtained for HsHtrII analogues. Interestingly, The  $\alpha$ -helical contents of HsHtrII [1-398 $\Delta$ LBD] slightly decreased in the  $\alpha$ -helical contents from 87.3 (4M salt buffer) to 82 % (50 mM salt buffer). The marginal differences in helical content might reflect the minor alteration in the relatively small portion of the change in extramembrane with stable transmembrane assembly. These observations indicate that HsHtrII protein fold into predominantly  $\alpha$ -helical secondary structure at high salt concentration. Thus, the observed gain in negative ellipticity could be attributed to the formation of a higher degree of  $\alpha$ -helical contents induced by high salt concentration. The HsHtrII proteins seemed to be partially unfolded because of the increases of random coil contents at low salt concentration.

**Table. 7. CD analysis of HsHtrII constructs and Tar chemoreceptor (REF:(144))**

	salt concentration	$\alpha$ -helix(%)	$\beta$ -sheet(%)	turn(%)	random(%)
HtrII(1-765)	4M (membrane)	77	2	8.5	18.2
	4M (cytosolic)	72	3	10.4	24
	50mM	56.4	7.7	14.2	24.8
HtrII(1-765 $\Delta$ LBD)	4M (membrane)	83	1.3	5.1	10.1
	50mM	68.8	6.7	12.6	22.4
HtrII(1-398)	4M ( membrane)	60	4.2	15.6	26.6
	4M ( cytosolic)	54	5.1	17.5	30.4
	50mM	46	10.3	19.3	34.6
HtrII(1-398 $\Delta$ LBD)	4M	87.3	6	7.9	16.1
	50mM	82	9	4.2	22.1
Tar (1-553)	4M	69.2	5.3	10	35.4
	50mM (membrane)	73((78)(REF))	2	4	24((22)(REF))
	50mM (cytosolic)	68.7	4.5	6.3	37.3

## RESULTS

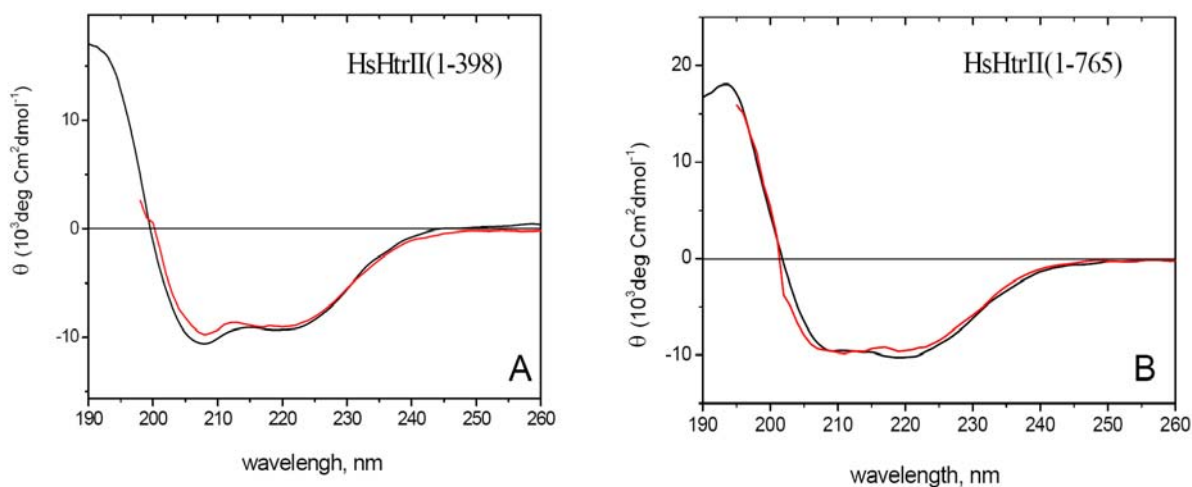


Figure 3-22. CD spectra of (A) HsHtrII[1-765] and (B) HsHtrII[1-398]. Proteins in 4M KF, 20 mM KPi, 20 mM KPi, 0.05% DDM, pH 6.0 (black curve) and proteins in 50 mM KF, 20 mM KPi, pH 6.0 (red curve). The CD signal is given in arbitrary units. Protein was diluted in the respective buffer to a concentration suited for CD spectroscopy. Data collection was performed at 20°C.

For further investigation was necessary to establish the integrity of detergent free HsHtrII. The secondary structure of detergent-free HsHtrII protein was analyzed. Apparently, the CD spectra of detergent free HsHtrII constructs are almost identical to the detergent solubilized HsHtrII constructs, as shown in Figure 3-22A and 22B (red curve). Both detergent-free HsHtrII[1-765] and HsHtrII [1-398] proteins exhibited  $\alpha$ -helical contents of 72% and 54%, respectively. It reveals that the detergent free HsHtrII[1-765] and HsHtrII[1-398] contain quite similar  $\alpha$ -helical secondary structure to the detergent solubilized samples.

CD analysis of HsHtrII-LBD [42-285] and HsHtrII-HAMP [303-465]; To examine the properties of ligand binding domain (LBD) and HAMP domain, CD analysis was performed in different salt conditions. Since extracellular domain and HAMP domain are expected to be involved in signal transfer, each functional domain can provide direct information on the conformational changes in the secondary structure. Figure 3-23 shows the CD spectra of HAMP and LBD protein in 50 mM KF and 4 M KF at pH 6 to characterize and compare the salt dependency. The CD spectra of LBD showed characteristic

## RESULTS

minima at 200 nm which is typical for random coils (Figure 3-23A, black curve).

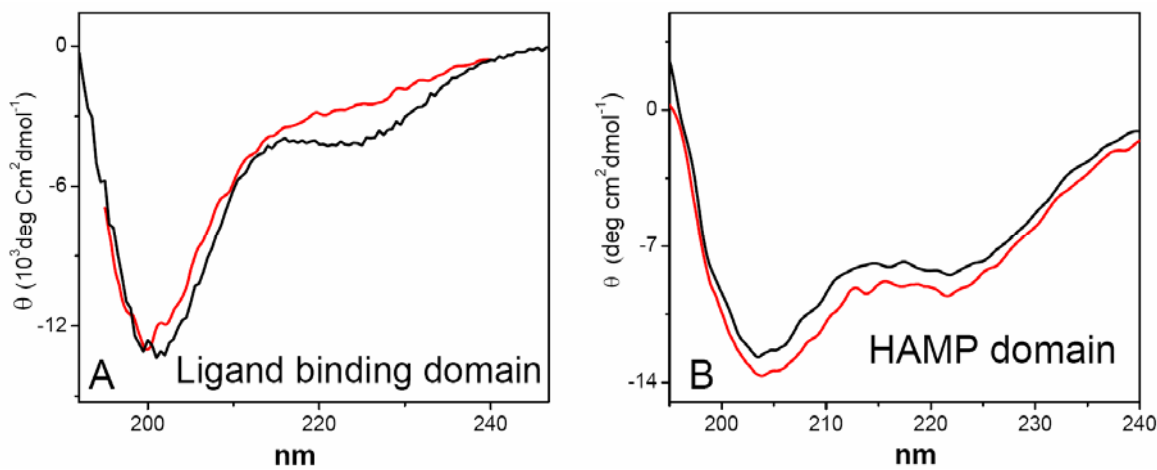


Figure 3-23. CD spectra of HsHtrII-LBD [42-285] and HsHtrII-HAMP [303-465] in 4 M KF, 20 mM KPi, pH 6.0 (black curve) and proteins in 50 mM KF, 20 mM KPi, pH 6.0 (red curve). The CD signal is given in arbitrary units. Protein was diluted in the respective buffer to a concentration suited for CD spectroscopy. Data were collection was performed at 20°C.

The random coil content is 92.4% and  $\alpha$ -helical content contribute 5% at high salt concentration. CD spectra of the analyzed LBD resulted only in minor changes of the secondary structure at low salt concentration. The secondary structure of LBD was estimated to consist of 89.4% random coil contents. One can conclude that LBD was not correctly folded since  $\alpha$ -helical contents in both high and low salt conditions were not observed.

The CD spectrum of HAMP domain reveals an  $\alpha$ -helical content of 17% and random coil (64%). The CD data of HAMP domain showed a slight salt-dependency with  $\alpha$ -helical content decreasing from 17% at higher salt concentration to 11% at low salt concentration. The crystal structure of the ligand binding domain of Tar chemoreceptor showed that it consists of four antiparallel  $\alpha$ -helices in a four-helix bundle (145,146). In contrast to HAMP domain, as judged from the total  $\alpha$ -helical content of the LBD, a loss of  $\alpha$ -helical content occurred. It indicates that LBD is not fold into their characteristic and functional tertiary structure(147).

## RESULTS

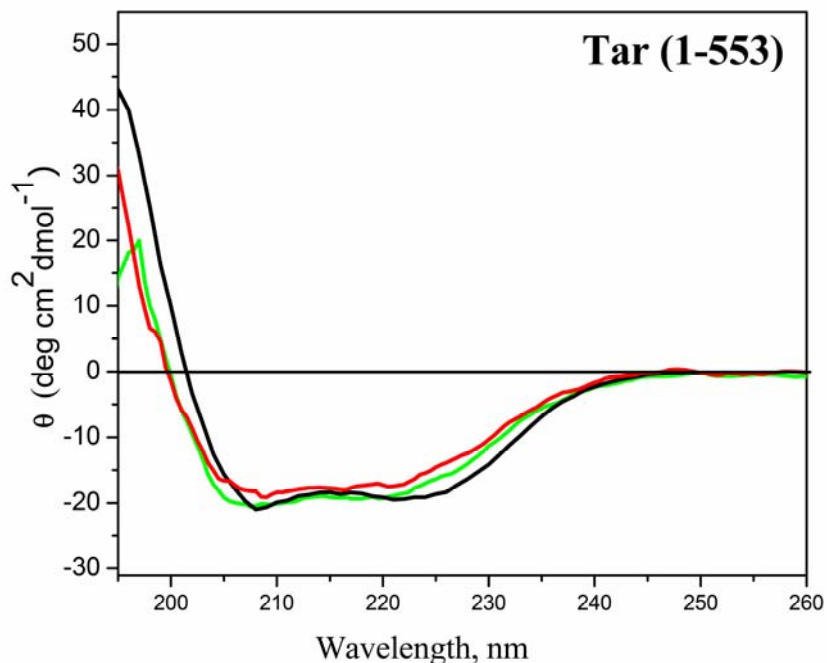


Figure 3-24. CD spectra of Tar chemoreceptor [1-553]. Salt-induced conformational changes of membrane Tar[1-553] (green curve) in 4M KF, 20 mM KPi, 0.05% DDM, pH 7.0 and proteins in 50 mM KF, 20 mM KPi, 0.05% DDM, pH 7.0 (black curve) and protein in 50 mM KF, 20 mM KPi, pH 7.0 (red curve). The CD signal is given in arbitrary units. Data collection was performed at 20°C.

CD analysis of Aspartate chemoreceptor: The CD spectra of Tar chemoreceptor at 20°C are shown in Figure 3-24. The  $\alpha$ -helical contents of Tar [1-553] in 4M KF buffer (69.2%) (green curve) and those in 50 mM KF buffer (73%)(black curve) were observed. Detergent free Tar [1-553] reveals the  $\alpha$ -helical contents of 64.7%. Notably, the  $\alpha$ -helical contents of the Tar chemoreceptor at low salt concentration(73%) is well line with previous observations, which demonstrate 78% helix for the aspartate chemoreceptor (144). Although, the CD spectrum of detergent free Tar chemoreceptor resulted in slight decreases in the  $\alpha$ -helical contents from 73 to 68.7%, it folds into mostly  $\alpha$ -helical secondary structure. The salt dependence of CD spectra indicating that at different salt concentration does not impair the secondary structure of Tar chemoreceptor.

## RESULTS

Temperature dependence of HsHtrII constructs: The thermal denaturation was further used to gain more insight into the possible role of salt effect on the structural stability of the protein (Figure 3-25). An attempt was made to compare the thermal stability of HsHtrII by monitoring the CD signal change at 220 nm as a function of temperature under high and low salt buffer condition.

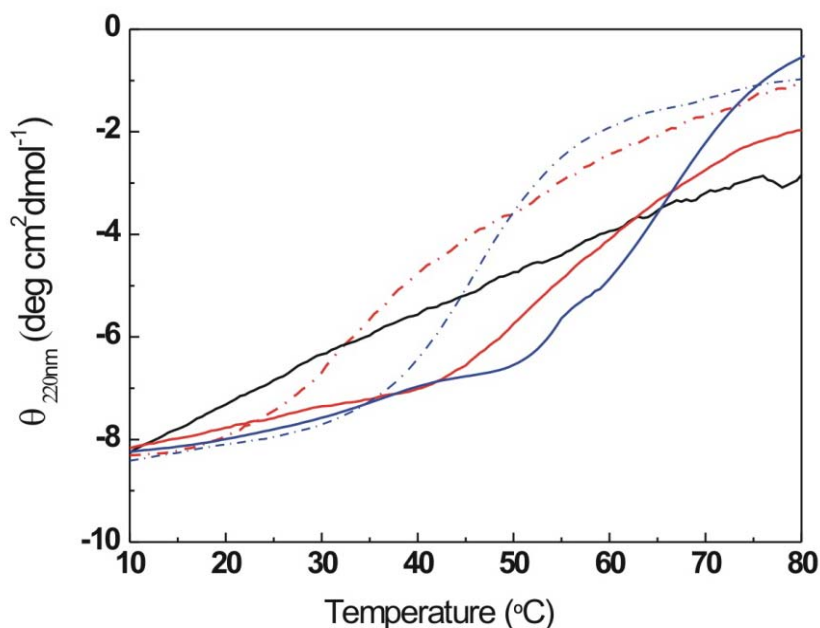


Figure 3-25. CD spectra of heat denaturation of HsHtrII. CD spectra of HsHtrII[1-398](red) in 50 mM NaCl(dashed line) and 500 mM NaCl(solid line); HsHtrII[1-765](blue) in 50 mM NaCl(dashed line), 500 mM NaCl(solid line) and 1 M NaCl (black). Normalized CD signal at 222 nm plotted as a function increasing from 10 to above 85°C at 1°C per min with 500 mM NaCl (solid line) or 50 mM (dotted line). The thermal denaturation behavior for 1 M salt showed no transition between 10 °C and 85 °C. Proteins were diluted in the respective buffer to a concentration range suitable for CD spectroscopy.

With increase in temperature from 10 to 85 °C, HsHtrII constructs gradually underwent thermal denaturation, leading to the decrease of CD signal which indicated loss of  $\alpha$ -helical content. As shown in Figure 3-27, with the exception of HsHtrII [1-765] in 1 M NaCl buffer(black curve), both 50 mM (blue dashed curve) and 500 mM NaCl (blue solid curve) buffer with HsHtrII constructs exhibited a cooperative two state mode for unfolding, with a characteristic melting temperature ( $T_m$ ). The mid-points of the thermal transitions were obtained for HsHtrII[1-765] in 50 mM NaCl (47 °C) and 500

## RESULTS

---

mM NaCl (65 °C). The spectra of HsHtrII[1-765] in 1 M NaCl showed gradual loss in its helical content with increasing temperature. The mid-points of the thermal transitions were obtained for HsHtrII[1-398] in 50 mM NaCl (34°C) and 500 mM NaCl (45°C). In comparison with HsHtrII [1-398], HsHtrII [1-765] shows increased melting temperature, indicating that HsHtrII [1-765] is more thermally stable than HsHtrII [1-398]. The mid-point of the thermal transitions for HsHtrII [1-398] constructs in high salt condition also occurred at a much higher temperature than that of low salt condition. These results indicate that HsHtrII requires high salt concentrations to maintain its native fold.



### 3.3. Functional characterization of HsHtrII and Tar chemoreceptor

#### 3.3.1. Isothermal titration calorimetry (ITC) of HsHtrII-serine interaction

To analyze serine binding of HsHtrII constructs, ITC measurements were performed. Shown in Figure 3-29 are the results of the titration experiments, in which serine was titrated against HsHtrII (Figure 3-29A) and HsHtrII-HsSRII complex (Figure 3-29B). The experiments, with HsHtrII[1-398] alone and in combination with HsSRII, were done close to native conditions at 4 M NaCl.

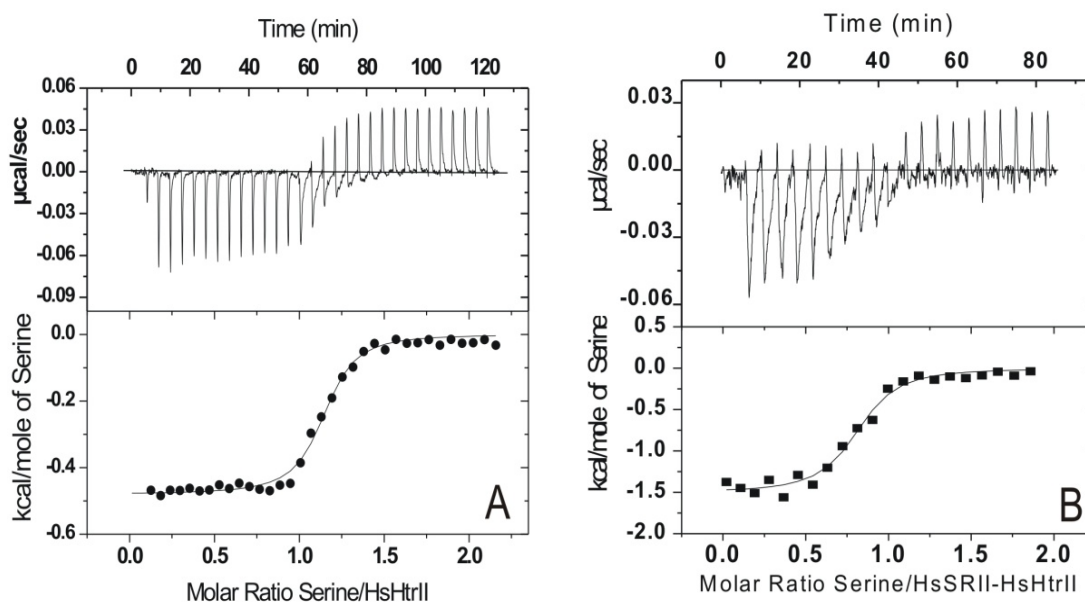


Figure 3-26. Isothermal calorimetric titration of (A) Serine (500 μM) into a HsHtrII[1-398] solution (20 μM) and titration of (B) Serine (500 μM) into a solution of HsSRII-HsHtrII complex (20 μM) in 50 mM MES, 4 M NaCl, 0.05% DDM pH 6. The upper panels represent the raw data after baseline correction. In the lower panels the integral of the upper spikes (enthalpy change) are plotted against the molar ratio of serine to transducer proteins.

From the ITC experiments, Serine binds to HsHtrII[1-398] with a  $K_D = 4.62\mu\text{M}$  with a 1:1 stoichiometry. Upon serine binding, the HsSRII-HsHtrII complex is almost unaffected ( $K_D = 5.35\mu\text{M}$ ). Interestingly, the stoichiometry of serine binding to HsHtrII-HsSRII complex is 0.5 (Figure 3-26B). This stoichiometry indicated that serine binding sites have negative cooperative

## RESULTS

effect. The aspartate receptor of *Escherichia coli* is a dimer that shows negative cooperativity with a stoichiometry of one aspartate per dimer. When only one binding site is occupied by aspartate, an aspartate-induced conformational change reduces or eliminates affinity for the aspartate at the second binding site (145). Removing the extracellular domain of HsHtrII[1-765 $\Delta$ 38-280] and HsHtrII[1-398 $\Delta$ 38-280] yielded no binding affinity to serine. It was also found that HsHtrII in low salt concentration (50 mM NaCl) has extremely reduced binding activity ( $K_D > 200 \mu\text{M}$ ) (data not shown). For this reason, it is clear that the HsHtrII in high salt concentration bears not only significant structural stability but also serine binding activity.

### 3.3.2. Isothermal titration calorimetry (ITC) of Tar-aspartate interaction

The aspartate-binding chemoreceptor is one of the strongest responses of *E. coli* cell (148). To explore the nature of an efficient ligand binding event without membrane, water soluble Tar chemoreceptor was studied by measuring the interaction with aspartate by isothermal titration calorimetry.

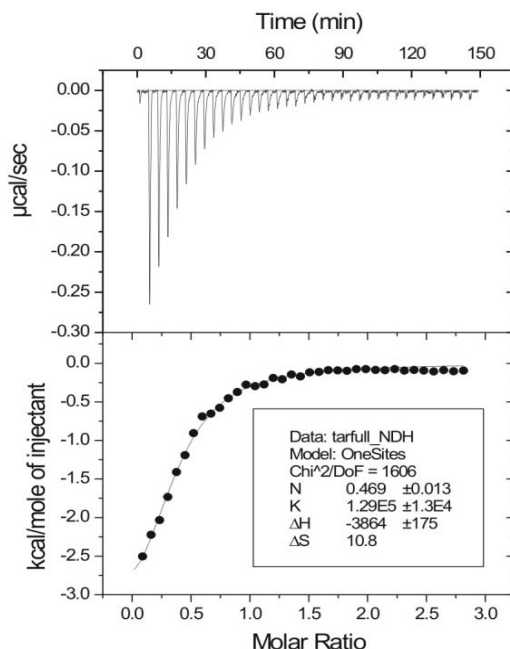


Figure 3-27. Isothermal calorimetric Titration of Tar with aspartate at 25°C. Aspartate (1 mM) binding to Tar receptor[1-553] (50  $\mu\text{M}$ ) in 25 mM Tris-HCl, 5% glycerol, 150 mM NaCl, pH 7. The upper panels represent the raw data after baseline correction. In the lower panels the

## RESULTS

---

integral of the upper spikes (enthalpy change) are plotted against the molar ratio of serine to transducer proteins. The titration data were fitted by a binding curve. Tar: Asp titration curves were corrected by subtraction of blank titration curves obtained by titration of the buffer alone.

Representative raw data of a typical titration with Asp is shown in the upper panel of Figure 3-27. After integration of the peaks the enthalpy values were plotted as a function of the aspartate-Tar protein molar ratio. The heat effect observed during titration indicates an exothermic binding reaction ( $\Delta H = -3.86$  kcal mol<sup>-1</sup>) and entropy ( $\Delta S = 10.8$  cal mol<sup>-1</sup>) with a dissociation constant  $K_D = 7$   $\mu$ M. In addition to enthalpy and entropy values, the Gibbs free energy was calculated to be  $\Delta G = -7.02$  for the binding of aspartate. This finding showed that water soluble Tar receptor has similar affinity to Asp as the membrane Tar receptor, whose affinity was calculated by using radioactive isotope labeled aspartate ( $K_D = \sim 5$   $\mu$ M)(148).

### 3.3.3. Intrinsic tryptophan fluorescence

Intrinsic fluorescence of proteins mainly results from tryptophan which is the dominating residue due to higher absorbance and higher quantum yield of emission. Trp fluorescence depends on protein local environment. Besides, folding intermediates and natively folded proteins are distinguishable by their respective tryptophan spectra (149). This well-known effect is illustrated in Figure 3-28. Trp residues which are highly exposed to solvent have emission maxima ( $\lambda_{max}$ ) in the range of 350-360 nm, whereas Trp residues in hydrophobic environments have maxima ranging between 330-350 nm (150).

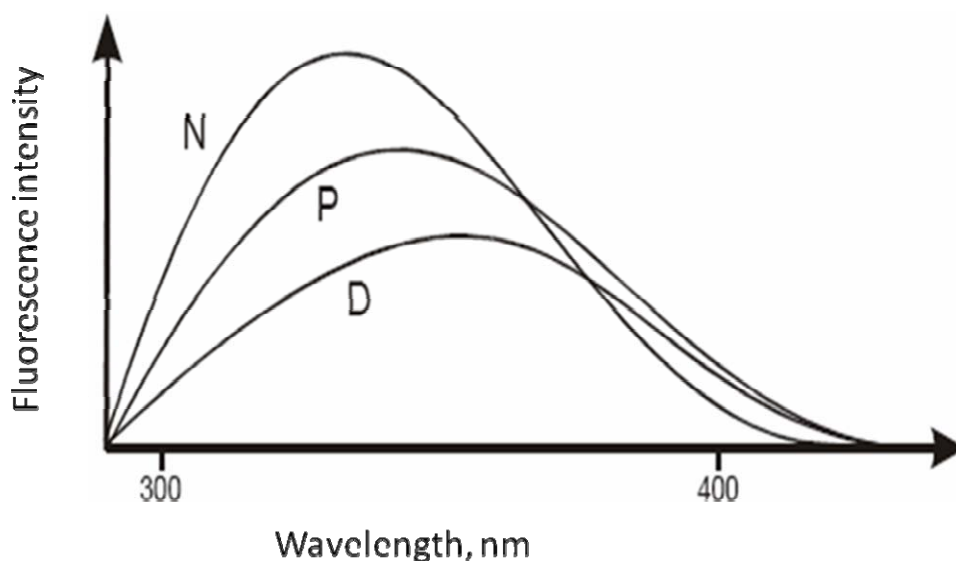


Figure 3-28. Hypothetical protein fluorescence spectra N, P and D indicate spectra of native, partially folded and unfolded protein, respectively. This figure was adapted from Royer C.A., *et al*, (149).

Trp residues in native state(N) of protein exhibits the wavelength of fluorescent maximum ( $\lambda_{max}$ = ca. 330 nm) with higher intensity than that of partially folded(P) ( $\lambda_{max}$ = 330-350 nm) and unfolded state (D) ( $\lambda_{max}$ = 350-360 nm) of protein(Figure 3-28). It indicates that the tryptophan residues in native protein are buried in a hydrophobic interior of the protein. Upon folding from native state to unfolded state, the wavelength of fluorescence maximum

## RESULTS

exhibits a large red shift in fluorescence with smaller intensities (i.e. lower energy) and therefore the tryptophan residues are more solvent exposed. The occurrence of such a shift from red to blue can be used for monitor the folding or unfolding of protein. As observed in most proteins, a relatively high fluorescence intensity at 330nm is an indicator for natively folded protein (149,151-154).

### 3.3.4. Trp fluorescence emission spectra of HsHtrII

The structural changes of HsHtrII were characterized using chemical denaturant guanidine hydrochloride (GuHCl). Intrinsic Trp fluorescence was selected to monitor GuHCl-induced denaturation of HsHtrII. In HsHtrII, there are two tryptophan residues in the periplasmic domain: the first Trp65 residue is close to the region of TM1 and the second Trp261 is positioned proximal to TM2.

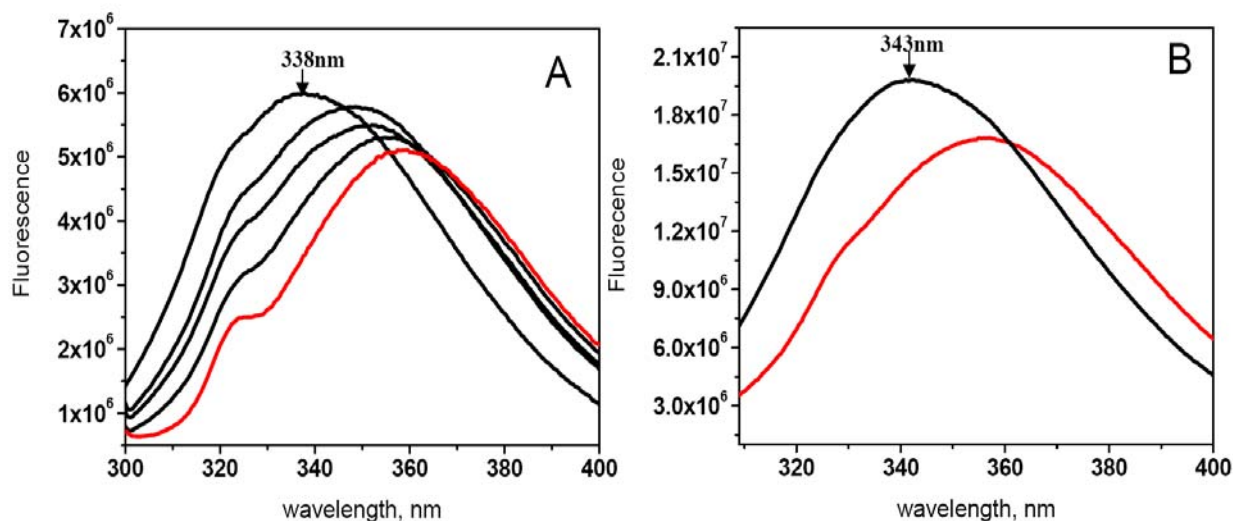


Figure 3-29. Intrinsic tryptophan fluorescence of HsHtrII [1-398] and HsHtrII[1-765]: (A) GuHCl-induced unfolding HsHtrII[1-398] (left) fluorescence versus GuHCl concentration (from the top to the bottom: 0 M, 1 M, 2 M, 4 M and 6 M (red solid line), respectively); (B) HsHtrII[1-765] in GuHCl 0 M (black line), 6 M (red line); The samples were excited at 295 nm and spectra were taken from 305 nm to 405 nm in 50 mM MES, 4 M NaCl, pH 6.

Figure 3-29 shows the scanning of Trp fluorescence emission for HsHtrII constructs upon GuHCl denaturation. The fluorescence emission was

## RESULTS

---

measured with increasing concentration of GuHCl. The emission spectra of HsHtrII constructs are detectable in HsHtrII constructs. Red lines are fluorescence emission spectra of both samples from 6 M GuHCl denaturation. Complete unfolding of HsHtrII by GuHCl resulted in a decrease of fluorescence emission maximum and red shift. It revealed that the completely denatured HsHtrII[1-398] showed a red shift of the fluorescence emission maximum from 338 nm to 356 nm. In comparison with maximum peak at 343 nm for HsHtrII[1-765], the emission maximum of the GuHCl-induced denaturation also caused a red shift to 360 nm. These red shifts from 343nm to 360nm indicate a transition from folded to unfolded states of HsHtrII. The tryptophan fluorescence of HsHtrII at 360 nm (unfolded state) indicates that tryptophan residues are close to the solvent in a more hydrophilic environment. In addition, the tryptophan fluorescence in HsHtrII [1-398] ( $\lambda_{\max}$ = 338 nm) displays a relatively large blue shift of 5 nm than HsHtrII [1-765] ( $\lambda_{\max}$ = 343 nm).

### 3.3.5. Binding of serine to HsHtrII by intrinsic tryptophan fluorescence

As shown above (Figure 3-29), Trp fluorescence changes in HsHtrII were observed by using a denaturant. In order to examine HsHtrII structural changes on serine binding, the intrinsic Trp fluorescence changes were measured.

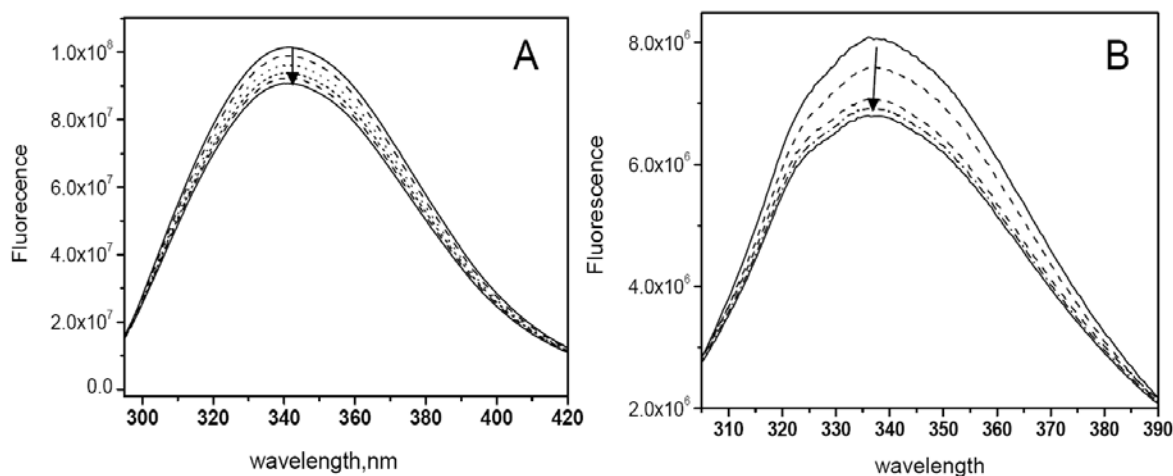


Figure 3-30. Intrinsic tryptophan fluorescence of HsHtrII[1-765] and HsHtrII[1-398] with serine: (A) Intrinsic Trp fluorescence emission spectra of HsHtrII[1-765](1 μM) with increasing concentration of serine from top (0 μM) to bottom(5 μM) in 1 μM steps. (B) HsHtrII [1-398] (0.5 μM) with increasing concentration of serine from top (0 μM) to bottom (2.5 μM) in 0.5 μM steps. The excitation was at 295 nm and the emission was scanned from 290 nm to 450 nm in 50 mM MES, 4 M NaCl, pH 6.

The intrinsic tryptophan fluorescence of HsHtrII was measured of five different serine concentrations. The emission spectra were recorded from 295 to 400 nm with fixed excitation at 295nm (Figure 3-30).

For both, HsHtrII [1-765] and HsHtrII [1-398] fluorescence quenching was induced by serine binding. The decrease of HsHtrII fluorescence of about 10-15 % of the initial fluorescence was proportional to the amount of serine added.

When serine was added to HsHtrII [1-765], the Trp fluorescence in HsHtrII [1-765] decreased by about 10 %, while HsHtrII [1-398] binding to serine

## RESULTS

caused more reduction of the fluorescence intensity approximately 15 %. These results reflect more structural changes in HsHtrII[1-398] than those in HsHtrII[1-765]. In addition, HsHtrII [1-398] showed a minor blue shift of the maximum from 338 nm to 335 nm, in the presence of serine. The minor blue shift can be explained that the tryptophan residues shift into a more hydrophobic interior of HsHtrII [1-398] on serine binding. An evident fluorescence shift in Trp fluorescence for HsHtrII [1-765] was not observed. This may reflect that tryptophan residues (Trp 65, Trp 261) are quenched by serine but are positioned in the same protein environment and a lower degree of conformational change has occurred in HsHtrII [1-765] than in HsHtrII [1-398].

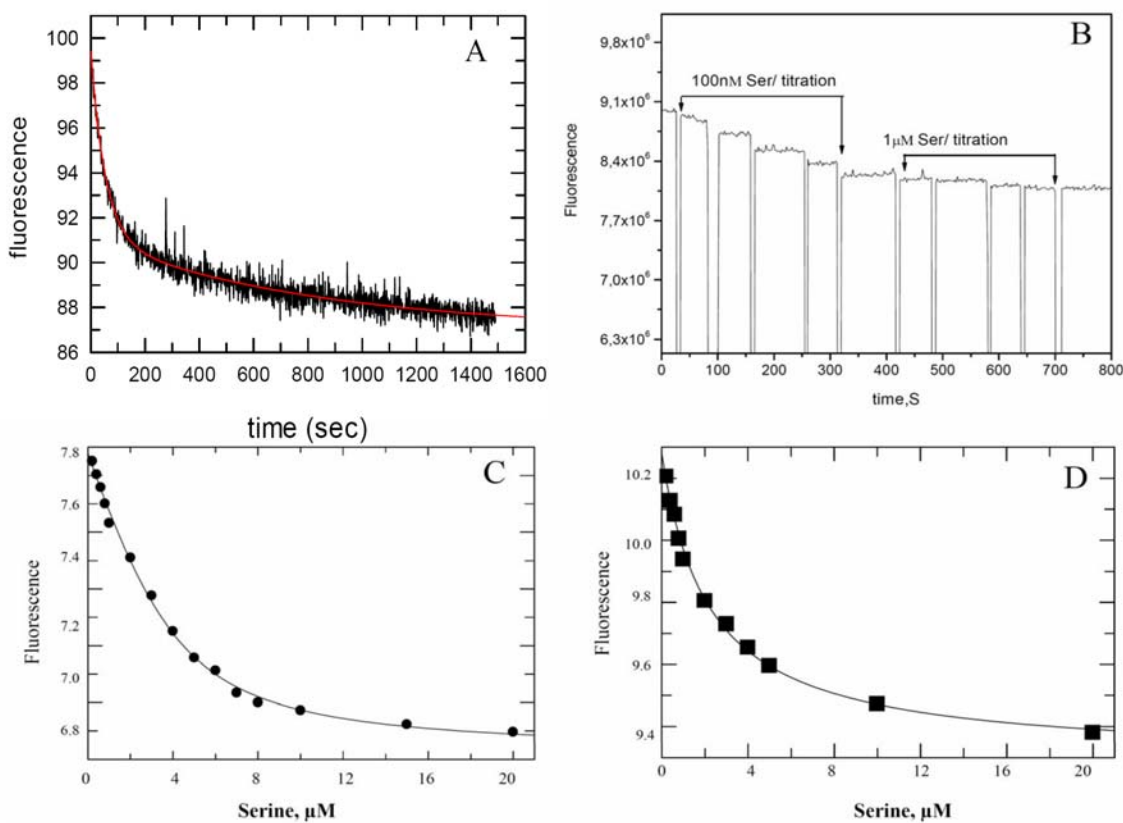


Figure 3-31. Intrinsic trp fluorescence of HsHtrII : (A)Time course of change in HsHtrII [1-765]. Trp fluorescence upon mixing 10 μM serine. 1 μM of HsHtrII[1-765] with serine(red dot), and with buffer (black) respectively. (B) Raw data for a titration of serine in 100 nM and 1 μM steps into the solution of HsHtrII [1-398]. Titration of serine into the solution of 1 μM of HsHtrII[1-765] (C) and 3.4 μM of HsHtrII[1-398] (D). Fluorescence was excited at 295 nm and spectra were recorded at 340 nm at 20 °C in 50 mM MES, 4 M NaCl, pH 6. Titrations were



## RESULTS

---

corrected for normalized, averaged, and the values fit to a GRAFIT program using quadratic equation.

In order to analyze the kinetics of serine binding, stop flow experiments were performed. Figure 3-31A shows the time course of Trp fluorescence of HsHtrII [1-765]. Mixing of HsHtrII [1-765] with serine led to a decrease in the tryptophan fluorescence. Two observed rate constants ( $k_{\text{obs}} = 1.8 \pm 0.6 \times 10^{-2} \text{ s}^{-1}$  and  $1.2 \pm 0.9 \times 10^{-3} \text{ s}^{-1}$ ) were obtained using the program GraFit 5.0.

The results were further confirmed by titration of HsHtrII with serine. A multistep equilibrium titration was performed with increasing concentration of serine (Figure. 3-31B). Serine was added to two HsHtrII constructs in a range of concentrations from 1 nM to 2  $\mu\text{M}$ . In the first set of titrations, serine was added to HsHtrII to reach the absorption maxima at equilibrium. Each equilibrium titration was subsequently plotted against serine concentration (Figure. 3-31 C and D). Fitting of the equilibrium titration data was done by plotting normalized fluorescence intensity against serine concentration. Evaluation of the titration curves by fitting a quadratic equation yielded dissociation constants ( $K_D$ ) values of  $2.4 \pm 0.6$  and  $3 \pm 0.8 \mu\text{M}$  for HsHtrII [1-765] and HsHtrII [1-398], respectively. Fluorescence titrations at equilibrium show that HsHtrII[1-765] and HsHtrII[1-398] have similar affinities for serine, although results indicate that HsHtrII[1-765] has a slightly higher affinity than HsHtrII[1-398]. The binding affinity obtained with ITC ( $K_D=5\mu\text{M}$ ) is consistent with the values derived from titration data for HsHtrII [1-398]. The fluorescence data indicated that serine is an effective quencher for tryptophan residues in HsHtrII constructs. The results provide direct structural evidence for intrinsic Trp fluorescence of HsHtrII [1-398] and demonstrate that serine binding induces a local conformational change. However, it remains to be seen which tryptophan residue is affected by the presence of serine.

### 3.3.6. ANS fluorescence emission spectra

8-Anilino-1-naphthalenesulfonic acid (ANS) is a useful indicator of hydrophobic regions in a protein and is believed to mimic structures formed during the folding process. A common application of ANS is directly linked to

## RESULTS

the molten globule state, which conserves a native-like secondary structure content but it lacks tertiary structure (112,155).

Efficient receptor function requires conformational changes upon ligand binding, which can be explained by its molten globule character which has a much more dynamic or more open state than a fully folded protein. In other words, a small amount of hydrophobic surface area is shielded upon ligand binding and functions as a probe for the accessibility of hydrophobic regions.

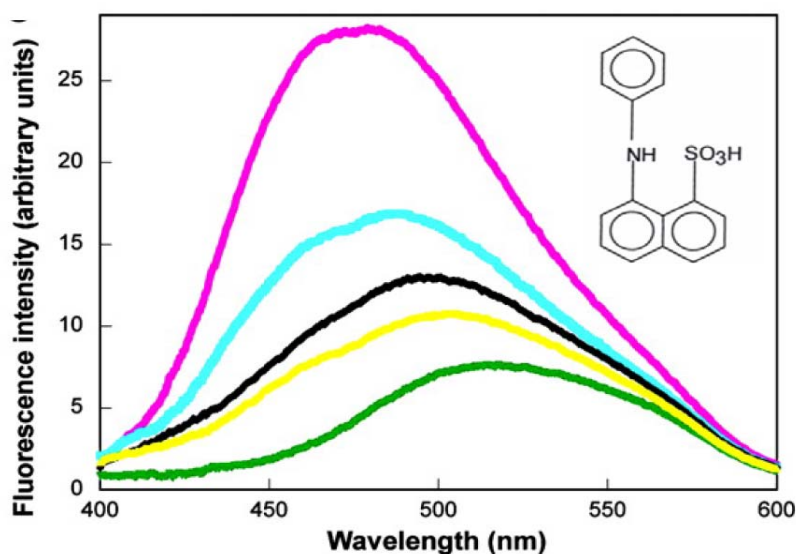


Figure 3-32. Chemical structure of 8-anilino naphthalene-1-sulphonic acid (1,8-ANS) and ANS emission spectra of the free and ligand-bound enzymes from *Methanococcus jannaschii*. Monomeric chorismate mutase enzyme in the absence (magenta curve) and in the presence (cyan curve) of ligand. Dimeric chorismate mutase in the absence (black curve) and in the presence (yellow curve) of ligand and ANS alone (green line). This figure was taken from Katherina Vamvaca *et al* (156).

The availability of water soluble HsHtrII and Tar allowed us to exclude lipidic environment for monitoring its interaction with protein and ligand. One of the conformational changes on ligand can be well explained by the molten globule structure which is shown in Figure 3-32. Katherina *et al* (156) performed ANS binding experiment to monitor the molten globule like structure of chorismate mutase. The fluorescence intensity of ANS increases when it is bound accessible hydrophobic sites in unliganded chorismate enzyme (magenta curve) which is typical for molten globules. This monomer enzyme (magenta

## RESULTS

curve) binds more to the environmentally sensitive hydrophobic dye ANS than the dimeric enzyme (black curve), giving rise to significantly enhanced fluorescence with a characteristic blue shift of the emission maximum. Binding of ligand to monomeric enzyme (cyan curve) causes a decrease in ANS fluorescence. Similar effects were also seen with the dimeric enzyme (yellow curve) in the presence of ligand, indicating that it becomes more structured upon ligand binding. As a result, the fluorescence increase, as seen for ANS in the presence of the wild-type dimer, is more typical for a conventionally folded protein than a monomer.

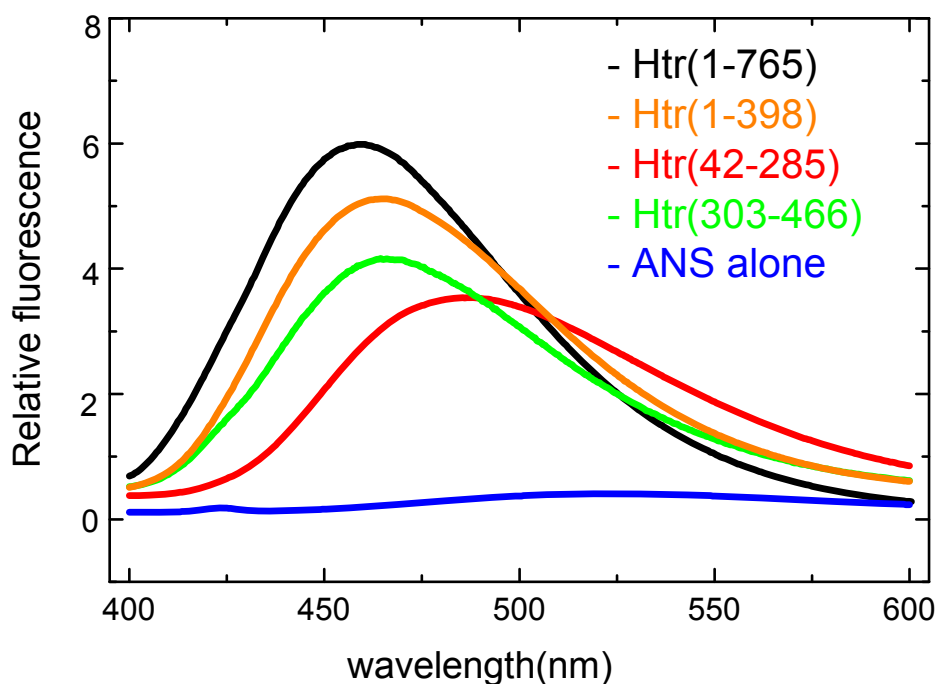


Figure 3-33. ANS fluorescence spectra from the mixtures of 10  $\mu\text{M}$  ANS and proteins: 1  $\mu\text{M}$  of HsHtrII[1-765](black), 1.4  $\mu\text{M}$  of HsHtrII[1-398](orange), 1  $\mu\text{M}$  of HsHtrII (HAMP,303-466)(green), 1.5  $\mu\text{M}$  HsHtrII (ligand binding domain, 42-285)(red) and buffer (blue). The data presented here are averages from two or more experiments. Fluorescence was excited at 370 nm and spectra were recorded between 420 and 600 nm. In each case, the spectrum of ANS in buffer was subtracted.

To analyze structural features of HsHtrII and its analogues, ANS fluorescence was measured. As shown in Figure 3-33, addition of ANS to

## RESULTS

HsHtrII and its analogues led to enhancement in fluorescence. It was observed that ANS-bound HsHtrII[1-765] had higher intensity of emission spectra with a blue shift ( $\lambda_{\max}=458$ ), compared to HsHtrII[1-398] ( $\lambda_{\max}=466$ ) at the same concentration. The maximum absorption of blue shift of 8nm can be explained that HsHtrII [1-765] contains more molten globule like structure than HsHtrII [1-398]. The other construct, HAMP domain (303-465) exhibited a maximum peak ( $\lambda_{\max}=460$ ), similar to that of HsHtrII [1-765]. It displayed decrease in fluorescence intensity probably due to smaller molecule size. The ligand binding domain (42-285) resulted in a remarkable red shift ( $\lambda_{\max}=458$ ), indicating that ligand binding domain(42-285) adopts less molten globule like structure relative to the other HsHtrII constructs, which is consistent with 90% of random coils or dramatic decrease of secondary helical structure as observed from CD spectrum (see chapter 3.2.7.).

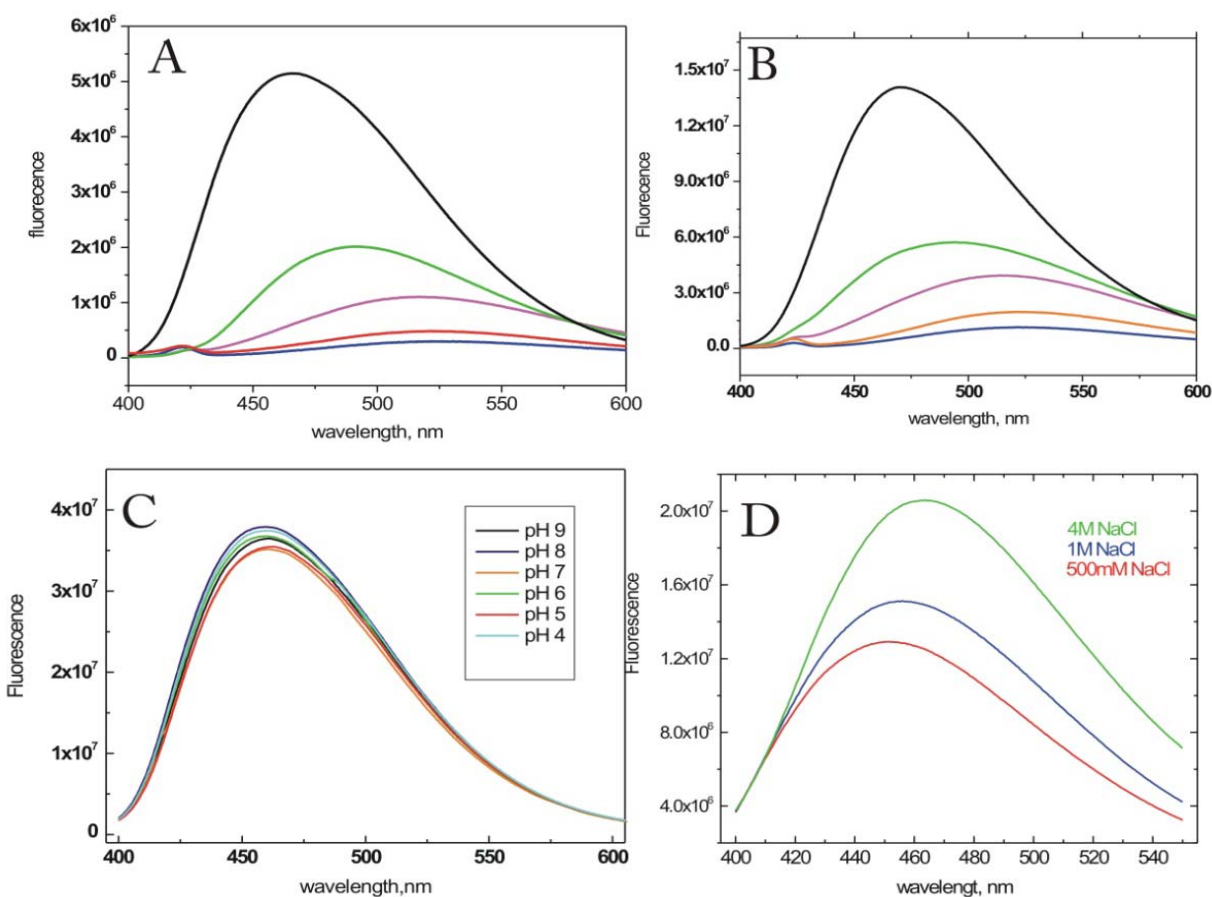


Figure 3-34. ANS fluorescence spectra of (A) HsHtrII [1-765] and (B) HsHtrII[1-398] varying concentrations of GuHCl as follows : A significant decrease in fluorescence is detected in

## RESULTS

---

presence of GuHCl. black(0 M), green (2 M), pink (4 M), red( 5 M), blue (6 M) respectively.  
(C) ANS emission spectra of 1.5  $\mu$ M HsHtrII[1-398], varying the pH in the range from 4 to 9.  
(D) ANS fluorescence of HsHtrII[1-398] in the presence of 4 M, 1 M and 500 mM NaCl respectively.

To further monitor the conformational changes, HsHtrII constructs with ANS were applied to change in pH, salt and GuHCl concentration. First, to test whether chemically-induced denaturation affects the ANS fluorescence in the protein, the ANS fluorescence intensity and wavelengths were monitored after the protein was equilibrated with increasing concentrations of GuHCl (Figure.3-34A and B). Both HsHtrII [1-765] and HsHtrII[1-398] resulted in dramatic decreases in fluorescence and blue shifts of the emission maximum ranging from 460 to 520nm which indicate unfolding of the protein with increasing GuHCl concentration. Second, as shown in Figure 3-34C, no fluorescence changes of HsHtrII[1-398] were observed when pH was varied in the range 4 to 9. For salt dependency, the fluorescence spectrum of ANS was also recorded in the presence of 50 mM, 1 M and 4 M NaCl. HsHtrII[1-398] showed an increase in fluorescence with a red shift of the emission spectra from 450 nm to 460 nm in 4 M NaCl buffer condition (Figure.3-34D). The protein was found to be a more molten globule at high salt than protein at a low salt concentration. This conclusion agrees with the observation that the CD spectra of HsHtrII [1-398] indicated a similar salt-dependency.

## RESULTS

### 3.3.7. Ligand induced conformational changes of HsHtrII and Tar chemoreceptor

To link the ANS fluorescence study with the ligand-binding properties of HsHtrII and Tar chemoreceptor, ligand induced structural changes were further analyzed. As shown in Figure 3-35A, addition of ANS to HsHtrII[1-765]-serine complex caused a decrease in ANS fluorescence of about 12 % than that of serine free HsHtrII[1-765]. Just like the results of HsHtrII[1-765] fluorescence experiments, the fluorescence intensity of HsHtrII[1-398]-serine decreased by 14 % compared to HsHtrII[1-398] (Figure.3-35B).

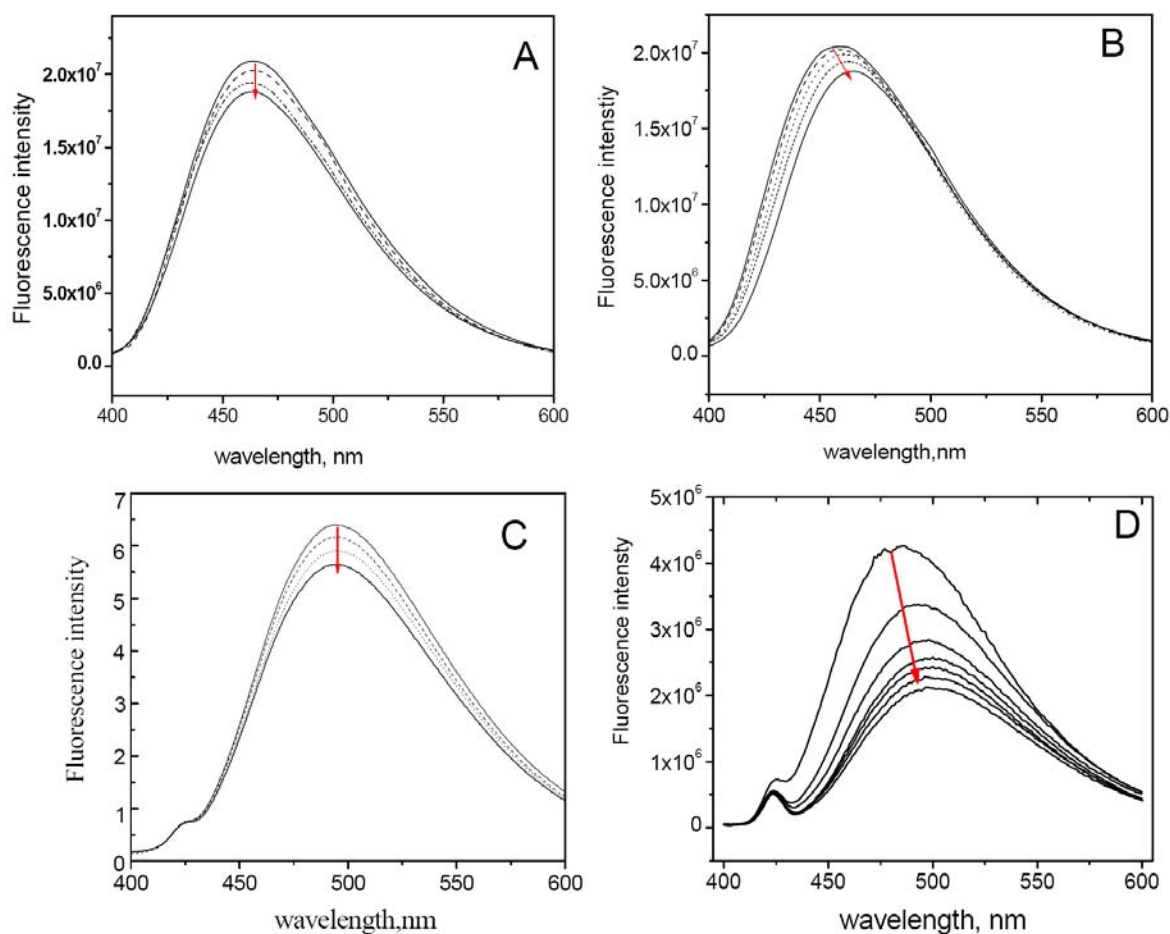


Figure 3-35. Fluorescence emission spectra of ANS binding to HsHtrII in the presence of various concentrations of serine: (A) 1.5  $\mu\text{M}$  of HsHtrII[1-765] and 5  $\mu\text{M}$  ANS mixture with increasing serine concentration from 1  $\mu\text{M}$  to 10  $\mu\text{M}$  as indicated by arrow (red); (B) 3.2  $\mu\text{M}$  of HsHtrII [1-398] and 5  $\mu\text{M}$  ANS mixture with increasing serine concentration from 1  $\mu\text{M}$  to 10  $\mu\text{M}$  as indicated by arrow (red). (C) 1.4  $\mu\text{M}$  of Tar [1-553] and 5  $\mu\text{M}$  ANS mixture with

## RESULTS

---

increasing serine concentration from 0.1  $\mu\text{M}$  to 5  $\mu\text{M}$  as indicated by arrow (red). (D) 0.5  $\mu\text{M}$  of Tar [1-265] and 5  $\mu\text{M}$  ANS mixture with increasing serine concentration from 50 nM to 1  $\mu\text{M}$  as indicated by arrow (red). The data presented here are averages from two or more experiment. Fluorescence was excited at 370 nm and spectra were recorded between 400 and 600 nm. In each case, the spectrum of ANS in buffer was subtracted.

Water soluble Tar constructs also displayed similar spectral properties upon complex formation with aspartate (Figure.3-35 C and D). Interestingly, it was found that binding of aspartate to Tar [1-265] strongly attenuated the fluorescence intensity by 35% than that of aspartate to Tar [1-553](16%). Furthermore, there are differences in emission maxima not only between HsHtrII[1-765] and HsHtrII[1-398] but also Tar [1-553] and Tar [1-265]. In the presence of ligand, HsHtrII [1-765] and Tar [1-553] exhibited very little red shifts of about 2 nm in the emission maxima (Figure.3-35 A and C), whereas the maximum of HsHtrII[1-398] a red shift from 460 nm to 470 nm (Figure.3-35 B). Also, Tar [1-265] showed a red shift of 20nm from 475nm to 495nm with concomitant decrease in fluorescence intensity (Figure.3-35 D). ANS binding to HsHtrII[1-398]-Ser as well as Tar(1-265)-Asp resulted in a red shift of the ANS fluorescence emission maximum and is accompanied by decrease in fluorescence intensity. These results indicate that hydrophobic surface area is shielded when binding sites are occupied, which leads to less molten globule or more compact conformation than ligand-free HsHtrII and Tar chemoreceptor.

### 3.3.8. Determination of the number of ANS binding sites

Scatchard plot analysis of HsHtrII: In order to provide information about the number of ANS and the location of the binding sites in different constructs, Scatchard plot analysis was used for calculating number of ANS binding site (see materials and methods 2.6.2). Scatchard plot is capable of fitting nonlinear regression into a linear relationship, where the straight line reveals the number of ANS binding sites. Thus, the number of ANS binding sites can be determined from X intercept values of the linear fit (Figure.3-36B, D and F). Titration of HsHtrII solutions with an increasing concentration of ANS provides

## RESULTS

information on the number of binding sites. The number of ANS-binding sites was determined by monitoring the change in ANS fluorescence intensity as a function of ANS concentration.

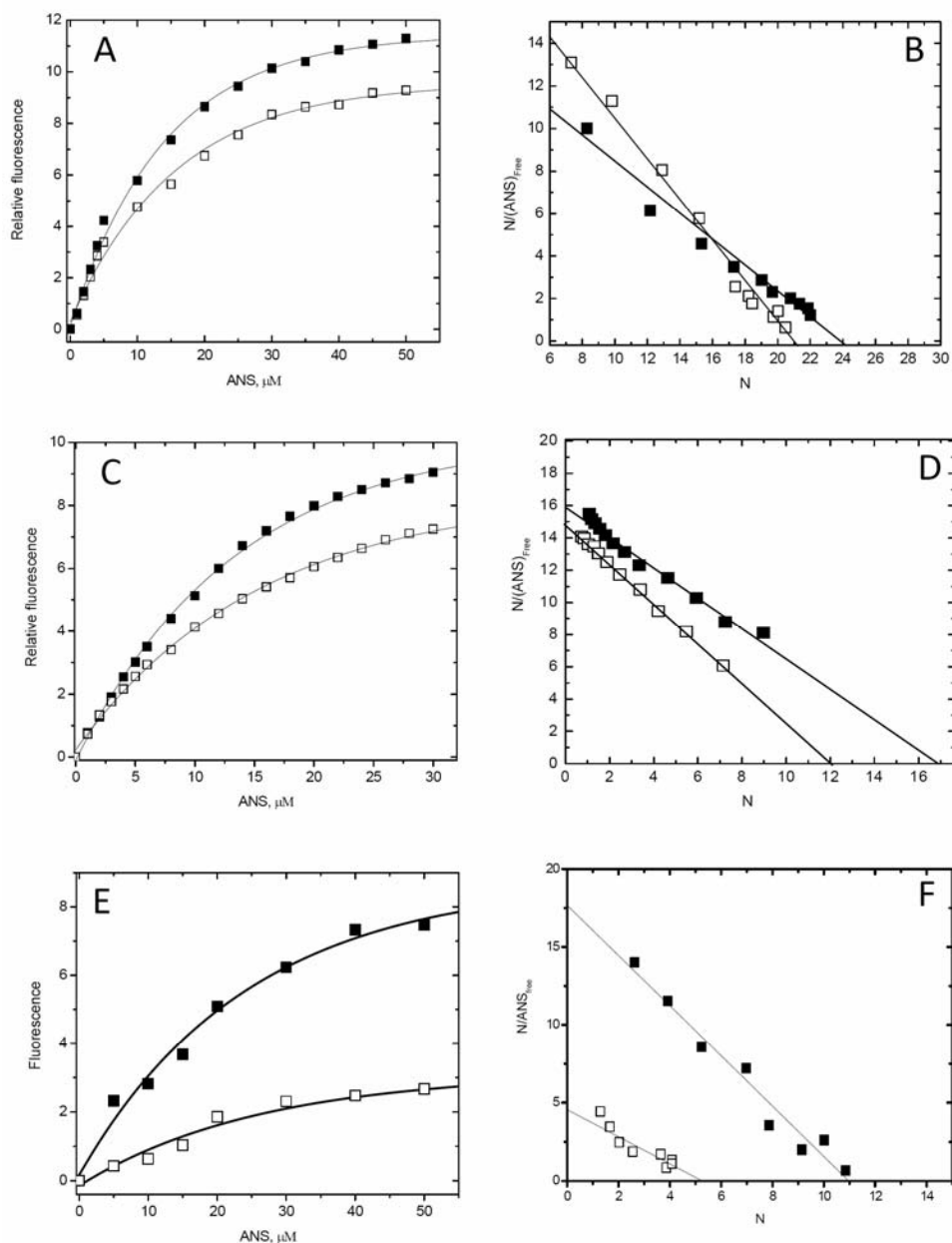


Figure 3-36 Determination of the number of ANS binding site for HsHtrII constructs with serine. ANS titration of HsHtrII constructs in the absence and presence of 10  $\mu\text{M}$  serine: (A) 0.5  $\mu\text{M}$  HsHtrII[1-765]( closed square), HsHtrII[1-765]-serine(open square). (B) Scatchard plot for the binding of ANS to HsHtrII[1-765](closed square) and HsHtrII[1-765]-serine(open square). (C) 1.2  $\mu\text{M}$  HsHtrII[1-398](closed square) and HsHtrII[1-398]-serine(open square).



## RESULTS

---

(D) Scatchard plot for the binding of ANS to HsHtrII[1-398](closed square), HsHtrII[1-765]-serine (open square). (E) 1  $\mu$ M HAMP (303-466) (closed square), 1.7 $\mu$ M LBD (42-285) (open square) (F) Scatchard plot for the binding of ANS to HAMP (303-466)(closed square), LBD (42-285) (open square). The concentration of ANS was added stepwise to the equilibrium mixture and varied from 0 to 50 $\mu$ M. The letter r denotes the amount of ANS bound/protein and ANS<sub>free</sub> denotes free ANS which do not bound proteins. The raw data were corrected for dilution and inner filter effect. The excitation and emission wavelength were 370 nm and 460 nm respectively.

The fluorescence reached saturation when ANS was fully bound to HsHtrII proteins (Figure 3-36A, C and E). ANS with HsHtrII constructs were excited at 370 nm and emission maxima at 460 nm was recorded. In all cases, the spectrum of the buffer was subtracted to normalize ANS spectra. ANS was titrated against a fixed concentration of HsHtrII constructs and its complex with serine. Initial titration of ANS from 0 to 2  $\mu$ M showed that similar emission spectra between HsHtrII[1-765] and HsHtrII[1-765]-serine complex (Figure 3-36A). However, upon increasing ANS concentration from 2 to 50 $\mu$ M, ANS fluorescence intensities of HsHtrII[1-765]-serine complex decreased more than those of HsHtrII alone. This indicates that less ANS is bound to HsHtrII[1-765]-serine complex as compared to HsHtrII[1-765]. Similar decrease in fluorescence was observed in HsHtrII[1-398] with serine(Figure 3-36C). The data fits for HsHtrII[1-765] (Figure 3-36B) and HsHtrII[1-398] (Figure 3-36D) to the Scatchard equation give  $R^2=0.933$  and  $R^2=0.901$ , respectively. However, for the determination of the exact number of ANS binding sites, a Scatchard transformation may not be the best alternative for the HAMP domain ( $R^2=0.573$ ) and LBD ( $R^2=0.493$ ) of HsHtrII(Figure 3-36E and F), as it showed non-linearity and may reflect heterogeneity of ANS binding mode on the components of HsHtrII and difference in the size of molecules with different affinities. In the absence of serine, the molar ratio of HsHtrII[1-765] to ANS indicated that a HsHtrII[1-765] molecule binds 24 molecules of ANS per HsHtrII. HsHtrII[1-398], HAMP(303-466) domain and LBD (42-285) were bind to 17, 11 and 5 molecules of ANS per protein, respectively. By comparison, less ANS molecules are bound to the HsHtrII-serine complex. In comparison to HsHtrII in the absence of serine, HsHtrII [1-765]-serine complex (12 ANS molecules) and HsHtrII[1-398]-serine complex

## RESULTS

(22 ANS molecules) lost two and four ANS binding site, respectively. The binding of HsHtrII constructs to serine lead to a decrease of hydrophobic surface area and a subsequent loss of ANS binding sites.

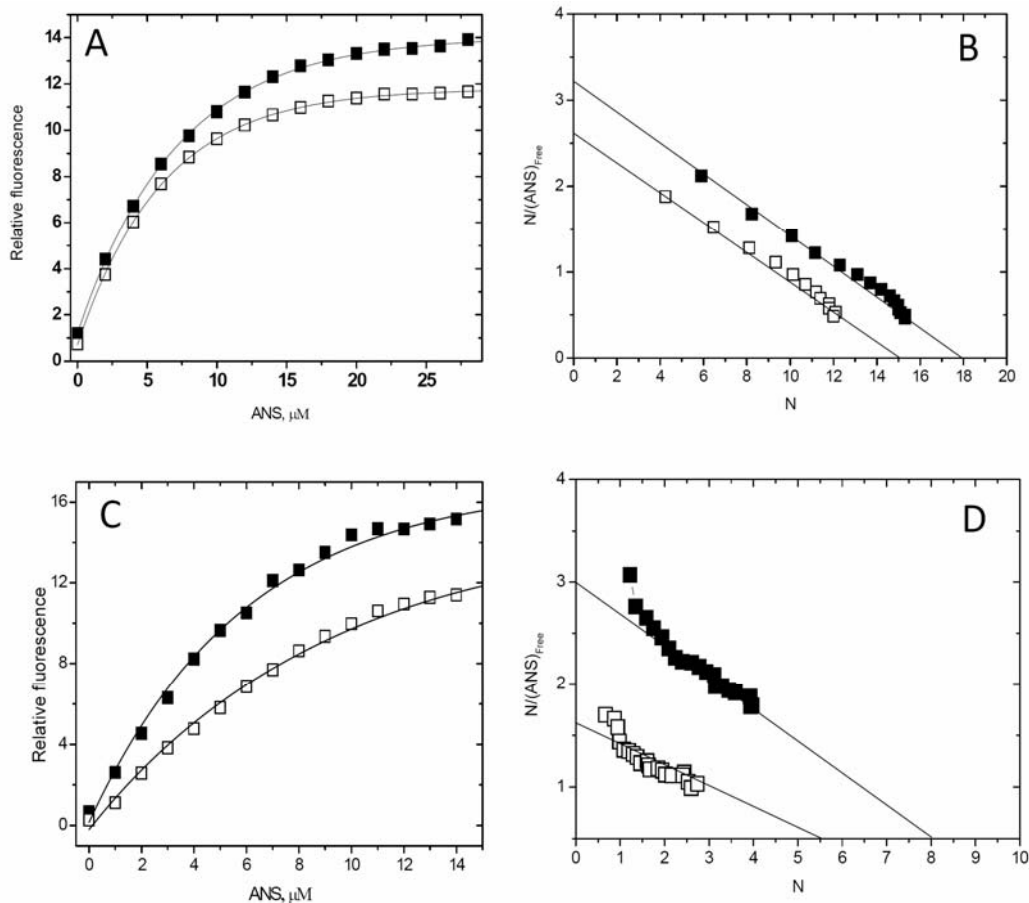


Figure 3-37. Comparison of ANS binding to Tar proteins. ANS titration of Tar constructs in the absence and presence of 10  $\mu\text{M}$  aspartate: (A) ANS titration of 1  $\mu\text{M}$  Tar [1-553] (closed square), Tar-aspartate (open square) (B) Scatchard plot for the binding of ANS to Tar [1-553](closed square) and Tar [1-553]-aspartate (open square). (C) ANS titration of 1  $\mu\text{M}$  Tar LBD (26-184) (closed square), Tar LBD(26-184) -aspartate (open square) (D) Scatchard plot for the binding of ANS to Tar LBD (26-184)(closed square) and Tar LBD (26-184)-aspartate (open square). The letter N denotes the amount of ANS bound per protein and  $\text{ANS}_{\text{free}}$  denotes free ANS. The Fluorescence was excited at 370 nm and spectra were recorded at 480 nm in 20 mM Tris-HCl, 150 mM NaCl, pH 7. The values of ANS bound per protein from HsHtrII constructs and Tar constructs in the presence and absence of ligand. The plot represents averaged fluorescence values from three or more experiments.

## RESULTS

---

Scatchard plot analysis of Tar chemoreceptor: A similar results were obtained when ANS was titrated against Tar constructs(1-553) and Tar LBD(26-184) in the presence of aspartate (Figure 3-37). Monitoring of intensity change showed that fluorescence intensity of aspartate-associated Tar was lower than aspartate-free form. In order to quantify the binding site of ANS on aspartate binding, either Tar with aspartate or Tar alone was titrated with increasing concentration of ANS from 2 to 50  $\mu\text{M}$ . To examine the binding stoichiometry, a Scatchard analysis was performed for the Tar constructs. ANS bound to aspartate free Tar constructs exhibited values of 18 molecules for Tar [1-553] (Figure 3-37B) and 8 molecules for Tar-LBD (26-184) (Figure 3-37D), respectively. The ANS binding sites for aspartate binding of Tar [1-553] and Tar-LBD (26-184) were found to be 16 and 5 molecules, respectively. These observations indicate that the conformation and number of ANS binding sites are affected by aspartate which is quite similar to the dynamic behavior of the serine associated HsHtrII constructs. Therefore one can conclude that less hydrophobic regions of both ligand associated HsHtrII and Tar chemoreceptor can bind less hydrophobic ANS dye. It suggests that the ligand associated receptors reduced its hydrophobic environment, which led to the optimization of the compact and less dynamic structure.

## 4. DISCUSSION

## 4. Discussion

The photosensors sensory rhodopsin I and II are responsible for phototaxis signaling in *Halobacterium salinarum* (126,132,157-159). Sensory rhodopsin II, a blue light photoreceptor from *H. salinarum* (HsSRII), in complex with its cognate transducer protein (HsHtrII) triggers the photophobic response of the bacteria. HsHtrII possess a dual functionality as it can act also as a chemotransducer sensing serine as a substrate via its large periplasmic ligand binding domain. Since the signal transduction of HsHtrII is similar to a chemotactic system structural and functional data obtained for chemoreceptors like Tar or Tsr from *E. Coli* can also be applied to the archaeal photosensory system. For example, the tertiary structure of the cytoplasmic domain of bacterial chemoreceptor can be taken as a model also for the corresponding domain of HsHtrII. Quite a few additional data comes from other biochemical and structural analysis so that one can depict a model of the complex and that in analogy to the *N. pharaonis* NpSRII/NpHtrII complex the first steps of signal transfer can be envisioned. However, it is not clear how membrane proximal signaling events are triggered by extracellular and/or membrane associated ligand binding. In addition, it is not well understood how signals are recognized and how sensitivity combined with a dynamic range is tuned for adequate signaling. It is the aim of the present work to shed light into these questions.

The model systems to study transmembrane signal transduction consist of the chemosensory domain of HsHtrII and its cognate photoreceptor HsSRII. Because of their functional and structural similarities the bacterial aspartate (Tar) chemoreceptor was included in this study. Main focus of the work was the elucidation of ligand binding to their receptors and analysis of the subsequent conformational changes across the membrane.

### 4.1. Biochemical and biophysical characterization of HsSRII

First HsSRII were purified in high yields (5-7mg/L). Purification of HsSRII expressed in *E.coli* was achieved by introducing a C-terminal seven histidine tag. Since the recombinantly expressed HsSRII shows the same

## DISCUSSION

---

characteristic spectroscopic properties as SRII isolated from *H.salinarum*, it can be concluded that neither the *E.coli* expression system nor the C-terminal histidine tag alters the functionality of HsSRII. UV-Vis spectroscopy also revealed that about 90% of HsSRII shows the characteristic absorption maximum ( $\lambda_{\max} = 487\text{nm}$ ) at high salt concentrations (4M NaCl). However, lowering the salt concentration (<2M NaCl) rendered HsSRII unstable and more than 60% of denatured HsSRII was observed reflecting the natural habitat of halophilic archaea.

HsSRII displays a typical photocycle of archaeal photosensors with prolonged kinetics. To optimize the stability of HsSRII, the purified membrane protein was solubilized in detergent (DDM) at high salt concentration (4M NaCl) and reconstituted in purple membrane lipids (PMLs). The photocycle kinetics of detergent solubilized and lipid reconstituted HsSRII were analyzed by recording the transient absorption changes at three different wavelengths (360, 490 and 520 nm). The wavelengths of 360, 490 and 520nm were selected to follow the rise and decay of the characteristic photocycle intermediates of M-, ground- and O state, respectively. Analysis of the photocycle kinetics of HsSRII in detergent revealed eight distinct kinetic components (rate constants). Despite the fact that the absorption maximum ( $\lambda_{\max} = 487\text{nm}$ ) of HsSRII is not altered either solubilized by detergent or reconstituted in PMLs, the photocycle of HsSRII is considerably affected by different chemical conditions. In the PML-reconstituted HsSRII the half life times were generally faster and an acceleration of the M-decay was observed as compared to the HsSRII in detergent.

The photocycles of HsSRII showed that turnover and rate constants are almost not affected by binding of HsHtrII to HsSRII. Only minor differences are observed in the HsSRII photocycle upon transducer binding, causing the reduction of amplitude of the O-intermediate and small alteration of rate constants. Interestingly, binding of HsHtrII to the homologous natronobacterial receptor NpSRII also reduced the amplitude of the O-intermediate. Apparently, a functional complex was formed indicating that the interaction surface is not species selective. These observations suggest

that transducer binding must be exact in order to guarantee specific signal transfer.

### 4.2. Binding of serine to HsHtrII

The extracellular domain of HsHtrII was proposed to be a serine binding receptor(63). In order to determine whether this assumption is correct, the dissociation constant of serine binding to HsHtrII was determined to be about 5  $\mu\text{M}$  as observed from ITC experiment. This conclusion agrees with the observation that Tar chemoreceptor yields similar affinity ( $K_D=5.6\mu\text{M}$ ) upon complex formation with aspartate. Furthermore, the affinity of HsHtrII with serine was also determined by intrinsic tryptophan fluorescence. Addition of serine to HsHtrII showed decrease in Trp fluorescence. The titration of serine to HsHtrII yields dissociation constants in the micromolar range ( $K_D=3-4\mu\text{M}$ ) as observed by Trp fluorescence quenching. These results strongly suggest that the extracellular domain indeed is a serine receptor.

Two observed rate constants ( $k_{\text{obs}} = 1.8 \pm 0.6 \times 10^{-2} \text{ s}^{-1}$  and  $1.2 \pm 0.9 \times 10^{-3} \text{ s}^{-1}$ ) were obtained for HsHtrII-Ser complex formation by stop flow measurement. The two steps of reaction presumably lie with some level of cooperativity. The kinetic value of  $1.8 \pm 0.6 \times 10^{-2} \text{ s}^{-1}$  might reflect a first binding site for serine and the smaller kinetic value of  $1.2 \pm 0.9 \times 10^{-3} \text{ s}^{-1}$  might reflect a second binding site for serine. The interactions formed upon binding the first serine is occupied in the homodimer, resulting in diminished binding at the second binding sites, which can be explained by negative cooperativity of the bacterial attractant binding response.

The exact mechanism of the archeobacterial chemotaxis still remains unclear, particularly in the area concerning signal propagation from the receptor unit to the signaling domain. The lack of any structural information for HsHtrII protein clearly hampers the study of the signal relay. The elucidation of the distribution, dynamics, and function of membrane proteins in signal transduction is essential for the understanding of their cellular functions. A major issue is how to correlate the conformational changes and ligand binding event of HsHtrII and Tar chemoreceptor.

## DISCUSSION

The mechanism of serine-induced conformational changes of HsHtrII has not yet been clarified. However, the ligand induced conformational change is accompanied by a change in Trp fluorescence which reflects the changes in the protein local environment. In response to serine binding tryptophan fluorescence is significantly quenched. Thus the binding of serine to HsHtrII[1-398] might be due to a conformational change that would allow solvent penetration in the hydrophobic core of protein.

Comparing the primary sequence of Tar chemoreceptor with that of HsHtrII reveals a common domain structure including the extracellular receptor-, transmembrane-, and cytoplasmic domain (Figure 4-1).

Protein	TM 1 domain	Ligand binding domain	TM 2 domain
HsHtrII	26 VLSVGVGTFVYQQT	TTQLET DVRADLTGSADARADHLDAW-----WSVLVRAPHDRALG	FVASSLVGLVLITI 292
EcTar	16 GV FALLQLISGSLF	FSSLHHSQKSFVVS NQLREQQELTS-----SEKLYRDI VTDNADDYR	FAQWQLAVIALVVV 202

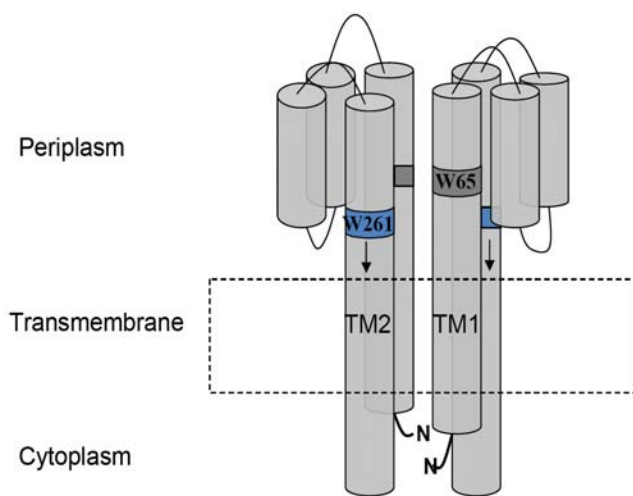


Figure 4-1 Sequences alignment of the HsHtrII and Tar chemoreceptor (upper panel) and schematic representation of piston model for HsHtrII (lower panel). Trp 261 and Trp 65 are represented blue and gray boxes, respectively. Upon binding serine, TM2 is proposed to be displaced towards the cytoplasm.

It appears that the aspartate binding domain likely possesses a very similar architecture to the ligand binding domain of HsHtrII so that one can use the structural information of Tar to model in first approximation Ser receptor domain of HsHtrII. This allows placing Trp within the structure



(Figure 4-1, lower panel). The binding of aspartate induces a displacement of signaling helices that was explained by the piston movement, which is a 1-2 Å displacement of the TM 2 domain towards the cytoplasm (160,161). The two tryptophan residues (Trp 65, Trp 261) which are positioned in periplasmic domain could be altered the fluorescence emission properties by one or both tryptophans being close to water in a more hydrophilic environment. This result defines more clearly the role of the ligand binding event and suggests that serine binding to HsHtrII results in some ligand induced motion in periplasmic domain. Especially, Trp 261 in the periplasmic domain is predicted to be close to the N-terminus of the TM 2 domain of HsHtrII which might induce the transmembrane signaling (Figure 4.1 lower panel). Using the same reasoning of the piston movement for Tar chemoreceptor, serine binding could cause a similar piston movement of HsHtrII. Therefore, the displacement of Trp 261 induced by serine binding may disrupt the helical packing interface to allow water exposure. The results presented here provide the first structural explanation for signaling of HsHtrII as observed by intrinsic Trp fluorescence.

Previous SDSL EPR studies (85-87) suggested that light activation of NpSRII leads to a displacement of Helix F, which in turn triggers a rotational motion of TM 2 in NpHtrII. Therefore, it could suggest that HsHtrII in the presence of an attractant seems to employ piston-based communication mechanism, whereas the light-induced rotational TM 2 motion appears to trigger the repellent signaling state of NpHtrII.

### **4.3. Ligand-induced conformational changes of HsHtrII and Tar chemoreceptor**

Molten globule state has been suggested to be involved in many important physiological processes, including signal transduction and interactions with molecules(162). For example, activation of chemotaxis receptor and phototransducer occurs through very subtle small helix movements during the activation(163,164). The molten globule like structure proposed here

## DISCUSSION

---

could contribute to the mechanism for activation such as modulation of kinase activity.

In order to investigate conformational changes of HsHtrII as a serine chemosensor and identify folding intermediate such as molten globule like protein, chemical ANS fluorescence probes were used to validate predicted structural changes in HsHtrII constructs. Used as a fluorescent probe, ANS shows an increase in the quantum yield of fluorescence and a blue shift of the emission spectrum when it interacts with the hydrophobic regions of a protein. It allowed detection of the molten globule like structure and function of protein. The molten globule state is a compact structure with significant native-like secondary structure, but with disrupted tertiary interaction (165). Well-folded proteins do not bind the dye strongly, but those possessing molten or more dynamic hydrophobic cores bind ANS typically with micro molar affinities, resulting in a large increase in fluorescence (112,113). In addition, the titration of ANS also provides detailed information about stoichiometry of protein-ANS, properties and location of binding sites. This method, however, has a limitation that it can only be used to monitor water-soluble protein. Membrane proteins, being in a more complex physiological surrounding with lipids or if isolated in detergents, limit the application of this method. Unspecific binding of ANS to lipids and detergents result in high background of non-specific fluorescence. To overcome this problem, the detergent-free HsHtrII and Tar protein were purified to determine whether the affinity of serine is a potent ligand of HsHtrII. However, detergent free condition may lead to variations of highly flexible states of HsHtrII and Tar chemoreceptor which are non-physiological. Since water-soluble membrane proteins were produced without detergent, it suggests that more than 80% of water-soluble extramembrane part is able to solubilize the transmembrane part (~20%) of the protein. Moreover, the detergent free HsHtrII and Tar protein purified from cytosolic fraction were folded into well-defined secondary  $\alpha$ -helical structure as indicated by CD spectroscopy. This implies that most of the water soluble Tar and HsHtrII protein retain their function during the course of the experiment. Therefore, the results presented in this study characterize detergent free HsHtrII as a suitable

## DISCUSSION

object for studying ligand-dependent conformational changes with hydrophobic fluorescence probes.

To determine how the ligand affects the hydrophobic packing of the interior of the protein and conformational changes, the binding of ANS to the HsHtrII as well as to the Tar chemoreceptor was investigated.

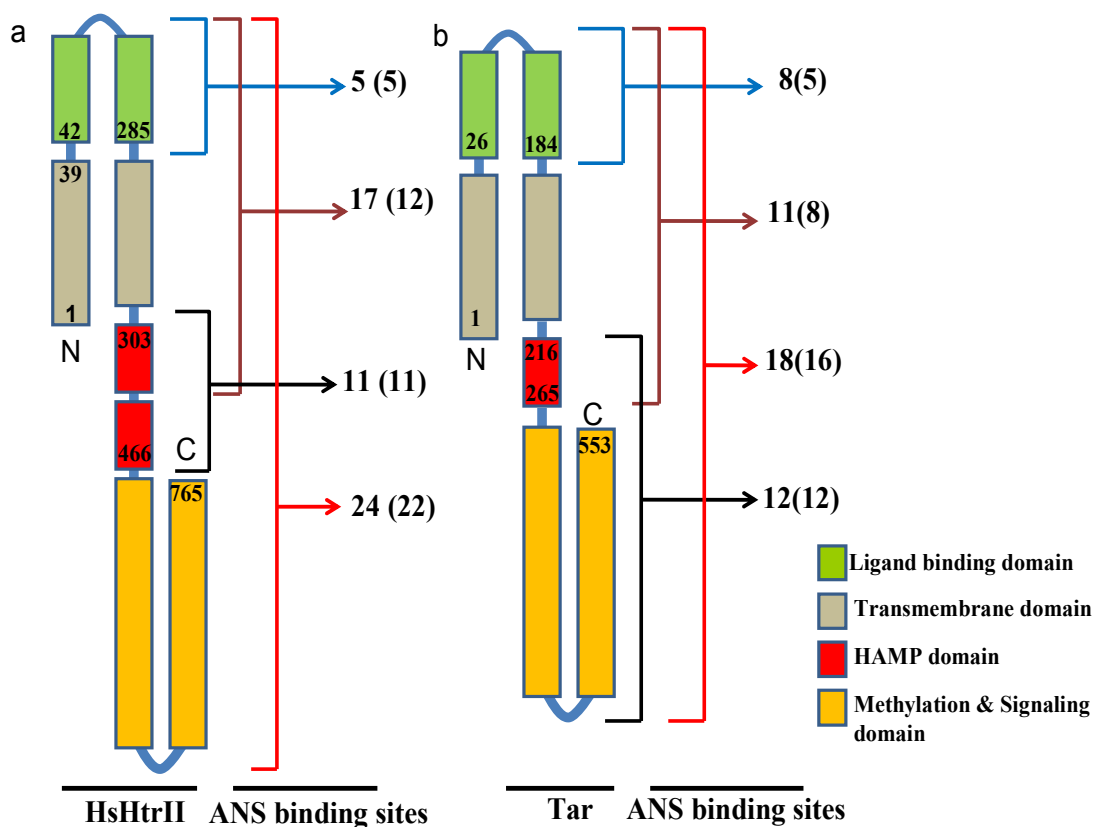


Figure 4-2. The stoichiometry of ANS bound to the protein. (a)HsHtrII, (b)Tar chemoreceptor. A round bracket indicates the number of ANS binding sites in the presence of ligands (serine for HsHtrII, aspartate for Tar chemoreceptor).

The conformational changes of HsHtrII upon binding to serine resulted in a decreased hydrophobic surface area and a subsequent decrease in ANS fluorescence intensity of the HsHtrII-serine complex. A similar result was observed for Tar chemoreceptor in response to aspartate binding. Moreover, titrations of ANS provide detailed information about alterations in the stoichiometry of complex formation.

## DISCUSSION

---

Figure 4-2 summarizes the results from the ANS experiments. A comparison among different HsHtrII constructs and Tar constructs resulted in a distinct number of binding sites. The ANS titration of HsHtrII and Tar provided Scatchard plots which are distinguished depending on ligand binding. Both HsHtrII[1-765] and HsHtrII[1-398] resulted in loss of the number of ANS binding sites when serine is bound (Figure 4-2a). Full length HsHtrII [1-765] lost two ANS binding sites, whereas HsHtrII with one HAMP domain (HsHtrII [1-398]) lost five ANS binding sites in the presence of serine. The different loss of ANS binding sites for HsHtrII [1-398] may accompany by the conformational change of some of the missing components according to its dynamic properties. No change in ANS fluorescence for the ligand binding domain (LBD) of HsHtrII [42-285] was observed in the presence of serine. In contrast, a Scatchard plot analysis of the Tar-LBD [26-184] revealed that in the presence of aspartate (Figure 4-2b), three ANS binding sites are lost. Thus, the conformation of the HsHtrII-LBD [42-285] differs from that of Tar-LBD [26-184]. This was confirmed by CD spectroscopy which showed that secondary helical content of HsHtrII-LBD[42-285] is 90% of random coil, a conformation that does not bind ANS (166). The unfolded structure of the HsHtrII-LBD[42-285] may be due to the absence of other components of the system as the transmembrane and/or cytoplasmic domain which are needed to stabilize the tertiary structure of the ligand binding domain.

Because a molten globule conformation is characterized by maintenance of or increase in secondary structure (165), the HsHtrII-HAMP [303-466] domain to be about 20%  $\alpha$ -helical contents which is not indicative for molten globule like secondary structure. However, The HsHtrII-HAMP [303-466] domain has a relatively large amount of ANS binding sites (11 ANS binding sites, red box) reflecting a highly flexible or expanded structure which might be correlate to a molten globular state which is well in line with a molten globular type of HAMP domain from *N.pharaonis* proposed by Bordignon and co-workers(167). Compared to HAMP domain from NpHtrII at low salt concentration, the presence of high salt concentration induces less molten-globule-like state of HAMP domain(167). These findings, together with the

## DISCUSSION

---

presence of ANS, suggest that addition of ANS to HsHtrII-HAMP [303-466] may induce  $\alpha$ -helix formation and stabilization of a molten-globule-like state.

The structural integrity of HsHtrII and its analogues were further studied in a range of different temperatures and salt conditions using CD spectroscopy. The substantial increases in  $\alpha$ -helical content of the HsHtrII constructs at high salt concentrations indicate the adaptation of a molten globule like structure(165). These results are consistent with the salt dependency of ANS spectra of HsHtrII constructs. A two-fold higher number of ANS binding sites with high fluorescence intensity of HsHtrII[1-765] is observed at a high salt condition(4M NaCl, 24 ANS binding sites) as compared to a low salt condition (500 mM NaCl, 12 ANS binding sites) (see Figure 3-34D). This molten globule like behavior of HsHtrII may be important for the functionality of HsHtrII in a high salt environment.

HsHtrII has a high sequence homology with the cytoplasmic domain of the Tar chemoreceptor and displays a relatively dynamic structure in the absence of ligand. However, Tar chemoreceptor and HsHtrII are in a compact conformational state when aspartate and serine, respectively are bound as observed from ANS fluorescence experiments. In addition, no changes in the ANS binding sites of the cytoplasmic domains (HAMP, methylation and signaling domain), in the presence of ligand, are observed. Therefore, ligand-induced conformational changes in both proteins mainly affect the ligand binding site. Consequently, the presence of attractants shifts the ligand binding site into a more compact conformation.

CD spectra by thermal denaturation support the evidences that Tar chemoreceptor in the absence of ligand is somewhat less stable than those in the presence of ligand even in similar amount of  $\alpha$ -helical secondary contents. Therefore, it is plausible concept that the dynamics of HsHtrII and Tar chemoreceptor play an important role for transmembrane signal transduction.

It has been proposed that the conformational changes in the TM domain appear to be mechanically linked to those in the cytoplasmic and extracellular domains(99). The piston-like movement of aspartate-Tar chemoreceptor complex induce a closer association of both the cytoplasmic

## DISCUSSION

and extracellular domains(160,161). This ligand-induced motion generates other hydrophobic patches to occupy or contact its hydrophobic transmembrane domain. Thereby, it would provide the less hydrophobic cores of HsHtrII for ANS binding sites which may reflect the entirely less dynamic nature of protein.

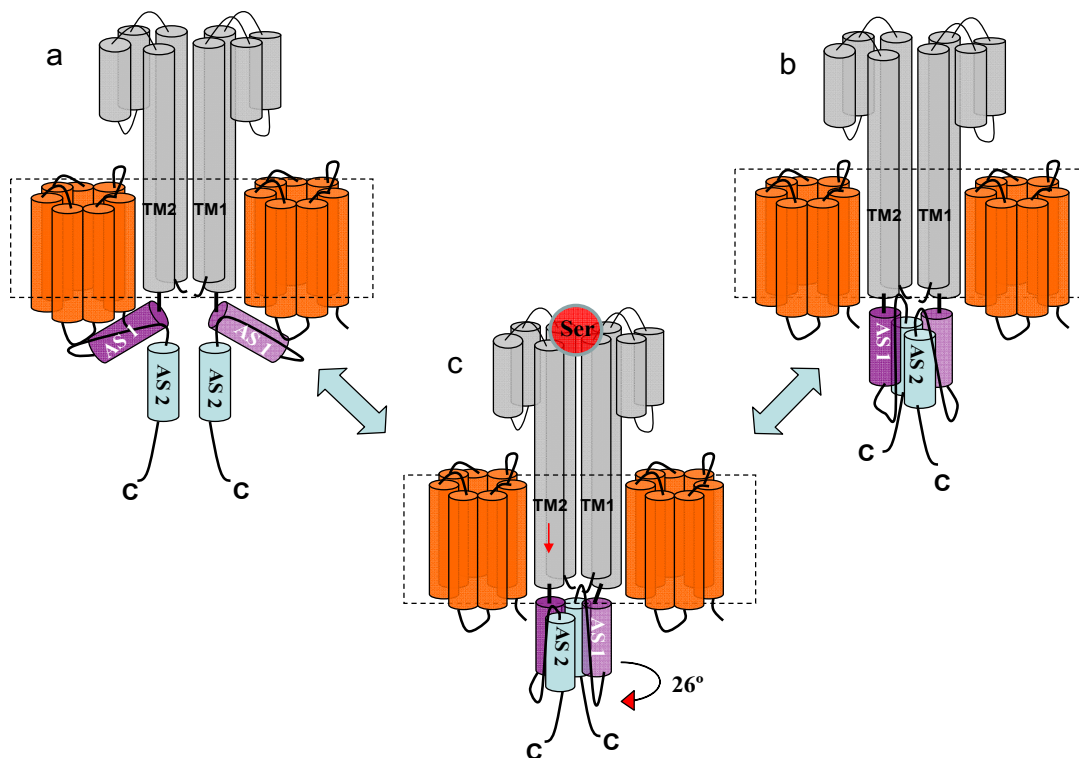


Figure 4-3. Two models for HsHtrII-HAMP conformational changes. The picture at the upper left (a) is based on data reported by Williams et al,(168). The picture at the upper right(b) is based on the data described previously by Hulko et al,(67). The bottom picture(c) shows the receptor in the presence of ligand (serine).

The HAMP domains are also able to adapt their sensitivity towards a variety of attractant and repellent inputs, induced by ligand binding to periplasmic domains and conformational changes of photoreceptors. Several evidences for a dynamic conformation of HAMP domain have been described in the literature (169-172). By screening for interaction HsHtrII with serine using ANS fluorescence, two models can be proposed to explain the dynamics of the HAMP domain as shown in Figure 4-3.

## DISCUSSION

---

Williams, S.B. and Stewart, V. (168) suggested that AS1 interacts with either AS2 or the cell membrane in different binding modes. During the activation of kinase (repellent binding), the AS1 helix of the HAMP domain is oriented nearly parallel to the inner face of cell membrane, with its hydrophobic residues in contact with the hydrophobic interior of the phospholipids bilayer and its hydrophilic face in contact with polar head groups. On the other hand, when the attractant binds to the receptor, AS1 might interact with AS2 and subsequently form stable arrangements. The other evidences showed that E-F loop of NpSRII bind to AS1 of NpHtrII and become even closer upon light activation as shown by FRET (173). Strong support has also been provided by increased solvent exposure of the AS1 helices as shown by introducing Trp residue (174). Taking into account the conformation of HAMP and NpSRII-NpHtrII signaling, the AS1 of HAMP domain might interact with an intact transmembrane domain and E-F loop region of HsSRII in the absence of serine (Figure 4-3a). Binding of serine might induce the interaction of AS1 with AS2 leading to a stabilized and less-dynamic tertiary structure of HAMP domain, which would be the attractant binding mode of the HsHtrII (Figure 4-3c).

Alternatively, the diagram in Figure 4-3b is based on the data described by Hulko *et al* (67). They proposed that signaling involves a 26° rotation of AS1 relative to AS2 that converts knob and knob packing to knob and hole packing. In the absence of serine, the four helix bundle is in one of its structurally stable arrangements with either knob and knob or knob and hole packing. After serine binding to HsHtrII, one of TM2 helices moves to an inward 1-2 Å piston displacement and AS1 might rotate by 26° which leads to the one of conformations (Figure 4-3c). Because both conformations are stable, a structural plasticity of HsHtrII could be mainly resulted from the conformation of ligand binding domain.

The study presented here is an investigation of water-soluble HsHtrII and Tar chemoreceptor functions to provide a plausible explanation how chemosensory machinery can process the change in the ligand binding domain. However, it remains to be seen whether similar conformational states are also observed in the presence of a membrane environment and

how the conformational change is affected by different osmotic conditions, as they are in the periplasmic and cytoplasmic region. Furthermore dynamic information is not easily obtained from static crystal structure. Clearly, new and innovative methods are needed to enable the comparison of light- and serine induced structural changes and rotary- or piston motion in HsHtrII. EPR and electron microscopy methods will shed light on these important issues.

#### 4.4. The HsSRII-HsHtrII complex formation

To further characterize the HsHtrII and HsSRII-HsHtrII complex, analytical gel filtration was performed. These experiments showed that HsHtrII[1-398] as well as the HsHtrII[1-398]-HsSRII complexes are present in several oligomeric forms. HsHtrII [1-398] does not contain the signaling tip which is mainly involved in the functional trimer of dimers formation but it forms with hexameric form (~330 kDa) in 4M NaCl buffer. Another possibility to form higher order oligomers is supported by Park et al(175). They observed that even though chemoreceptor from *Thermotoga martima* conserves most of the Tsr signaling tip, the MCPs stack in hedgerows in the crystal. Therefore, a similar assembly pattern may also happen to HsHtrII[1-398] as a large bundle of helices. Several minor shifted peaks (240, 310 and 470 kDa) were revealed when HsSRII was added to HsHtrII[1-398] in a 1:1 stoichiometry. The species at 240 is slightly larger than that determined for the dimer of HsHtrII[1-398]-HsSRII complex (~210kDa). However, taking the variation of DDM micelle size into account (50-70kDa), the other higher oligomeric forms in HsHtrII[1-398]-HsSRII complex could be explained by folding from dimer into hexamer in micellar environment. Especially for the shifted peak at 470 kDa, it is well in line with the hexamer of HsHtrII[1-398]-HsSRII complex, which is the functional unit of chemoreception.

Calorimetric techniques were applied to analyze the HsHtrII interaction with the HsSRII protein which provided information about the affinity and thermodynamic parameters of the binding process. This information is of general interest because it could be shown that isothermal titration



## DISCUSSION

---

calorimeter is a suitable method to directly study membrane protein-protein interactions which although performed in a micelle environment, will enlarge our knowledge about this class of proteins. Using an isothermal titration calorimeter (ITC), it was seen that HsHtrII [1-765] binds to HsSRII with a  $K_d$  value of about 1  $\mu\text{M}$  and HsHtrII lacking the extracellular and cytoplasmic domain is also sufficient to bind the HsSRII with a slightly lower affinity.

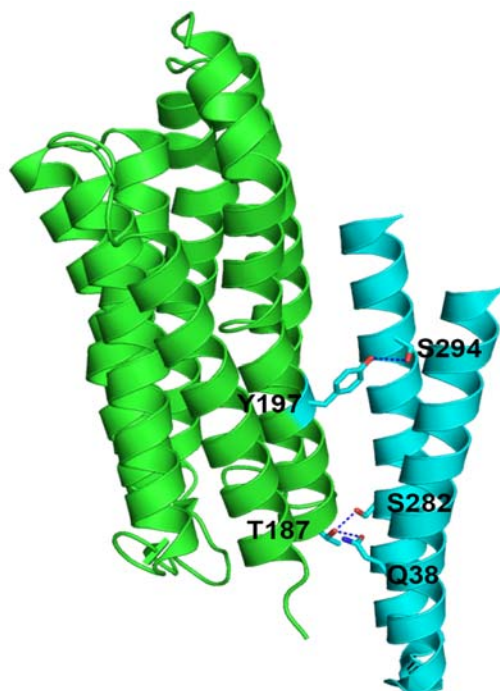


Figure 4-4. Interaction model of HsSRII-HsHtrII complex (side view) based on analogy of the NpSRII-NpHtrII complex (PDB ID code 1H2S). Three hydrogen bonding residues are depicted; Thr189 and Tyr199 in NpSRII corresponding to Thr 187 and Tyr 197 in HsSRII (green ribbon), respectively. Asn74, Ser 62 and Glu 43 in NpHtrII correspond to Ser 294, Ser 282 and Gln 38 in HsHtrII (blue ribbon).

The crystal structure of NpSRII-NpHtrII[1-114] complex has been determined to reveal amino acids (residues,1-82) of the transducer which associates with NpSRII helices F and G (17). The crystal structure of HsSRII is not known. However HsSRII shows around 53% sequence homology to NpSRII and mediates photophobic behaviour of cells through the NpHtrII (90). The HsHtrII region might also harbour the recognition site

## DISCUSSION

---

for its cognate photoreceptor HsSR<sub>II</sub>. Therefore, it is expected to form a structurally similar receptor-transducer interface.

It is shown that five amino acids were important for binding and function (Figure 4-4). This comprises T189 and Y199 in NpSR<sub>II</sub> which form hydrogen bonds with NpHtr<sub>II</sub> residues N74, S62, and E43 (17,137-139) and homologous amino acids are also found in *H. salinarum* system (NpSR<sub>II</sub>→HsSR<sub>II</sub>: T189→T187; Y199→Y197. NpHtr<sub>II</sub>→HsHtr<sub>II</sub>: N74→S294; S62→S282; E43→Q38) (140). These similarities suggest that HsHtr<sub>II</sub> might not only bind to its cognate receptor but also to NpSR<sub>II</sub>. This specificity of receptor-transducer was demonstrated by substitution of their native SR<sub>II</sub> receptors by site directed mutagenesis. Strong support for NpSR<sub>II</sub> binding to HsHtr<sub>II</sub> is provided by ITC ( $K_d \sim 2 \mu\text{M}$ ) and blue native gel electrophoresis. These results corroborate data obtained for NpHtr<sub>II</sub> showing that a minimal binding domain comprising the two transmembrane helices (NpHtr<sub>II</sub>[1-114]) is sufficient (135). Salt dependency of the complex formation was found to be negligible, indicating that mainly hydrophobic interactions contribute to the binding of HsHtr<sub>II</sub> to HsSR<sub>II</sub>, in agreement with the natural habitat of *H. salinarum*.

Previous ITC experiments showed that the N-terminal 114-residue fragment of NpHtr<sub>II</sub>, which contains the TM domain and 22 residues of the cytoplasmic extension, is sufficient for high affinity binding to NpSR<sub>II</sub> in detergent micelles, whereas the N-terminal 100-residue fragment did not bind (135). Hippler-Mreyen *et al* (135) suggested that the NpHtr<sub>II</sub> sequence of the residues from 101 to 114 (GDGDL DVELETRRE) is highly charged, including six negative and two positive charges, which provide for the electrostatic interactions with NpSR<sub>II</sub>. In addition, fluorescent probe showed that light-induced structural changes also occur in the cytoplasmic membrane-proximal region of the NpSR<sub>II</sub>-NpHtr<sub>II</sub> complex (173). HsHtr<sub>II</sub> from *H. salinarum* shows conserved residues from 323 to 334 (GDLDTDIDTSRN) with four of the acidic and one of the basic groups, which can be contributed to form complex by electrostatic interactions with HsSR<sub>II</sub> even under high ionic strength conditions. Therefore, these sites might be involved in the binding surface of the receptor to the transducer.

## DISCUSSION

---

These observations imply that the HtrII membrane-proximal domain interaction with the receptor might play an important role in the signal relay.

In addition, the calorimetric experiments allowed the calculation of heat capacity. The slope for  $\Delta H$  dependencies on temperature represents the heat capacity changes upon complex formation. Wegener, A.A *et al* (176) showed that the heat capacity of the interaction of NpSRII- NpHtrII(1-157) was found to be  $-1.7 \text{ kJ mol}^{-1} \text{ K}^{-1}$ , indicating the removal of hydrophobic surface area from the solvent as one would expect for complex assembly. However, in the case of complex formation of HsSRII and HsHtrII[1-398], the heat capacity ( $\Delta C_p$ ) showed positive values ( $0.82$  and  $1.9 \text{ kJ mol}^{-1} \text{ K}^{-1}$ ) ranging from  $20$  to  $30$  °C. A positive  $\Delta C_p$  of HsSRII-HsHtrII [1-398] complex formation appears to agree with the idea that a positive  $\Delta C_p$  is caused by the formation of the receptor and transducer complexes upon solvent exposure at higher temperature. At the same time, the equilibrium dissociation constants ( $K_d=1-3\mu\text{M}$ ) did not depend significantly on temperatures, which reflects interactions of transmembrane helices between the HsSRII and HsHtrII. Even though the increase of positive  $\Delta C_p$  values are obtained for HsSRII-HsHtrII [1-398] complex formation, substantial affinities of HsHtrII with HsSRII suggested that the stable transmembrane helix-helix contact is not influenced by water exposure. Therefore, one can conclude that protein solvent exposure of the positive  $\Delta C_p$  values appear to be mainly resulting from flexible extramembrane or water soluble regions of HsSRII and HsHtrII. However, the conformational flexibility of HsHtrII-HsSRII complexes has to be taken into account, if their function is influenced by its physical properties in their higher temperature environment, for example, why and how extramembrane becomes less helical conformation when bound to cognate partner protein at higher temperature.

## **5. SUMMARY**

## 5. Summary

Archaeobacterial photoreceptors mediate phototaxis by regulating cell mobility through the generation of intracellular two-component phosphorylation cascades. As a result, the cell modulates the direction of flagellar rotation and therefore migrates towards favorable surroundings. This sensory pathway also occurs in enteric bacteria in which the chemotaxis has been extensively studied. The model system employed here consists of chemosensory domain of cognate transducer (HsHtrII) and of the photoreceptor sensory rhodopsin II (HsSRII). HsHtrII has HsSRII binding domain and the periplasmic domains as a serine-receptor domain. An attempt was to bring together recent knowledge of general pattern of signal transduction processes in extreme halophilic archaea. High yield purification of HsSRII and HsHtrII proteins expressed in *E.coli* were achieved by introducing a C-terminal seven histidine tag. In order to investigate HsSRII photocycle in the favored nature mode, HsSRII in purple membrane lipid (PML) was monitored by laser flash photolysis method. HsSRII displays typical photocycle of archaeal photosensors with prolonged kinetics. Using an isothermal titration calorimetric (ITC) method, the dissociation constant of HsHtrII binding to the HsSRII was determined to be  $\sim 1\mu\text{M}$ , which is similar to that of corresponding transducer-receptor pair from *Natronobacterium pharaonis*.

As another line of the study, because the mechanism of serine-induced conformational changes of HsHtrII is not yet clarified, hydrophobic dye, 1-Anilinonaphthalene-8-Sulfonic Acid (ANS) fluorescent was used to validate predicted molten globule states and dynamic properties of HsHtrII. Significant increase of ANS fluorescence spectra for HsHtrII constructs was observed at higher salt concentration, which is well line with CD spectra of HsHtrII proteins that these proteins adopt a molten globule structure. At high salt concentration (4M NaCl), the  $\alpha$ -helical contents of HsHtrII constructs were increased to a comparable extent than those at low salt concentration (50mM NaCl).

## SUMMARY

---

HsHtrII binding to serine resulted in decreased ANS fluorescence spectra. Similar result was obtained for Tar chemoreceptor in response to aspartate binding. Additionally, the titration of ANS provides detailed information about stoichiometry of ligand-receptor complex formation and alteration of the environment of the binding sites. Upon serine binding to HsHtrII, the loss of ANS binding sites is mainly due to decrease of hydrophobic surface area, which leads to ligand-induced packing conformational change.

The titration of serine to HsHtrII was further carried out to determine the binding affinity using Trp fluorescence and ITC experiments. The dissociation constants were found to be 3-5 $\mu$ M which can be validated the dual-method approach for detecting binding and determining the binding affinity. Tar chemoreceptor shows similar affinity ( $K_d \sim 6 \mu$ M) for aspartate-chemoreceptor complex formation. These results confirm the proposition that the HsHtrII indeed is a serine receptor.

Based on biophysical and biochemical data of HsHtrII, point mutational studies may show that the exchange of key residues of putative serine binding site leads to the expected increase or decrease in the intrinsic fluorescence and dynamic conformation how the exact signal transduction mechanism involved in ligand interaction. Although sufficient amounts of water soluble HsHtrII and Tar chemoreceptor were isolated, their stability was apparently insufficient for crystallization. Therefore, optimizing crystallization conditions would be a major challenge for addressing issues related to ligand binding specificity and provide an explanation of how chemosensor machinery can process folding and conformational changes for general pattern of signal transduction pathway.

## Zusammenfassung

Die Phototaxis der Archaeobakterien wird durch Histidin-Kinase gekoppelte Rezeptoren und eine Zwei-Komponenten Signalkaskade reguliert. Durch die Signalübertragung über das Zwei-Komponenten System wird die Rotationsrichtung der Flagellen bestimmt, und die Zelle bewegt sich in Richtung günstiger Umweltbedingungen. Für Enterobakterien, die die Fähigkeit zur Chemotaxis besitzen, wurde ebenfalls eine Signalübertragung über ein Zwei-Komponenten System gefunden, welches bereits intensiv untersucht wurde.

Mit Hilfe dieser Arbeit sollen die generellen Modelle des Signaltransduktionsprozesse in extrem halophilen Archaeobakterien mit aktuellen Forschungsdaten verbunden werden. Das untersuchte Modellsystem besteht aus dem Photorezeptor Sensorhodopsin II (HsSRII) und der chemosensorischen Domäne des zugehörigen Transducers (HsHtrII). HsHtrII weist zusätzlich zu der HsSRII-Bindungsdomäne und der zytoplasmatischen Domäne eine extrazelluläre Serinrezeptordomäne auf. Die Expression der beiden Proteine HsSRII und HsHtrII erfolgte heterolog in *E. coli* und die Aufreinigung wurde über einen C-terminalen Histidin-Tag erreicht.

Um den Photozyklus von HsSRII zu untersuchen, wurde das Membranprotein in Purpurmembranlipide rekonstituiert und der Photozyklus mittels Laserblitz-Absorptionsspektroskopie gemessen. HsSRII zeigt einen für archaebakterielle Photosensoren typischen Photozyklus mit anhaltender Kinetik.

Mit Hilfe der Isothermen-Titrationskalorimetrie (ITC) konnte für den Transducer-Rezeptor-Komplex eine Dissoziationskonstante von 1  $\mu\text{M}$  bestimmt werden, welche dem homologen Komplex aus *Natronobacterium pharaonis* ähnlich ist.

Ein weiterer Schwerpunkt dieser Arbeit war es den Mechanismus der Serin induzierten Konformationsänderung im Rezeptor HsHtrII aufzuklären. Hierzu wurden Fluoreszenzmessungen mit dem hydrophoben Farbstoff 1-Anilinonaphthalen-8-Sulfonsäure (ANS) durchgeführt, um die dynamischen

## SUMMARY

---

Eigenschaften und den *molten globule* Zustand des Transducers HsHtrII zu charakterisieren. Es wurde ein Anstieg der ANS-Fluoreszenz für HsHtrII unter Hochsalzbedingungen beobachtet, was in Übereinstimmung mit CD-Spektroskopie Daten liegt, die den *molten globule* Zustand des Rezeptors zeigen. Unter Hochsalzbedingungen von 4 M NaCl wurde für den Transducer HsHtrII ein höherer  $\alpha$ -helikaler Anteil gefunden als unter niedrigen Salzkonzentrationen (50 mM NaCl). Die Bindung von Serin bewirkt eine Abnahme der ANS-Fluoreszenz beim HsHtrII-Serin-Komplex. Ähnliche Ergebnisse wurden für die Aspartatbindung an den Chemorezeptor Tar beobachtet.

Zusätzlich lassen sich aus Fluoreszenzmessungen, bei denen ANS zu HsHtrII titriert wird, Informationen über die Stöchiometrie der Ligand-Rezeptor Komplexbildung und der Änderung in der Umgebung der Bindetaschen gewinnen. Die Bindung des Serins an den Rezeptor HsHtrII verringert die hydrophobe Oberfläche des Proteins, was in einer Abnahme der ANS-Fluoreszenz des HsHtrII-Serin-Komplexes resultiert. Dies weist auf einen Liganden-induzierte Konformationsänderung im Protein hin.

Die Bindungsaffinität von Serin zu dem Transducer HsHtrII wurde durch Messung der Trp Fluoreszenz und ITC Experimente bestimmt. Durch diesen dualen Ansatz konnte der Nachweis der Bindung und die Berechnung der Bindungsaffinität erfolgen und so eine Dissoziationskonstante von 3-5  $\mu\text{M}$  ermittelt werden. Der Chemorezeptor Tar zeigt eine ähnliche Affinität ( $K_d \sim 6 \mu\text{M}$ ) für die Bildung des Aspartat-Chemorezeptor Komplexes. Diese Ergebnisse bestätigen die Annahme, dass HsHtrII ein Serinrezeptor ist.

Basierend auf den biophysikalischen und biochemischen Daten des HsHtrII könnten Punktmutationsstudien durchgeführt werden, bei denen Aminosäuren ausgetauscht werden, welche vermeintlich an der Serinbindung beteiligt sind und somit zu einer Erniedrigung beziehungsweise Erhöhung der intrinsischen Fluoreszenz und der dynamischen Konformation führen. Bis jetzt ist es noch nicht vollkommen geklärt, wie der exakte Signaltransduktionsmechanismus während der Interaktion des Liganden mit dem Chemorezeptor funktioniert.



## SUMMARY

---

Obwohl ausreichende Mengen von löslichem HsHtrII und Tar-Chemorezeptor isoliert werden konnten, ist ihre Stabilität für eine Kristallisation nicht ausreichend. Deshalb stellt die Optimierung der Kristallisationsbedingungen eine große Herausforderung dar, um die Frage nach der Ligandenbindungsspezifität zu beantworten. Desweiteren könnte dadurch die Aufklärung der Struktur der Chemosensoren und der Konformationsänderungen während der Signaltransduktion erfolgen.

## 6. REFERENCES

## REFERENCES

---

### REFERENCES

1. Bibikov, S. I., R. Biran, K. E. Rudd, and J. S. Parkinson (1997) A signal transducer for aerotaxis in *Escherichia coli*. *Journal of Bacteriology* **179**, 4075-4079.
2. Mesibov, R. and J. Adler (1972) Chemotaxis Toward Amino-Acids in *Escherichia-Coli*. *Journal of Bacteriology* **112**, 315-&.
3. Rebbapragada, A., M. S. Johnson, G. P. Harding, A. J. Zuccarelli, H. M. Fletcher, I. B. Zhulin, and B. L. Taylor (1997) The Aer protein and the serine chemoreceptor Tsr independently sense intracellular energy levels and transduce oxygen, redox, and energy signals for *Escherichia coli* behavior. *Proceedings of the National Academy of Sciences of the United States of America* **94**, 10541-10546.
4. Wadhams, G. H. and J. P. Armitage (2004) Making sense of it all: bacterial chemotaxis. *Nat. Rev. Mol. Cell Biol.* **5**, 1024-1037.
5. Hazelbauer, G. L., J. J. Falke, and J. S. Parkinson (2008) Bacterial chemoreceptors: high-performance signaling in networked arrays. *Trends Biochem. Sci.* **33**, 9-19.
6. Endres, R. G., O. Oleksiuk, C. H. Hansen, Y. Meir, V. Sourjik, and N. S. Wingreen (2008) Variable sizes of *Escherichia coli* chemoreceptor signaling teams. *Molecular Systems Biology* **4**.
7. Sourjik, V. (2006) Dynamics of the bacterial chemotaxis pathway. *Journal of General Physiology* **128**.
8. Sourjik, V. and H. C. Berg (2004) Functional interactions between receptors in bacterial chemotaxis. *Nature* **428**, 437-441.
9. Falke, J. J. and S. H. Kim (2000) Structure of a conserved receptor domain that regulates kinase activity: the cytoplasmic domain of bacterial taxis receptors. *Curr. Opin. Struct. Biol.* **10**, 462-469.
10. Falke, J. J. and G. L. Hazelbauer (2001) Transmembrane signaling in bacterial chemoreceptors. *Trends Biochem. Sci.* **26**, 257-265.
11. LeMoual, H. and D. E. Koshland (1996) Molecular evolution of the C-terminal cytoplasmic domain of a superfamily of bacterial receptors involved in taxis. *Journal of Molecular Biology* **261**, 568-585.
12. Falke, J. J., R. B. Bass, S. L. Butler, S. A. Chervitz, and M. A. Danielson (1997) The two-component signaling pathway of bacterial chemotaxis: A molecular view of signal transduction by receptors, kinases, and adaptation enzymes. *Annual Review of Cell and Developmental Biology* **13**, 457-512.
13. Gardina, P. J., A. F. Bormans, M. A. Hawkins, J. W. Meeker, and M. D. Manson (1997) Maltose-binding protein interacts simultaneously and asymmetrically with both subunits of the Tar chemoreceptor. *Molecular Microbiology* **23**, 1181-1191.
14. Kossmann, M., C. Wolff, and M. D. Manson (1988) Maltose Chemoreceptor of *Escherichia-Coli* - Interaction of Maltose-Binding Protein and the Tar Signal Transducer. *Journal of Bacteriology* **170**, 4516-4521.

## REFERENCES

---

15. Trivedi, V. D. and J. L. Spudich (2003) Photostimulation of a sensory rhodopsin II/HtrII/Tsr fusion chimera activates CheA-autophosphorylation and CheY-phosphotransfer in vitro. *Biochemistry* **42**, 13887-13892.
16. Jung, K. H., E. N. Spudich, V. D. Trivedi, and J. L. Spudich (2001) An archaeal photosignal-transducing module mediates phototaxis in *Escherichia coli*. *J. Bacteriol.* **183**, 6365-6371.
17. Gordeliy, V. I., J. Labahn, R. Moukhametzianov, R. Efremov, J. Granzin, R. Schlesinger, G. Buldt, T. Savopol, A. J. Scheidig, J. P. Klare, and M. Engelhard (2002) Molecular basis of transmembrane signalling by sensory rhodopsin II-transducer complex. *Nature* **419**, 484-487.
18. Hess, J. F., K. Oosawa, P. Matsumura, and M. I. Simon (1987) Protein phosphorylation is involved in bacterial chemotaxis. *Proc. Natl. Acad. Sci. U. S. A* **84**, 7609-7613.
19. Hess, J. F., R. B. Bourret, K. Oosawa, P. Matsumura, and M. I. Simon (1988) Protein phosphorylation and bacterial chemotaxis. *Cold Spring Harb. Symp. Quant. Biol.* **53 Pt 1**, 41-48.
20. Bren, A., M. Welch, Y. Blat, and M. Eisenbach (1996) Signal termination in bacterial chemotaxis: CheZ mediates dephosphorylation of free rather than switch-bound CheY. *Proceedings of the National Academy of Sciences of the United States of America* **93**, 10090-10093.
21. Bren, A. and M. Eisenbach (1998) The N terminus of the flagellar switch protein, FliM, is the binding domain for the chemotactic response regulator, CheY. *Journal of Molecular Biology* **278**, 507-514.
22. Welch, M., K. Oosawa, S. I. Aizawa, and M. Eisenbach (1993) Phosphorylation-Dependent Binding of A Signal Molecule to the Flagellar Switch of Bacteria. *Proceedings of the National Academy of Sciences of the United States of America* **90**, 8787-8791.
23. Aizawa, S., C. S. Harwood, and R. J. Kadner (2000) Signaling components in bacterial locomotion and sensory reception. *Journal of Bacteriology* **182**, 1459-1471.
24. Hegemann, P. (2008) Algal sensory photoreceptors. *Annu. Rev. Plant Biol.* **59**, 167-189.
25. Zhai, Y. F., W. H. M. Heijne, D. W. Smith, and M. H. Saier (2001) Homologues of archaeal rhodopsins in plants, animals and fungi: structural and functional predications for a putative fungal chaperone protein. *Biochimica et Biophysica Acta-Biomembranes* **1511**, 206-223.
26. Filipek, S., D. C. Teller, K. Palczewski, and R. Stenkamp (2003) The crystallographic model of rhodopsin and its use in studies of other G protein-coupled receptors. *Annu. Rev. Biophys. Biomol. Struct.* **32**, 375-397.
27. Bhandawat, V., J. Reisert, and K. W. Yau (2005) Elementary response of olfactory receptor neurons to odorants. *Science* **308**, 1931-1934.

## REFERENCES

---

28. Heck, M., S. A. Schadel, D. Maretzki, F. J. Bartl, E. Ritter, K. Palczewski, and K. P. Hofmann (2003) Signaling states of rhodopsin. Formation of the storage form, metarhodopsin III, from active metarhodopsin II. *J. Biol. Chem.* **278**, 3162-3169.
29. Birnbaumer, L. and A. M. Brown (1990) G proteins and the mechanism of action of hormones, neurotransmitters, and autocrine and paracrine regulatory factors. *Am. Rev. Respir. Dis.* **141**, S106-S114.
30. Birnbaumer, L. and M. Birnbaumer (1995) Signal transduction by G proteins: 1994 edition. *J. Recept. Signal. Transduct. Res.* **15**, 213-252.
31. Hargrave, P. A. and J. H. McDowell (1992) Rhodopsin and phototransduction: a model system for G protein-linked receptors. *FASEB J.* **6**, 2323-2331.
32. Stoeckenius, W., E. K. Wolff, and B. Hess (1988) A rapid population method for action spectra applied to Halobacterium halobium. *J. Bacteriol.* **170**, 2790-2795.
33. Wolff, E. K., R. A. Bogomolni, P. Scherrer, B. Hess, and W. Stoeckenius (1986) Color discrimination in halobacteria: spectroscopic characterization of a second sensory receptor covering the blue-green region of the spectrum. *Proc. Natl. Acad. Sci. U. S. A* **83**, 7272-7276.
34. Marwan, W., M. Alam, and D. Oesterhelt (1991) Rotation and switching of the flagellar motor assembly in Halobacterium halobium. *J. Bacteriol.* **173**, 1971-1977.
35. Alam, M., M. Claviez, D. Oesterhelt, and M. Kessel (1984) Flagella and motility behaviour of square bacteria. *EMBO J.* **3**, 2899-2903.
36. Alam, M. and D. Oesterhelt (1984) Morphology, function and isolation of halobacterial flagella. *J. Mol. Biol.* **176**, 459-475.
37. Stoeckenius, W. and R. H. Lozier (1974) Light energy conversion in Halobacterium halobium. *J. Supramol. Struct.* **2**, 769-774.
38. Hildebrand, E. and N. Dencher (1975) Two photosystems controlling behavioural responses of Halobacterium halobium. *Nature* **257**, 46-48.
39. Marwan, W. and D. Oesterhelt (1987) Signal formation in the halobacterial photophobic response mediated by a fourth retinal protein (P480). *J. Mol. Biol.* **195**, 333-342.
40. Sperling, W. and A. Schimz (1980) Photosensory retinal pigments in Halobacterium halobium. *Biophys. Struct. Mech.* **6**, 165-169.
41. Spudich, J. L. and W. Stoeckenius (1980) Light-regulated retinal-dependent reversible phosphorylation of Halobacterium proteins. *J. Biol. Chem.* **255**, 5501-5503.
42. Ghosh, M. and H. M. Sonawat (1998) Krebs's TCA cycle in Halobacterium salinarum investigated by C-13 nuclear magnetic resonance spectroscopy. *Extremophiles* **2**, 427-433.
43. Kushwaha, S. C., M. Kates, and W. Stoeckenius (1976) Comparison of purple membrane from Halobacterium cutirubrum and Halobacterium halobium. *Biochim. Biophys. Acta* **426**, 703-710.

## REFERENCES

---

44. Hartmann, R., H. D. Sickinger, and D. Oesterhelt (1980) Anaerobic growth of halobacteria. *Proc. Natl. Acad. Sci. U. S A* **77**, 3821-3825.
45. Oesterhelt, D. and G. Krippahl (1983) Phototrophic growth of halobacteria and its use for isolation of photosynthetically-deficient mutants. *Ann. Microbiol. (Paris)* **134B**, 137-150.
46. Lanyi, J. K. and D. Oesterhelt (1982) Identification of the retinal-binding protein in halorhodopsin. *J. Biol. Chem.* **257**, 2674-2677.
47. Spudich, J. L. and R. A. Bogomolni (1988) Sensory rhodopsins of halobacteria. *Annu. Rev. Biophys. Chem.* **17**, 193-215.
48. Oesterhelt, D. and J. Tittor (1989) Two pumps, one principle: light-driven ion transport in halobacteria. *Trends Biochem. Sci.* **14**, 57-61.
49. Avetisyan, A. V., A. D. Kaulen, V. P. Skulachev, and B. A. Feniouk (1998) Photophosphorylation in alkalophilic halobacterial cells containing halorhodopsin: chloride-ion cycle? *Biochemistry (Mosc.)* **63**, 625-628.
50. Lanyi, J. K., A. Duschl, G. W. Hatfield, K. May, and D. Oesterhelt (1990) The primary structure of a halorhodopsin from *Natronobacterium pharaonis*. Structural, functional and evolutionary implications for bacterial rhodopsins and halorhodopsins. *J. Biol. Chem.* **265**, 1253-1260.
51. Schafer, G., M. Engelhard, and V. Muller (1999) Bioenergetics of the Archaea. *Microbiol. Mol. Biol. Rev.* **63**, 570-620.
52. Spudich, J. L. and R. A. Bogomolni (1983) Spectroscopic discrimination of the three rhodopsinlike pigments in *Halobacterium halobium* membranes. *Biophys. J.* **43**, 243-246.
53. Spudich, J. L., D. A. McCain, K. Nakanishi, M. Okabe, N. Shimizu, H. Rodman, B. Honig, and R. A. Bogomolni (1986) Chromophore/protein interaction in bacterial sensory rhodopsin and bacteriorhodopsin. *Biophys. J.* **49**, 479-483.
54. Patel, A. B., E. Crocker, M. Eilers, A. Hirshfeld, M. Sheves, and S. O. Smith (2004) Coupling of retinal isomerization to the activation of rhodopsin. *Proceedings of the National Academy of Sciences of the United States of America* **101**, 10048-10053.
55. Choi, G., J. Landin, J. F. Galan, R. R. Birge, A. D. Albert, and P. L. Yeagle (2002) Structural studies of metarhodopsin II, the activated form of the G-protein coupled receptor, rhodopsin. *Biochemistry* **41**, 7318-7324.
56. Oesterhelt, D. and W. Stoeckenius (1971) Rhodopsin-like protein from the purple membrane of *Halobacterium halobium*. *Nat. New Biol.* **233**, 149-152.
57. Blaurock, A. E. and W. Stoeckenius (1971) Structure of the purple membrane. *Nat. New Biol.* **233**, 152-155.
58. Spudich, J. L. (1998) Variations on a molecular switch: transport and sensory signalling by archaeal rhodopsins. *Mol. Microbiol.* **28**, 1051-1058.
59. Alam, M., M. Lebert, D. Oesterhelt, and G. L. Hazelbauer (1989) Methyl-accepting taxis proteins in *Halobacterium halobium*. *EMBO J.* **8**, 631-639.

## REFERENCES

---

60. Ng, W. V., S. P. Kennedy, G. G. Mahairas, B. Berquist, M. Pan, H. D. Shukla, S. R. Lasky, N. S. Baliga, V. Thorsson, J. Sbrogna, S. Swartzell, D. Weir, J. Hall, T. A. Dahl, R. Welti, Y. A. Goo, B. Leithauser, K. Keller, R. Cruz, M. J. Danson, D. W. Hough, D. G. Maddocks, P. E. Jablonski, M. P. Krebs, C. M. Angevine, H. Dale, T. A. Isenbarger, R. F. Peck, M. Pohlschroder, J. L. Spudich, K. W. Jung, M. Alam, T. Freitas, S. Hou, C. J. Daniels, P. P. Dennis, A. D. Omer, H. Ebhardt, T. M. Lowe, P. Liang, M. Riley, L. Hood, and S. Dassarma (2000) Genome sequence of Halobacterium species NRC-1. *Proc. Natl. Acad. Sci. U. S A* **97**, 12176-12181.
61. Ng, W. V., B. R. Berquist, J. A. Coker, M. Capes, T. H. Wu, P. DasSarma, and S. Dassarma (2008) Genome sequences of Halobacterium species. *Genomics* **91**, 548-552.
62. Hazelbauer, G. L., J. J. Falke, and J. S. Parkinson (2008) Bacterial chemoreceptors: high-performance signaling in networked arrays. *Trends Biochem. Sci.* **33**, 9-19.
63. Hou, S. B., A. Brooun, H. S. Yu, T. Freitas, and M. Alam (1998) Sensory rhodopsin II transducer HtrII is also responsible for serine chemotaxis in the archaeon Halobacterium salinarum. *Journal of Bacteriology* **180**, 1600-1602.
64. Diercks, T., M. Coles, and H. Kessler (1999) An efficient strategy for assignment of cross-peaks in 3D heteronuclear NOESY experiments. *Journal of Biomolecular Nmr* **15**, 177-180.
65. Jin, T. and M. Inouye (1994) Transmembrane signaling. Mutational analysis of the cytoplasmic linker region of Taz1-1, a Tar-EnvZ chimeric receptor in Escherichia coli. *J. Mol. Biol.* **244**, 477-481.
66. Aravind, L. and C. P. Ponting (1999) The cytoplasmic helical linker domain of receptor histidine kinase and methyl-accepting proteins is common to many prokaryotic signalling proteins. *FEMS Microbiol. Lett.* **176**, 111-116.
67. Hulko, M., F. Berndt, M. Gruber, J. U. Linder, V. Truffault, A. Schultz, J. Martin, J. E. Schultz, A. N. Lupas, and M. Coles (2006) The HAMP domain structure implies helix rotation in transmembrane signaling. *Cell* **126**, 929-940.
68. Koretke, K. K., A. N. Lupas, P. V. Warren, M. Rosenberg, and J. R. Brown (2000) Evolution of two-component signal transduction. *Mol. Biol. Evol.* **17**, 1956-1970.
69. Scharf, B., B. Pevec, B. Hess, and M. Engelhard (1992) Biochemical and photochemical properties of the photophobic receptors from Halobacterium halobium and Natronobacterium pharaonis. *Eur. J. Biochem.* **206**, 359-366.
70. Royant, A., P. Nollert, K. Edman, R. Neutze, E. M. Landau, E. Pebay-Peyroula, and J. Navarro (2001) X-ray structure of sensory rhodopsin II at 2.1-Å resolution. *Proc. Natl. Acad. Sci. U. S A* **98**, 10131-10136.
71. Luecke, H., B. Schobert, J. K. Lanyi, E. N. Spudich, and J. L. Spudich (2001) Crystal structure of sensory rhodopsin II at 2.4 angstroms: insights into color tuning and transducer interaction. *Science* **293**, 1499-1503.
72. Kunji, E. R., E. N. Spudich, R. Grisshammer, R. Henderson, and J. L. Spudich (2001) Electron crystallographic analysis of two-dimensional crystals of sensory rhodopsin II: a 6.9 Å projection structure. *J. Mol. Biol.* **308**, 279-293.

## REFERENCES

---

73. Klare, J. P., E. Bordignon, M. Engelhard, and H. J. Steinhoff (2004) Sensory rhodopsin II and bacteriorhodopsin: light activated helix F movement. *Photochem. Photobiol. Sci.* **3**, 543-547.
74. Klare, J. P., V. I. Gordeliy, J. Labahn, G. Buldt, H. J. Steinhoff, and M. Engelhard (2004) The archaeal sensory rhodopsin II/transducer complex: a model for transmembrane signal transfer. *FEBS Lett.* **564**, 219-224.
75. Hippler-Mreyen, S., J. P. Klare, A. A. Wegener, R. Seidel, C. Herrmann, G. Schmies, G. Nagel, E. Bamberg, and M. Engelhard (2003) Probing the sensory rhodopsin II binding domain of its cognate transducer by calorimetry and electrophysiology. *J. Mol. Biol.* **330**, 1203-1213.
76. Chen, X. and J. L. Spudich (2002) Demonstration of 2:2 stoichiometry in the functional SRI-HtrI signaling complex in Halobacterium membranes by gene fusion analysis. *Biochemistry* **41**, 3891-3896.
77. Hippler-Mreyen, S., J. P. Klare, A. A. Wegener, R. Seidel, C. Herrmann, G. Schmies, G. Nagel, E. Bamberg, and M. Engelhard (2003) Probing the sensory rhodopsin II binding domain of its cognate transducer by calorimetry and electrophysiology. *J. Mol. Biol.* **330**, 1203-1213.
78. Hippler-Mreyen, S., J. P. Klare, A. A. Wegener, R. Seidel, C. Herrmann, G. Schmies, G. Nagel, E. Bamberg, and M. Engelhard (2003) Probing the sensory rhodopsin II binding domain of its cognate transducer by calorimetry and electrophysiology. *J. Mol. Biol.* **330**, 1203-1213.
79. Sudo, Y., M. Iwamoto, K. Shimono, and N. Kamo (2002) Association of pharaonis phoborhodopsin with its cognate transducer decreases the photo-dependent reactivity by water-soluble reagents of azide and hydroxylamine. *Biochim. Biophys. Acta* **1558**, 63-69.
80. Lozier, R. H., R. A. Bogomolni, and W. Stoerkenius (1975) Bacteriorhodopsin: a light-driven proton pump in Halobacterium Halobium. *Biophys. J.* **15**, 955-962.
81. Hirayama, J., Y. Imamoto, Y. Shichida, N. Kamo, H. Tomioka, and T. Yoshizawa (1992) Photocycle of phoborhodopsin from haloalkaliphilic bacterium (*Natronobacterium pharaonis*) studied by low-temperature spectrophotometry. *Biochemistry* **31**, 2093-2098.
82. Imamoto, Y., Y. Shichida, J. Hirayama, H. Tomioka, N. Kamo, and T. Yoshizawa (1992) Chromophore configuration of pharaonis phoborhodopsin and its isomerization on photon absorption. *Biochemistry* **31**, 2523-2528.
83. Chizhov, I., G. Schmies, R. Seidel, J. R. Sydor, B. Luttenberg, and M. Engelhard (1998) The photophobic receptor from *Natronobacterium pharaonis*: temperature and pH dependencies of the photocycle of sensory rhodopsin II. *Biophys. J.* **75**, 999-1009.
84. Klare, J. P., V. I. Gordeliy, J. Labahn, G. Buldt, H. J. Steinhoff, and M. Engelhard (2004) The archaeal sensory rhodopsin II/transducer complex: a model for transmembrane signal transfer. *FEBS Lett.* **564**, 219-224.
85. Klare, J. P., E. Bordignon, M. Engelhard, and H. J. Steinhoff (2004) Sensory rhodopsin II and bacteriorhodopsin: light activated helix F movement. *Photochem. Photobiol. Sci.* **3**, 543-547.



## REFERENCES

---

86. Wegener, A. A., I. Chizhov, M. Engelhard, and H. J. Steinhoff (2000) Time-resolved detection of transient movement of helix F in spin-labelled pharaonis sensory rhodopsin II. *J. Mol. Biol.* **301**, 881-891.
87. Wegener, A. A., J. P. Klare, M. Engelhard, and H. J. Steinhoff (2001) Structural insights into the early steps of receptor-transducer signal transfer in archaeal phototaxis. *EMBO J.* **20**, 5312-5319.
88. Yan, B., T. Takahashi, R. Johnson, and J. L. Spudich (1991) Identification of signaling states of a sensory receptor by modulation of lifetimes of stimulus-induced conformations: the case of sensory rhodopsin II. *Biochemistry* **30**, 10686-10692.
89. Sudo, Y., M. Iwamoto, K. Shimono, M. Sumi, and N. Kamo (2001) Photo-induced proton transport of pharaonis phoborhodopsin (sensory rhodopsin II) is ceased by association with the transducer. *Biophys. J.* **80**, 916-922.
90. Spudich, E. N. and J. L. Spudich (1993) The photochemical reactions of sensory rhodopsin I are altered by its transducer. *J. Biol. Chem.* **268**, 16095-16097.
91. Sasaki, J. and J. L. Spudich (1998) The transducer protein HtrII modulates the lifetimes of sensory rhodopsin II photointermediates. *Biophys. J.* **75**, 2435-2440.
92. Zhang, X. N., J. Y. Zhu, and J. L. Spudich (1999) The specificity of interaction of archaeal transducers with their cognate sensory rhodopsins is determined by their transmembrane helices. *Proceedings of the National Academy of Sciences of the United States of America* **96**, 857-862.
93. Moukhametzianov, R., J. P. Klare, R. Efremov, C. Baeken, A. Goppner, J. Labahn, M. Engelhard, G. Buldt, and V. I. Gordeliy (2006) Development of the signal in sensory rhodopsin and its transfer to the cognate transducer. *Nature* **440**, 115-119.
94. Bergo, V., E. N. Spudich, K. L. Scott, J. L. Spudich, and K. J. Rothschild (2000) FTIR analysis of the SII540 intermediate of sensory rhodopsin II: Asp73 is the Schiff base proton acceptor. *Biochemistry* **39**, 2823-2830.
95. Bergo, V., E. N. Spudich, J. L. Spudich, and K. J. Rothschild (2003) Conformational changes detected in a sensory rhodopsin II-transducer complex. *J. Biol. Chem.* **278**, 36556-36562.
96. Hein, M., A. A. Wegener, M. Engelhard, and F. Siebert (2003) Time-resolved FTIR studies of sensory rhodopsin II (NpSRII) from *Natronobacterium pharaonis*: implications for proton transport and receptor activation. *Biophys. J.* **84**, 1208-1217.
97. Hughson, A. G. and G. L. Hazelbauer (1996) Detecting the conformational change of transmembrane signaling in a bacterial chemoreceptor by measuring effects on disulfide cross-linking in vivo. *Proceedings of the National Academy of Sciences of the United States of America* **93**, 11546-11551.
98. Chervitz, S. A. and J. J. Falke (1996) Molecular mechanism of transmembrane signaling by the aspartate receptor: a model. *Proc. Natl. Acad. Sci. U. S A* **93**, 2545-2550.
99. Kim, S. H., W. R. Wang, and K. K. Kim (2002) Dynamic and clustering model of bacterial chemotaxis receptors: Structural basis for signaling and high sensitivity.

## REFERENCES

---

- Proceedings of the National Academy of Sciences of the United States of America* **99**, 11611-11615.
100. Doebber, M., E. Bordignon, J. P. Klare, J. Holterhues, S. Martell, N. Mennes, L. Li, M. Engelhard, and H. J. Steinhoff (2008) Salt-driven equilibrium between two conformations in the HAMP domain from *Natronomonas pharaonis*: the language of signal transfer? *J. Biol. Chem.* **283**, 28691-28701.
  101. Khursigara, C. M., X. Wu, P. Zhang, J. Lefman, and S. Subramaniam (2008) Role of HAMP domains in chemotaxis signaling by bacterial chemoreceptors. *Proc. Natl. Acad. Sci. U. S A* **105**, 16555-16560.
  102. Milburn, M. V., G. G. Prive, D. L. Milligan, W. G. Scott, J. Yeh, J. Jancarik, D. E. Koshland, Jr., and S. H. Kim (1991) Three-dimensional structures of the ligand-binding domain of the bacterial aspartate receptor with and without a ligand. *Science* **254**, 1342-1347.
  103. Klostermeier, D., R. Seidel, and J. Reinstein (1998) Functional properties of the molecular chaperone DnaK from *Thermus thermophilus*. *Journal of Molecular Biology* **279**, 841-853.
  104. Hohenfeld, I. P., A. A. Wegener, and M. Engelhard (1999) Purification of histidine tagged bacteriorhodopsin, pharaonis halorhodopsin and pharaonis sensory rhodopsin II functionally expressed in *Escherichia coli*. *FEBS Lett.* **442**, 198-202.
  105. Shimono, K., M. Iwamoto, M. Sumi, and N. Kamo (1997) Functional expression of pharaonis phoborhodopsin in *Escherichia coli*. *FEBS Lett.* **420**, 54-56.
  106. EHRESMAN.B, P. Imbault, and J. H. Weil (1973) Spectrophotometric Determination of Protein Concentration in Cell Extracts Containing Transfer-Rna and Ribosomal-Rnas. *Analytical Biochemistry* **54**, 454-463.
  107. Kates, M. (1982) Lipids of Purple Membrane from Extreme Halophiles and of Methanogenic Bacteria. *Biochem. Soc. Symp.* **58**, 51-72.
  108. Laemmli, U. K. (1970) Cleavage of Structural Proteins During Assembly of Head of Bacteriophage-T4. *Nature* **227**, 680-&.
  109. Ossipow, V., P. Descombes, and U. Schibler (1993) Ccaat Enhancer-Binding Protein Messenger-Rna Is Translated Into Multiple Proteins with Different Transcription Activation Potentials. *Proceedings of the National Academy of Sciences of the United States of America* **90**, 8219-8223.
  110. Schagger, H. and G. Vonjagow (1991) Blue Native Electrophoresis for Isolation of Membrane-Protein Complexes in Enzymatically Active Form. *Analytical Biochemistry* **199**, 223-231.
  111. Yu, X. C. and H. W. Strobel (1997) Hydroperoxide-mediated cytochrome P450-dependent 8-anilino-1-naphthalenesulfonic acid destruction, product formation and P450 modification. *Molecular and Cellular Biochemistry* **167**, 159-168.
  112. Moller, M. and A. Denicola (2002) Study of protein-ligand binding by fluorescence. *Biochemistry and Molecular Biology Education* **30**, 309-312.

## REFERENCES

---

113. Ogasahara, K., K. Koike, M. Hamada, and T. Hiraoka (1976) Interaction of hydrophobic probes with the apoenzyme of pig heart lipoamide dehydrogenase. *J. Biochem.* **79**, 967-975.
114. Bulheller, B. M., A. Rodger, and J. D. Hirst (2007) Circular and linear dichroism of proteins. *Physical Chemistry Chemical Physics* **9**, 2020-2035.
115. Chizhov, I., D. S. Chernavskii, M. Engelhard, K. H. Mueller, B. V. Zubov, and B. Hess (1996) Spectrally silent transitions in the bacteriorhodopsin photocycle. *Biophys. J.* **71**, 2329-2345.
116. Klostermeier, D., R. Seidel, and J. Reinstein (1998) Functional properties of the molecular chaperone DnaK from *Thermus thermophilus*. *Journal of Molecular Biology* **279**, 841-853.
117. Dubendorff, J. W. and F. W. Studier (1991) Controlling Basal Expression in An Inducible T7 Expression System by Blocking the Target T7 Promoter with Lac Repressor. *Journal of Molecular Biology* **219**, 45-59.
118. Hippler-Mreyen, S., J. P. Klare, A. A. Wegener, R. Seidel, C. Herrmann, G. Schmies, G. Nagel, E. Bamberg, and M. Engelhard (2003) Probing the sensory rhodopsin II binding domain of its cognate transducer by calorimetry and electrophysiology. *J. Mol. Biol.* **330**, 1203-1213.
119. Scharf, B., B. Pevec, B. Hess, and M. Engelhard (1992) Biochemical and photochemical properties of the photophobic receptors from *Halobacterium halobium* and *Natronobacterium pharaonis*. *Eur. J. Biochem.* **206**, 359-366.
120. Yu, J. H., Z. Hamari, K. H. Han, J. A. Seo, Y. Reyes-Dominguez, and C. Scazzocchio (2004) Double-joint PCR: a PCR-based molecular tool for gene manipulations in filamentous fungi. *Fungal Genetics and Biology* **41**, 973-981.
121. Brownleader, M. D., O. Byron, A. Rowe, M. Trevan, K. Welham, and P. M. Dey (1996) Investigations into the molecular size and shape of tomato extensin. *Biochemical Journal* **320**, 577-583.
122. Marshall, C. B., A. Chakrabarty, and P. L. Davies (2005) Hyperactive antifreeze protein from winter flounder is a very long rod-like dimer of alpha-helices. *Journal of Biological Chemistry* **280**, 17920-17929.
123. Mennes, N., J. P. Klare, I. Chizhov, R. Seidel, R. Schlesinger, and M. Engelhard (2007) Expression of the halobacterial transducer protein HtrII from *Natronomonas pharaonis* in *Escherichia coli*. *FEBS Lett.* **581**, 1487-1494.
124. Mironova, O. S., R. G. Efremova, B. Person, J. Heberle, I. L. Budyak, G. Buldt, and R. Schlesinger (2005) Functional characterization of sensory rhodopsin II from *Halobacterium salinarum* expressed in *Escherichia coli*. *Febs Letters* **579**, 3147-3151.
125. Scharf, B., B. Hess, and M. Engelhard (1992) Chromophore of sensory rhodopsin II from *Halobacterium halobium*. *Biochemistry* **31**, 12486-12492.
126. Takahashi, T., B. Yan, P. Mazur, F. Derguini, K. Nakanishi, and J. L. Spudich (1990) Color regulation in the archaeobacterial phototaxis receptor phoborhodopsin (sensory rhodopsin II). *Biochemistry* **29**, 8467-8474.

## REFERENCES

---

127. Birge, R. R. (1990) Nature of the primary photochemical events in rhodopsin and bacteriorhodopsin. *Biochim. Biophys. Acta* **1016**, 293-327.
128. Chang, C. H., R. Jonas, R. Govindjee, and T. G. Ebrey (1988) Regeneration of Blue and Purple Membranes from Deionized Bleached Membranes of Halobacterium-Halobium. *Biophysical Journal* **53**, A383.
129. Olson, K. D., P. Deval, and J. L. Spudich (1992) Absorption and photochemistry of sensory rhodopsin--I: pH effects. *Photochem. Photobiol.* **56**, 1181-1187.
130. Klare, J. P., I. Chizhov, and M. Engelhard (2008) Microbial rhodopsins: scaffolds for ion pumps, channels, and sensors. *Results Probl. Cell Differ.* **45**, 73-122.
131. Tomioka, H., T. Takahashi, N. Kamo, and Y. Kobatake (1986) Flash Spectrophotometric Identification of A 4Th Rhodopsin-Like Pigment in Halobacterium-Halobium. *Biochemical and Biophysical Research Communications* **139**, 389-395.
132. Sasaki, J. and J. L. Spudich (1999) Proton circulation during the photocycle of sensory rhodopsin II. *Biophys. J.* **77**, 2145-2152.
133. Chizhov, I. and M. Engelhard (2001) Temperature and halide dependence of the photocycle of halorhodopsin from Natronobacterium pharaonis. *Biophys. J.* **81**, 1600-1612.
134. Strop, P. and A. T. Brunger (2005) Refractive index-based determination of detergent concentration and its application to the study of membrane proteins. *Protein Sci.* **14**, 2207-2211.
135. Hippler-Mreyen, S., J. P. Klare, A. A. Wegener, R. Seidel, C. Herrmann, G. Schmies, G. Nagel, E. Bamberg, and M. Engelhard (2003) Probing the sensory rhodopsin II binding domain of its cognate transducer by calorimetry and electrophysiology. *J. Mol. Biol.* **330**, 1203-1213.
136. Sudo, Y., M. Iwamoto, K. Shimono, and N. Kamo (2001) Pharaonis phoborhodopsin binds to its cognate truncated transducer even in the presence of a detergent with a 1:1 stoichiometry. *Photochem. Photobiol.* **74**, 489-494.
137. Sudo, Y., M. Iwamoto, K. Shimono, and N. Kamo (2002) Tyr-199 and charged residues of pharaonis Phoborhodopsin are important for the interaction with its transducer. *Biophys. J.* **83**, 427-432.
138. Sudo, Y. and J. L. Spudich (2006) Three strategically placed hydrogen-bonding residues convert a proton pump into a sensory receptor. *Proc. Natl. Acad. Sci. U. S A* **103**, 16129-16134.
139. Sudo, Y., M. Yamabi, S. Kato, C. Hasegawa, M. Iwamoto, K. Shimono, and N. Kamo (2006) Importance of specific hydrogen bonds of archaeal rhodopsins for the binding to the transducer protein. *J. Mol. Biol.* **357**, 1274-1282.
140. Zhang, W. S., A. Brooun, M. M. Mueller, and M. Alam (1996) The primary structures of the Archaeon Halobacterium salinarium blue light receptor sensory rhodopsin II and its transducer, a methyl-accepting protein. *Proceedings of the National Academy of Sciences of the United States of America* **93**, 8230-8235.

## REFERENCES

---

141. Zhang, X. N., J. Zhu, and J. L. Spudich (1999) The specificity of interaction of archaeal transducers with their cognate sensory rhodopsins is determined by their transmembrane helices. *Proc. Natl. Acad. Sci. U. S A* **96**, 857-862.
142. Jung, K. H. and J. L. Spudich (1996) Protonatable residues at the cytoplasmic end of transmembrane helix-2 in the signal transducer HtrI control photochemistry and function of sensory rhodopsin I. *Proc. Natl. Acad. Sci. U. S A* **93**, 6557-6561.
143. Brouillette, C. G., D. D. Muccio, and T. K. Finney (1987) Ph-Dependence of Bacteriorhodopsin Thermal Unfolding. *Biochemistry* **26**, 7431-7438.
144. Foster, D. L., S. L. Mowbray, B. K. Jap, and D. E. Koshland, Jr. (1985) Purification and characterization of the aspartate chemoreceptor. *J. Biol. Chem.* **260**, 11706-11710.
145. Chervitz, S. A. and J. J. Falke (1996) Molecular mechanism of transmembrane signaling by the aspartate receptor: a model. *Proc. Natl. Acad. Sci. U. S A* **93**, 2545-2550.
146. Yeh, J. I., H. P. Biemann, G. G. Prive, J. Pandit, D. E. Koshland, and S. H. Kim (1996) High-resolution structures of the ligand binding domain of the wild-type bacterial aspartate receptor. *Journal of Molecular Biology* **262**, 186-201.
147. Alberts, B. and J. L. M. R. K. R. a. P. W. Alexander Johnson (2002) "The Shape and Structure of Proteins". *Molecular Biology of the Cell; Fourth Edition. New York and London: Garland Science* **1016**.
148. Lin, L. N., J. Y. Li, J. F. Brandts, and R. M. Weis (1994) The Serine Receptor of Bacterial Chemotaxis Exhibits Half-Site Saturation for Serine Binding. *Biochemistry* **33**, 6564-6570.
149. Royer, C. A. (1995) Fluorescence Studies of Folding and Binding Equilibria in Proteins. *Abstracts of Papers of the American Chemical Society* **209**, 27-HYS.
150. Streicher, W. W., M. M. Lopez, and G. I. Makhatadze (2009) Annexin I and Annexin II N-Terminal Peptides Binding to S100 Protein Family Members: Specificity and Thermodynamic Characterization. *Biochemistry* **48**, 2788-2798.
151. Elalaoui, A., G. Divita, G. Maury, J. L. Imbach, and R. S. Goody (1994) Intrinsic Tryptophan Fluorescence of Bovine Liver Adenosine Kinase, Characterization of Ligand-Binding Sites and Conformational-Changes. *European Journal of Biochemistry* **221**, 839-846.
152. Nelson, S. W., C. V. Iancu, J. Y. Choe, R. B. Honzatko, and H. J. Fromm (2000) Tryptophan fluorescence reveals the conformational state of a dynamic loop in recombinant porcine fructose-1,6-bisphosphatase. *Biochemistry* **39**, 11100-11106.
153. Verjovskialmeida, S. and J. L. Silva (1981) Different Degrees of Cooperativity of the Ca<sup>2+</sup>-Induced Changes in Fluorescence Intensity of Solubilized Sarcoplasmic-Reticulum Atpase. *Journal of Biological Chemistry* **256**, 2940-2944.
154. Xu, Y., J. Johnson, H. Kohn, and W. R. Widger (2003) ATP binding to Rho transcription termination factor - Mutant F355W ATP-induced fluorescence quenching reveals dynamic ATP binding. *Journal of Biological Chemistry* **278**, 13719-13727.

## REFERENCES

---

155. Celej, M. S., C. G. Montich, and G. D. Fidelio (2003) Protein stability induced by ligand binding correlates with changes in protein flexibility. *Protein Science* **12**, 1496-1506.
156. Vamvaca, K., B. Vogeli, P. Kast, K. Pervushin, and D. Hilvert (2004) An enzymatic molten globule: efficient coupling of folding and catalysis. *Proc. Natl. Acad. Sci. U. S. A* **101**, 12860-12864.
157. Bogomolni, R. A. and J. L. Spudich (1982) Identification of a third rhodopsin-like pigment in phototactic *Halobacterium halobium*. *Proc. Natl. Acad. Sci. U. S. A* **79**, 6250-6254.
158. Hoff, W. D., K. H. Jung, and J. L. Spudich (1997) Molecular mechanism of photosignaling by archaeal sensory rhodopsins. *Annu. Rev. Biophys. Biomol. Struct.* **26**, 223-258.
159. Kamo, N., K. Shimono, M. Iwamoto, and Y. Sudo (2001) Photochemistry and photoinduced proton-transfer by pharaonis phoborhodopsin. *Biochemistry (Mosc.)* **66**, 1277-1282.
160. Miller, A. S. and J. J. Falke (2004) Side chains at the membrane-water interface modulate the signaling state of a transmembrane receptor. *Biochemistry* **43**, 1763-1770.
161. Ottemann, K. M., W. Z. Xiao, Y. K. Shin, and D. E. Koshland (1999) A piston model for transmembrane signaling of the aspartate receptor. *Science* **285**, 1751-1754.
162. Ashbaugh, H. S. and H. W. Hatch (2008) Natively unfolded protein stability as a coil-to-globule transition in charge/hydrophobicity space. *Journal of the American Chemical Society* **130**, 9536-9542.
163. Bass, R. B. and J. J. Falke (1998) Detection of a conserved alpha-helix in the kinase-docking region of the aspartate receptor by cysteine and disulfide scanning. *Journal of Biological Chemistry* **273**, 25006-25014.
164. Bass, R. B., M. D. Coleman, and J. J. Falke (1999) Signaling domain of the aspartate receptor is a helical hairpin with a localized kinase docking surface: Cysteine and disulfide scanning studies. *Biochemistry* **38**, 9317-9327.
165. Arai, M. and K. Kuwajima (2000) Role of the molten globule state in protein folding. *Advances in Protein Chemistry, Vol 53* **53**, 209-282.
166. Semisotnov, G. V., N. A. Rodionova, O. I. Razgulyaev, V. N. Uversky, A. F. Gripas, and R. I. Gilmanshin (1991) Study of the Molten Globule Intermediate State in Protein Folding by A Hydrophobic Fluorescent-Probe. *Biopolymers* **31**, 119-128.
167. Bordignon, E., J. P. Klare, M. Doebber, A. A. Wegener, S. Martell, M. Engelhard, and H. J. Steinhoff (2005) Structural analysis of a HAMP domain: the linker region of the phototransducer in complex with sensory rhodopsin II. *J. Biol. Chem.* **280**, 38767-38775.
168. Williams, S. B. and V. Stewart (1999) Functional similarities among two-component sensors and methyl-accepting chemotaxis proteins suggest a role for linker region amphipathic helices in transmembrane signal transduction. *Molecular Microbiology* **33**, 1093-1102.

## REFERENCES

---

169. Ames, P., Q. Zhou, and J. S. Parkinson (2008) Mutational analysis of the connector segment in the HAMP domain of Tsr, the Escherichia coli serine chemoreceptor. *Journal of Bacteriology* **190**, 6676-6685.
170. Bordignon, E., J. P. Klare, M. Doebber, A. A. Wegener, S. Martell, M. Engelhard, and H. J. Steinhoff (2005) Structural analysis of a HAMP domain - The linker region of the phototransducer in complex with sensory rhodopsin II. *Journal of Biological Chemistry* **280**, 38767-38775.
171. Doebber, M., E. Bordignon, J. P. Klare, J. Holterhues, S. Martell, N. Mennes, L. Li, M. Engelhard, and H. J. Steinhoff (2008) Salt-driven equilibrium between two conformations in the HAMP domain from Natronomonas pharaonis - The language of signal transfer? *Journal of Biological Chemistry* **283**, 28691-28701.
172. Khursigara, C. M., X. W. Wu, P. J. Zhang, J. Lefman, and S. Subramaniam (2008) Role of HAMP domains in chemotaxis signaling by bacterial chemoreceptors. *Proceedings of the National Academy of Sciences of the United States of America* **105**, 16555-16560.
173. Yang, C. S., O. Sineshchekov, E. N. Spudich, and J. L. Spudich (2004) The cytoplasmic membrane-proximal domain of the HtrII transducer interacts with the E-F loop of photoactivated Natronomonas pharaonis sensory rhodopsin II. *J. Biol. Chem.* **279**, 42970-42976.
174. Inoue, K., J. Sasaki, J. L. Spudich, and M. Terazima (2008) Signal transmission through the HtrII transducer alters the interaction of two alpha-helices in the HAMP domain. *J. Mol. Biol.* **376**, 963-970.
175. Park, S. Y., P. P. Borbat, G. Gonzalez-Bonet, J. Bhatnagar, A. M. Pollard, J. H. Freed, A. M. Bilwes, and B. R. Crane (2006) Reconstruction of the chemotaxis receptor-kinase assembly. *Nature Structural & Molecular Biology* **13**, 400-407.
176. Martin Engelhard, Georg Schmies and Ansgar A Wegener 2003. Photoreceptors and Light Signalling. Royal Society of Chemistry, 1-39. *Life Sci.* **71**, 751-757. 2003.

Ref Type: Generic

## **7. APPENDICES**



## APPENDICES

---

### Protein sequences

#### HsSRII [1-237]

10 20 30 40 50 60  
MALTTWFWVG AVGMLAGTVL PIRDCIRHPS HRRYDLVLAG ITGLAAIAYT TMGLGITATT  
70 80 90 100 110 120  
VGDRTVYLLAR YIDWLVTTPV IVLYLAMLAR PGHRTSAWLL AADV FVIAAG IAAALTTGVQ  
130 140 150 160 170 180  
RWLFFAVGAA GYAALLYGLL GTLPRALGDD PRVRS LFVTL RNITVVLWTL YPVVWLLSPA  
190 200 210 220 230 240  
GIGILQTEMY TIVVVYLDVI SKVAFVAFV LGADAVSRLV AADAAAPATA EPTPDGDENH

HHHHHH

**Number of amino acids: 246**

**Molecular weight: 26483.0 Da**

## APPENDICES

### HsHtrII [1-765]

10 20 30 40 50 60  
MGSGLVARIR GSYGTLKTLA LVVVVLSVG VGTFVYQQT TQLETDVRA D LTGSADARAD

70 80 90 100 110 120  
HLDAWLSNAR GQTQLASRHP VLASGNDTAI TRYLEGLAAS DERPDGVVAA HVYNTSTTTI

130 140 150 160 170 180  
EASSADAFTG VNPREQGAPF ATDPPSFAT SDVVVAAPFT VPAADFPVLS VLSPIPGTTD

190 200 210 220 230 240  
KALIYMVNVN TLTDDFGQNV AGSTTTVVA DGTYYVSHPDQ DRVLTGHDGP SRLLNQSR TQ

250 260 270 280 290 300  
PAYIDANGTV TAAAPVDGAP WSVLVRAPHD RAFALGDFVA SSLVGLVLIT IVSLSLIGVT

310 320 330 340 350 360  
VGSTTVTALR QFSRRADEMA AGDLDTDIDT SRNDEFGLA ESFRSMRDSL SESLTD AERA

370 380 390 400 410 420  
TARAEDARED AEQQRADAEA AREDAEAARK DAQETARALE SAAADYEEAL TAVADGDLTR

430 440 450 460 470 480  
RVDASRDHDA MARIGHALND MLDDIETSV AATAFSDHVS DAAQRVEADA GDAIDAGTDV

490 500 510 520 530 540  
STAVDEISDG ATEQTDRLHE VAGEVDDLSA SAEVAETVA SLADTAGQAA SAVDDGRQAT

550 560 570 580 590 600  
EDAVETMDDV ADDAEAAAADA MDALDSEMA IGEIVDVIAD IADQTNMLAL NASIEAARTG

610 620 630 640 650 660  
ADGDGFAVVA DEVKTLAEES RDAAE DIESR LLALQGQVSD VADEM RATS D TVSDGRATVG

670 680 690 700 710 720  
DAATALDDV SFVADTDAA GEIRAATDRQ AHAASRVASA VDEVAGISQE TAAQATAVAD

730 740 750 760 770  
SAATQDTLS SVDDAAADLA DRAAALDDL AEFDAHDDTE PEDYENHHHH HHH

**Number of amino acids: 773**

**Molecular weight: 80245.6 Da**

## APPENDICES

---

### HsHtrII LBD [42-285]

10 20 30 40 50 60  
MELETDVRAD LTGSADARAD HLDAWLSNAR GQTQLASRHP VLASGNDTAI TRYLEGLAAS  
70 80 90 100 110 120  
DERPDGRWFA GHVYNTSTTT IEASSADAFT GVNPREQGAP FATDPPSFAT TSDVVVAAPF  
130 140 150 160 170 180  
TVPAADFPVL SVLSPPIPGTT DKALIYMVNV NTLTDDFGQN VAGSTTTVVS ADGTYVSHPD  
190 200 210 220 230 240  
QDRVLTGHDG PSRLLNQSRT QPAYIDANGT VTAAAPVDGA PWSVLVRAPH DRAFANSHHH

HHHH

**Number of amino acids: 244**

**Molecular weight: 25840.2 Da**

### HsHtrII HAMP [303-465]

10 20 30 40 50 60  
MGSTTVTALR QFSRRADEMA AGDLDTDIDT SRNDEFGLA ESFRSMRDSL SESLTAERA  
70 80 90 100 110 120  
TARAEDAREDAEQQRADAEAREDAEAARK DAQETARALE SAAADYEEAL TAVADGDLTR  
130 140 150 160 170  
RVDASRDHDA MARIGHALND MLDDIETSVAAATAFSDHVS DAAQRENHHH HHHH

**Number of amino acids: 174**

**Molecular weight: 19005.1 Da**

## APPENDICES

---

### HsHtrII [1-398]

10 20 30 40 50 60  
MGSGLVARIR GSYGTKLTLA LVVVVLSVG VGTFFVYQQT TQLET DVRAD LTGSADARAD

70 80 90 100 110 120  
HLDAWLSNAR GQTQLASRHP VLASGNDTAI TRYLEGLAAS DERPDGRWFA GHVYNTSTTT

130 140 150 160 170 180  
IEASSADAFT GVNPREQGAP FATDPPSFAT TSDVVVAAPF TVPAADFVPL SVLSPPIGTT

190 200 210 220 230 240  
DKALIYMVNV NTLTDDFGQN VAGSTTTVVS ADGTYVSHPD QDRVLTGHDG PSRLLNQSRT

250 260 270 280 290 300  
QPAYIDANGT VTAAAPVDGA PWSVLVRAPH DRAFALGDFV ASSLVGLVLI TIVSLSLIGV

310 320 330 340 350 360  
TVGSTTVTAL RQFSRRADEM AAGDLDTDID TSRNDEFGLT AESFRSMRDS LSESLTDAER

370 380 390 400  
ATARAEDARE DAEQQRADAE AAREDAEAAR KDAQETAREN HHHHHHH

**Number of amino acids: 407**

**Molecular weight: 43155.4 Da**

### HsHtrII [1-398ΔLBD(39-281)]

10 20 30 40 50 60  
MGSGLVARIR GSYGTKLTLA LVVVVLSVG VGTFFVYQQVT AAAATGDAAA VQEAVASSLV

70 80 90 100 110 120  
GLVLITIVSL SLIGVTVGST TVTALRQFSR RADEMAAGDL DTDIDTSRND EFGTLAESFR

130 140 150 160 170 180  
SMRDSLSESL TDAERATARA EDAREDAEQQ RADAEEAARED AEAARKDAQE TARENHHHHH

HH

**Number of amino acids: 182**

**Molecular weight: 19289.2 Da**

## APPENDICES

---

### HsHtrII[1-765ΔLBD(39-281)]

10          20          30          40          50          60  
MGSGLVARIR GSYGTKLTLA LVVVVLSVG VGTFFVYQQVT AAAATGDAAA VQEAVASSLV

70          80          90          100          110          120  
GLVLITIVSL SLIGVTVGST TVTALRQFSR RADEMAAGDL DTDIDTSRND EFGTLAESFR

130          140          150          160          170          180  
SMRDSLSESL TDAERATARA EDAREDAEQQ RADAEAARED AEAARKDAQE TARALESAAA

190          200          210          220          230          240  
DYEEALTAVA DGDLTRRVDA SRDHDAMARI GHALNDMLDD IETSVAATA FSDHVSDAAQ

250          260          270          280          290          300  
RVEADAGDAI DAGTDVSTAV DEISDGATEQ TDRLHEVAGE VDDLSASAE E VAETVASLAD

310          320          330          340          350          360  
TAGQAASAVD DGRQATEDAV ETMDDVADDA EAAADAMDAL DSEMADIGEI VDVIADIADQ

370          380          390          400          410          420  
TNMLALNASI EAARTGADGD GFAVVADEVK TLAEESRDA E EDIESRLAL QGQVSDVADE

430          440          450          460          470          480  
MRATSDTVSD GRATVGDAAT ALDDVVSFVA DTDTAAGQIR AATDRQAHAA SRVASAVDEV

490          500          510          520          530          540  
AGISQETAQQ ATAVADSAAT QTDTLSSVDD AAADLADRAA ALDDLLEAFD AHDDTEPEDY

ENHHHHHHH

**Number of amino acids: 549**

**Molecular weight: 56655.7 Da**

## APPENDICES

---

### Tar [1-553]

10 20 30 40 50 60  
MINRIRVVTL LVMVLGVFAL LQLISGSLFF SSLHHSQKSF VVSNQLREQQ GELTSTWDLM

70 80 90 100 110 120  
LQTRINLSRS AVRMMMDSSN QQSNKVELL DSARKTLAQA ATHYKKFKSM APLPEMVATS

130 140 150 160 170 180  
RNIDEKYKNY YTALTELIDY LDYGNTGAYF AQPTQGMQNA MGEAFAQYAL SSEKLYRDIV

190 200 210 220 230 240  
TDNADDYRFA QWQLAVIALV VVLILLVAWY GIRRMMLTPL AKIIAHIREI AGGNLANTLT

250 260 270 280 290 300  
IDGRSEMDDL AQSVSHMQRS LTDTVTHVRE GSDAIYAGTR EIAAGNTDLS SRTEQQASAL

310 320 330 340 350 360  
EETAASMEQL TATVKQNADN ARQASQLAQS ASDTAQHGGK VVDGVXKTMH EIADSSKKIA

370 380 390 400 410 420  
DIISVIDGIA FQTNILALNA AVEAARAGEQ GRGFAVVAGE VRNLASRSAQ AAKEIKALIE

430 440 450 460 470 480  
DSVSRVDTGS VLVESAGETM NNIVDAVTRV TDIMGEIASA SDEQSRGIDQ VALAVSEMDH

490 500 510 520 530 540  
VTQQNASLVQ ESAAAAAALE EQASRLTQAV SAFRLAASPL TNKPQTPSRP ASEQPPAQPR

550 560  
LRIAEQDPNW ETFENHHHHH H

**Number of amino acids: 561**

**Molecular weight: 61003.9 Da**

## APPENDICES

---

### Tar [1-265]

10 20 30 40 50 60  
MINRIRVVT<sup>L</sup> LVMVLGVFAL LQLISGSLF<sup>F</sup> SSLHHSQKSF VVSNQLREQQ GELTSTWDL<sup>M</sup>

70 80 90 100 110 120  
LQTRINLSR<sup>S</sup> AVRMMMDSS<sup>N</sup> QQSNKVEL<sup>L</sup> DSARKTLAQ<sup>A</sup> ATHYKFKFS<sup>M</sup> APLPEMVAT<sup>S</sup>

130 140 150 160 170 180  
RNIDEKYKN<sup>Y</sup> YTALTELID<sup>Y</sup> LDYGNTGAY<sup>F</sup> AQPTQGMQNA MGEAFAQYAL SSEKLYRDIV

190 200 210 220 230 240  
TDNADDYRF<sup>A</sup> QWQLAVIAL<sup>V</sup> VVLILLVAW<sup>Y</sup> GIRRM<sup>L</sup>LTPL AKIIAHIREI AGGNLANTLT

250 260 270  
IDGRSEMGL<sup>L</sup> AQS<sup>V</sup>SHMQRS LTDTVENHHH HHHH

**Number of amino acids: 274**

**Molecular weight: 30987.5 Da**

## **8. ACKNOWLEDGMENTS**



### 8. Acknowledgments

First of all, I want to thank Prof. Dr. Roger Goody for giving me permission to do the necessary research work and to use departmental data. I have furthermore to thank the former coordinator for IMPRS, Dr. Jutta Rotter and the present coordinator Dr. Waltraud Hofmann-Goody and Christa Hornemann for their kind support and gave me a lot of helps to live in Germany.

I am deeply indebted to my supervisor Prof. Dr. Martin Engelhard for the overall opportunity to work in his group and of course for the many helpful and encouraging discussions. Moreover, I am especially grateful that he provide me with the freedom to independently pursue my research and stimulating suggestions and encouragement helped me in all the time of research for and writing of this thesis. I would like to express my gratitude to Priv.-Doz. Dr. Susanne Brakmann who gave me the possibility to complete this thesis and my Ph D work. Special thanks to Dr. Igor Chizov for his helps and valuable paper work. I am very grateful to Prof. Dr. Choe, Hui-woog for introducing me to the field of membrane protein and constant encouragement. I am obliged to Dr. Waltraud Hofmann-Goody for proofreading of the final version of the thesis for English style and grammar, correcting both and offering suggestions for improvement.

I am thankful to my former and present colleagues from the Department III (Department of Physical Biochemistry) who share with me lab, office, coffee and relaxed working atmosphere. Especially, I would like to thank for all their help, support, interest and valuable hints in my research work.

I thank my parents, parents in law, my brother and sister for their unconditional love and support from South Korea. Finally, but immensely, I would like to give my special thanks to my wife Chang, Eun-ju whose patient love enabled me to complete this work.

# CURRICULUM VITAE

Name: Kim, young jun

Date of birth: 18, 03, 1976

Gender: Male

Nationality: South Korea

## Education

09/2005- present Ph.D. thesis at Max-Planck Institute of Molecular Physiology, Dortmund, Germany

Supervisor: Prof. Dr. Martin Engelhard

Thesis title: Characterization of the sensory rhodopsin II/Transducer complexes from *Halobacterium salinarum*

02/2002~02/2004 M.Sc. in Biology, Chonbuk university, jeonju, south Korea

Supervisor: Prof. Dr. Park, chung wung

Thesis title: Study on anti-rheumatoid arthritis effects of *Sutellaria baicalensis* water extract

03/1995-02/2002 B.Sc. in Cell & Molecular biology, Chonbuk university,

Jeonju, south Korea

## Publication

A non-hydrolyzable ATP derivative generates a stable complex in a light-inducible two-component system.

Sharda S, Koay MS, Kim YJ, Engelhard M, Gärtner W.

*J Biol Chem.* 2009 Dec 4;284(49):33999-4004.

Functional expression of the signaling complex sensory rhodopsin II/transducer II from *Halobacterium salinarum* in *Escherichia coli*.

Kim YJ, Chizhov I, Engelhard M.

*Photochem Photobiol.* 2009 Mar-Apr;85(2):521-8. Epub 2008 Nov 19